Quantification of Temperature Implications and Investigation of Battery Design Options for Electrified Vehicles

Submitted in Partial Fulfillment of the Requirements for
the Degree of
Doctor of Philosophy

in

Mechanical Engineering

Tuğçe Yüksel

B.S. 2007 Mechanical Engineering, Middle East Technical University, Ankara, TURKEY

M.S. 2010 Mechanical Engineering, Middle East Technical University, Ankara, TURKEY

Carnegie Mellon University

Pittsburgh, PA

July 2015

To my dear family

ACKNOWLEDGEMENTS

I first would like to thank my advisor Professor Jeremy Michalek for giving me this unique research opportunity and for his invaluable guidance and support throughout the years. He was involved in every aspect of this dissertation, sharing his knowledge and expertise; pointing me to the right direction when I was lost; showing me the impact of my work whenever I was unaware; teaching me how to see the big picture without missing the importance of the details; encouraging me to explore new ideas and to engage in discussions with other researchers in the area. I would like to thank him for providing me a friendly and respectful research environment, valuing my opinions, acknowledging my work, and never hesitating to spare his lunch time to talk about my future goals, concerns and ideas whenever I asked for. I always felt very lucky to have Jeremy as my advisor and I hope to continue our collaboration in the future.

I was very fortunate to have an outstanding dissertation committee; all of who are well respected experts in their areas. Professor Shawn Litster, Professor Jay Whitacre and Doctor Kandler Smith have all contributed to this dissertation from the very beginning by sharing their knowledge and expertise, and by challenging me with their questions. The basics of the study in Chapter 2 were constructed in Professor Shawn Litster's Energy System Modeling course during my first year in the program and ever since he has been very helpful with my questions about model development. Professor Jay Whitacre was instrumental in developing my understanding of batteries whenever I was lost in the complicated world of electrochemistry. Doctor Kandler Smith was one of the first people who helped me understand battery degradation mechanisms, and he contributed directly to the study in Chapter 2 by providing the vehicle thermal network model. I appreciate all my committee members' feedback and support, which made this work possible.

Aside from my committee, I also had the chance to work with a great group of intelligent individuals who made direct contributions to this dissertation. I would like to thank Nan Gao for his work and contributions in understanding battery thermal management techniques and implications, and Darshit Mehta for putting together the optimization code in Chapter 5. I am grateful to my coauthors in the study leading to Chapter 4: Dr. Mili Tamayao, Professor Inês Azevedo and Professor Chris Hendrickson, who contributed directly to the study and made it possible to get its final form. They were also instrumental in developing my understanding of environmental impacts of vehicle electrification. I would like to thank Alex Mohammad and Siddharth Komini Babu for helping me in testing battery cells, which allowed me to understand battery modeling better; Professor Venkat Viswanathan for valuable discussions on battery modeling and degradation; Professor Huei Peng from University of Michigan for providing the hybrid electric vehicle powertrain control model; Kevin Stutenberg, Eric Rask and Forrest Jehlik from Argonne Energy Laboratory for sharing the dynamometer test data and helping me understand the aspects of the data; and Doctor Apurba Sakti for providing the battery cost model.

The discussions in Carnegie Mellon Vehicle Electrification Group meetings were invaluable in establishing my knowledge on various aspects of vehicle electrification. I would like to thank past and present members of Vehicle Electrification Group: Grace Haaf, Elizabeth Traut, Orkun Karabasoglu, Alan Jenn, Allison Weis, Scott Peterson, John Helveston and Costa Samaras for their feedback and support throughout the process. I also appreciate the feedback of Electrochemical Energy Group members in the study leading to Chapter 2.

In addition to people who made direct contributions to this dissertation, I am grateful to a great number of people, whose friendship made this journey fun and unforgettable. I would like to thank Bilge and Ersin Yumer for being by my side for all these years: it is not possible to list everything we shared together but I am grateful for all of it and looking forward to new adventures; Loubna El Abbadi for being my Moroccan reflection in the world, and keeping my attention alive to various other aspects of life with invaluable discussions on politics, history and music; Beril Cagla Cakir for keeping me company during long late night studies, for motivating me to keep up with recreational writing, and for all the amusing discussions about literature, purpose of life and future resolutions; Emrullah Korkmaz for always reminding me not to underestimate myself and not to forget what is actually important in life; Emre Can Kara for encouraging me to explore new ideas and opportunities for my career, and for his kind and thoughtful friendship; Melis Hazar for all the good food and activities she introduced me to and for showing me the importance of clarity and openness; and Arda Gozen for being one of my first guides into life in America and for all the fun times. I appreciate your support and thank you all for being my second family in Pittsburgh. There are also people I have been lucky to have in my life for quite a long time, and although they were thousands of miles away, they always made me feel they are by my side at both though and happy times: Diclehan Tezcaner Ozturk, Onur Taylan, Cumhur Kaman, Hatice Sinem Sas, Ozlem Demirkan Goksu and Cem Alper Ozen, thank you for all the phone calls/texts/emails/Skype conversations when I needed you the most. And finally, I would like to thank Bekir Bediz, for his endless support, patience and kindness; for bearing with me during all the stressful times; and for helping me to stay focused on the track.

I don’t believe words will ever be enough to express my gratitude to my family, but I would like to thank my parents Kadriye and Ali, who made every sacrifice for me to achieve what I want to achieve, supported my every decision and always believed in me; and my little brother Tolga who at many times became an older brother to me and provided support, love and perspective. I can’t thank them enough for everything they made for me to become the person I am today.

Finally, this work was supported partially by Fulbright Scholarship and Toyota Motor Corporation, and their supports are greatly acknowledged.

ABSTRACT

Battery cost, limited battery life and range anxiety are some barriers to widespread adoption of electrified vehicles. This thesis examines the implications of these issues with a particular focus of analyzing the effect of temperature by addressing several questions: How do range, emissions, and battery life vary with regional climate and driving patterns? How much does thermal management affect these outcomes? How does the cost-minimizing battery design change with chemistry?

A modeling and simulation approach is followed throughout the thesis, where physics based models, as well as models based on real world and experimental data are developed to address the aforementioned questions. Battery electrical, thermal and life models are created to estimate battery degradation under various different usage scenarios, and the effect of air-cooling on improving battery life is investigated. Real world driving data and dynamometer test data are used to estimate driving behavior, and are combined with regional effects of climate and electrical grid mix to evaluate emissions benefits of vehicle electrification across different regions. A battery cost model is used as an objective function in a mixed integer nonlinear program to find the battery design that minimizes the purchase cost for different battery chemistries. Sensitivity analyses are performed to understand the effect of modeling assumptions and design decisions on the results.

Results indicate that battery degradation is particularly sensitive to battery and vehicle design characteristics, such as battery size and powertrain control strategies. In addition, operational factors that change regionally, such as driving cycle and climate, can have significant implications. Aggressive driving can decrease battery life by 67% compared to average driving conditions, and battery life is about 46% shorter in Phoenix than in San Francisco. However battery life can be doubled if battery is thermally conditioned by air-cooling. Regional climate has also significant implications on battery electric vehicle range and energy consumption. Annual energy consumption of battery electric vehicles can increase by an average of 15% in the Upper Midwest or in the Southwest compared to the Pacific Coast due to temperature differences, and cold climate regions can encounter days with substantial reduction in EV range.

Environmental benefits of electrified vehicles vary substantially by vehicle model and region: The Nissan Leaf battery electric vehicle creates lower GHG emissions than the most efficient gasoline vehicle (Toyota Prius) in most of the country except in the Midwest and the South. The Chevrolet Volt plug-in hybrid electric vehicle has higher emissions than the Prius everywhere. Regional grid mix, temperature, driving patterns, and vehicle model all have significant implications on the relative benefits of PEVs versus gasoline vehicles.

Similar to degradation profile and environmental benefits, the cost minimizing design depends on battery energy requirement as well. As the energy requirement from the battery pack increases and the pack gets bigger, optimum design uses the maximum allowable cathode thickness. Among the chemistries explored, Lithium Manganese Oxide (LMO) provides the battery design with the least expensive production cost for vehicles with small size batteries; however as battery size increases it becomes comparable with other chemistries. Lithium Iron Phosphate (LFP) based batteries lead to most expensive design.

CONTENTS

LIST OF FIGURES

LIST OF TABLES

1 Introduction and Motivation

1.1 Background

1.1.1 Electrified Vehicles

Vehicle electrification has the potential to reduce operating cost, greenhouse gas (GHG) emissions, and petroleum consumption in transportation sector [1,2]. The transportation sector is responsible for 32% of U.S. CO_2 emissions and 28% of U.S. greenhouse gas emissions [3]. In addition, 70% of U.S. petroleum demand is consumed by the transportation sector [4]. Replacing the fuel source with electricity is promising to reduce transportation related emissions.

'*Electrified vehicles'* is a broad term used to describe various powertrain technologies that use electricity partly or solely as fuel source. Vehicle technologies that are considered in this thesis are summarized in Table 1.1.

Table 1.1 Vehicle technologies considered

		Vehicle technologies	**Energy Source**		**Power Convertor**
			Gasoline	Electricity	
		Conventional Vehicle (CV) (or gasoline vehicle)	+		Engine
Electrified Vehicles		Hybrid-electric vehicle (HEV)	+		Engine & Motor
Electrified Vehicles	Plug-in vehicles (PEV)	Plug-in hybrid electric vehicle (PHEV)	+	+	Engine & Motor
Electrified Vehicles	Plug-in vehicles (PEV)	Battery electric vehicle (BEV) (or Electric Vehicle (EV))		+	Motor

HEVs use gasoline as fuel source; however they utilize an electrical system to improve vehicle efficiency, therefore they can be categorized as an electrified vehicle.

PHEVs have two modes of operation. Charge depleting (CD) mode and charge sustaining (CS) mode. According to the control strategy in CD mode, PHEVs can further be grouped into two: 1) Blended PHEVs use a mix of gasoline and electricity until the usable battery charge is depleted, 2) Extended Range Electric Vehicles (EREVs) behave like a pure electric vehicle in CD mode, and switches to CS mode when charge is depleted. Toyota Prius PHEV is an example to a blended mode PHEV and GM Chevy Volt is an example for an EREV.

BEVs (or EVs) use electricity as the fuel source and propelled by an electric motor only. Note that, although the term EV usually refers to a battery electric vehicle, it is used inconsistently in public literature and press to refer to electrified vehicles in general.

Despite the benefits, there are various barriers to be overcome for widespread adoption of electrified vehicles such as high purchasing cost, range anxiety and battery life [5–9]. Batteries lose capacity and performance with time and use, therefore might not satisfy driver needs after a certain duration is exceeded. Battery is one of the most expensive components of electrified vehicles and if it has to be replaced before the vehicle's end of life, it increases the costs to the customers. Range anxiety, i.e. the fear of not having enough range to complete a trip, is particularly an issue for BEVs, since there is no engine to support for long trips and battery recharging can take long. Inherent battery and vehicle design characteristics determine the extent to which these issues will be significant. However, operational condition such as climate and driving patterns are also crucial.

1.1.2 Lithium Ion Batteries

An electrified vehicle battery pack consists of individual modules and cells. A cell is the smallest packaged form of a battery. Several cells are connected in series and/or parallel to construct a module. A pack is then constructed by connecting modules. Figure 1.1 shows Nissan Leaf battery pack for demonstrating this hierarchy. In public literature or presss, it is common to use the term 'battery' to refer to individual 'cells', although in the vehicle electrification context battery means the pack.

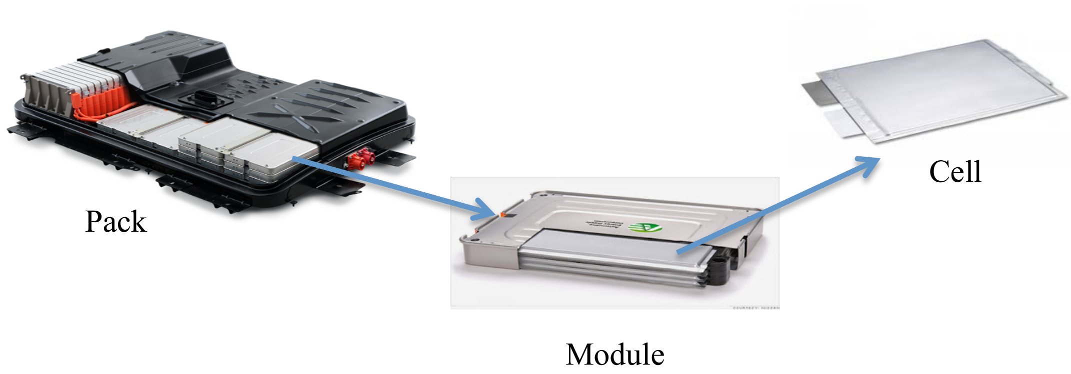

Figure 1.1 Nissan Leaf battery pack, module and cell (Image Source: livingleaf.info, [10])

The mainstream battery currently in use in vehicle electrification is lithium-ion (Li-ion). Li-ion batteries are rechargeable batteries in which lithium ions move back and forth between the positive electrode (cathode) and negative electrode (anode) during charge and discharge. Li-ion cells employ lithium intercalation compounds as cathode and anode [11]. The anode material is typically graphite. There are various cathode material alternatives. 'Li-ion battery chemistry' is a term usually used to refer to the differences in cathode material, which results in differences in performance, cost, and life characteristics. Table 1.2 shows the li-ion battery cathode materials currently in use in vehicle electrification.

In addition to chemistry, individual cells can also have different characteristics based on their physical specifications like dimensions, packaging alternatives (cylindrical or prismatic), and electrode thickness. In addition, two packs might still be different even if they use the exact same cells because of the variances in connection types, as well as in thermal management and energy management systems design. All of these design parameters and decisions have effects on cost, performance and safety.

Table 1.2 Li-ion cathode materials used in vehicle electrification. Values obtained from Nelson et al., 2012 [12]

	Vehicles/Batteries	Specific capacity (mAh/g)	Nominal voltage (V)	Cost per gram ($/g)
Lithium Nickel Manganese Cobalt Oxide, $LiNi_xMn_yCo_zO_2$ (NMC)	Chevy Volt Nissan Leaf	150	3.67	31
Lithium Manganese Oxide, $LiMn_2O_4$ (LMO)	Nissan Leaf Chevy Volt	100	3.95	10
Lithium Nickel Cobalt Aluminum Oxide, $LiNiCoAlO_2$ (NCA)	Tesla Model S	160	3.68	33
Lithium Iron Phosphate, $LiFePO_4$ (LFP)	A123 Systems Hymotion Battery Pack	150	3.28	20

1.1.3 Litium-Ion Battery Degradation and Life

Li-ion batteries experience capacity and power fade with time and use, and ageing mechanisms are complex. Degradation does not occur due to a single cause and it is usually a combination of various electrochemical reactions, as well as mechanical processes that causes ageing. Furthermore, different processes can also interact with each other in different ways and processes that occur change with chemistry.

Battery degradation mainly stems from ageing of the anode [13]. Most of the current li-ion batteries use graphite as anode material and degradation of the anode occurs due to various causes. Among these, the most significant causes can be summarized as follows [14,15].

1. Loss of lithium due to solid electrolyte interface (SEI) growth.
2. Loss of active material due to volume changes occurring during cycling
3. Impedance rise with SEI growth, decrease of accessible surface area and changes in volume due to cycling.

Degradation can also occur on the cathode side, and the degradation mechanism and profile depends on the cathode material. Some general causes of cathode ageing can be summarized as the wear of active mass, electrolyte degradation and interaction between the positive electrode element dissolved within the electrolyte and the negative electrode [13].

The dominant degradation mechanism changes between different batteries. For example, while the main degradation mechanism in LFP cells is SEI growth, in NCA the dominant mechanism is the substantial decrease in the electrode surface conductivity [16].

SEI growth occurs due to irreversible electrochemical decomposition of the electrolyte. It occurs in all Li-ion batteries that use graphite as anode, because typical electrolytes used in Li-ion batteries are not stable at the operating voltages of graphite during charging [16]. SEI is formed in the early cycles, and it is in fact useful for the cell since it prevents electrode's further interaction with the electrolyte. However, SEI continues to grow continuously during battery's life, although with a slower rate as time passes. It has been shown that, the time dependence of SEI growth shows depends on the square root of the time. In addition to time effects, cycling can induce new SEI formation. During cycling, volume expansion and contraction can create cracks in the SEI layer, exposing new areas of the graphite electrode to electrolyte, therefore forming new SEI [17,18].

Apart from material properties, storage and cycling conditions also have significant effects on battery degradation. Operational factors such as temperature, charge/discharge rate, depth of discharge (DOD) and state of charge (SOC) can all influence the aforementioned degradation mechanisms. As an example, SEI morphology and composition changes at high temperatures [14]. However, low temperatures can also induce ageing since the diffusion of lithium in the SEI layer and the graphite slows down at low temperatures, which can result in lithium plating and consequently loss of lithium [13,14]. Storage at both very low and SOCs can advance ageing [14]. In addition, high charge/discharge rates and depth of discharge can introduce new mechanisms that enhance ageing.

Due to its complex nature, characterizing battery degradation behavior and estimating battery life is a complicated and challenging task. Modeling and simulating electrified vehicle battery degradation under real world operation conditions introduce extra challenges. To obtain the exact battery life, cycling and storage tests would need to be performed at all possible conditions until the end of life is reached, which will require years of testing and therefore not practical. Using empirical models based on accelerated tests is one way for addressing this challenge. Accelerated tests can be performed at various stress factors by continuously cycling the cells and can provide invaluable predictions of battery life. However, the accelerated conditions can lead to different results than real world behavior. In addition, interaction between the stress factors may not be clearly understood since during tests usually one or two factors are varied at a time. Physics based models, which quantify degradation based on physical and electrochemical formulations provide better insight, however physical modeling requires identification of underlying mechanisms. There is currently no model in literature that can accurately model degradation under all conditions.

For electrified vehicles, a battery's end of life (EOL) is typically defined as the time when the battery capacity drops by 20% compared to its initial (beginning of life) value, or when 30% internal impedance growth is reached, whichever comes first [19]. However, it is not clear if this criteria will hold in real life applications. Saxena et al argues that, electric vehicles can satisfy the travel needs of 85% of the US drivers even after 20% capacity loss from the battery [20]. Individual drivers can make different decisions in terms of when to replace the vehicle battery.

1.1.4 Vehicle Greenhouse Gas (GHG) Emissions

Vehicle emissions can be broadly categorized as tailpipe emissions, emissions related to the production of the vehicle fuel source and vehicle production emissions. Battery electric vehicles have zero tailpipe emissions. However, there will still be greenhouse gas emissions associated with driving a battery electric vehicle that stems from the emissions during the production of electricity used to fuel the vehicle. This is strongly dependent on the source of electricity production. For example, electricity produced from coal has considerably higher emissions than electricity produced with natural gas. Therefore, GHG emissions associated with driving a BEV will show strong regional heterogeneity across different regions.

1.1.5 Temperature Effect and Thermal Management

Vehicle energy consumption, emissions and battery life will vary across different regions and drivers due to differences in operating conditions. One of the factors that is crucial is temperature. Battery degradation increases exponentially with rise in the temperature [21–23]. In addition, temperature affects vehicle and battery efficiency. At cold temperatures, the internal resistance of the battery increases, decreasing the power capability of battery in all types of xEVs. Cold temperatures will also decrease engine efficiency, causing it to consume more gasoline in case of HEVs and PHEVs. In addition, in cold weather, cabin heater will induce extra load, which is especially important in BEVs, since in BEVs there is no engine whose excess heat can be used, and the extra load due to heater use will be all on the battery. A similar decrease in efficiency is also observed at high temperatures due to air conditioning use. The efficiency decrease results in more energy consumption per miles driven and reduction in the electric range. Up to 40% decrease in battery electric vehicle range is reported when the vehicle is driven at cold ambient temperatures [24]. The change in vehicle and battery efficiency will also change the CO_2 emissions associated with the vehicle.

The battery temperature should therefore be controlled and kept at certain limits in order to improve battery life. This is achieved by thermal management systems. Thermal management techniques can be classified depending on the purpose (heating only versus heating and cooling[1]), the source (passive if ambient air is used without any pre-heating/cooling before entering the battery, active if a heating/cooling device is built-in to the system) and the cooling medium (air versus liquid) [25]. Currently, different vehicles in the market apply different cooling strategies. Toyota Prius PHEV uses air-cooling, whereas Chevy Volt has a complex active liquid cooling strategy. Nissan Leaf does not have a thermal management system, and it is claimed that pure electric vehicles do not need thermal management due to their high energy capacity and low heat generation characteristics. On the other hand, Tesla Model S, an electric vehicle with almost three times energy capacity than Nissan Leaf has an active liquid cooling system.

1.2 Thesis Scope

This thesis aims to investigate the implications of various operating scenarios and design decisions on the main challenges of vehicle electrification: battery cost, battery life, range and

[1] Heating will be required at cold temperatures for preconditioning purposes, to enhance the battery performance

emission benefits, with a particular focus on temperature. The scope of the thesis in terms of the addressed issues is summarized in Figure 1.2. The dissertation aims to answer the following research questions: How do electrified vehicle range, emissions, and battery life vary with regional climate and driving patterns? How much does thermal management affect these outcomes? How does the cost-minimizing battery design change with chemistry? In order to address these questions, 4 studies are presented each of which focuses on a certain portion of these questions.

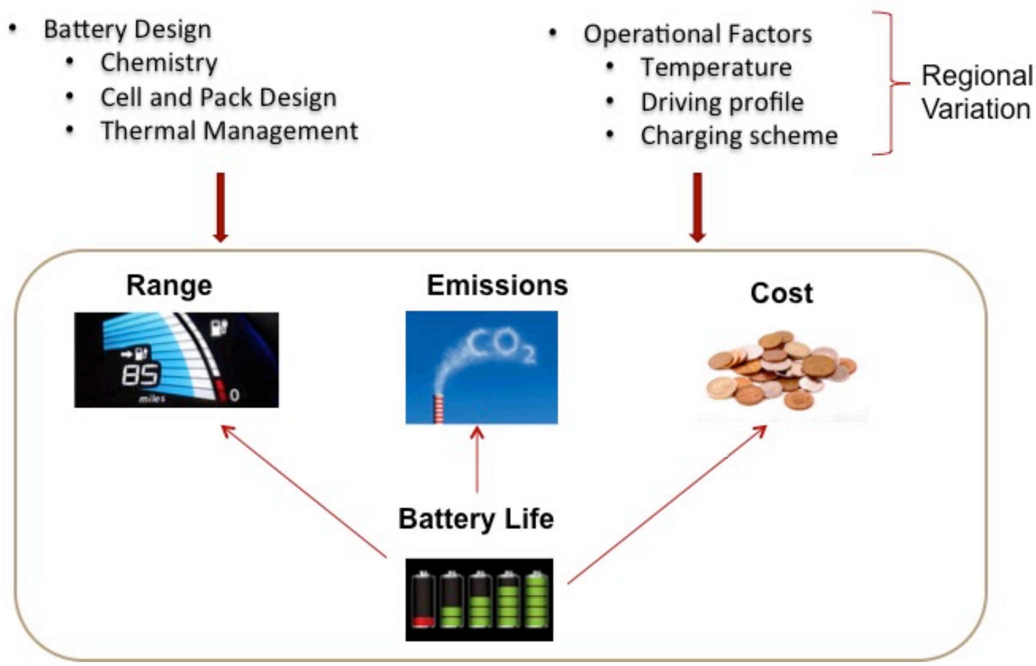

Figure 1.2 Challenges in vehicle electrification and factors affecting them (Images sources: evlanka.com, ecofriend.com, lifehacker.com, and stockfreeimages.com)

The rest of this document is organized as follows:

Chapter 2 aims to identify the change in battery life across climates and driving patterns, as well as to quantify the effect of thermal management on battery life. For this purpose, the study presented in this chapter creates a simulation model to simulate battery temperature, current and voltage profile, and subsequent degradation under different driving cycles in three cities from different regions. The vehicle technology focused on is a PHEV with a small 5 kWh battery. The main reason behind this selection is the fact that, due to its small size, a PHEV battery is more prone to temperature increase and issues from high charge/discharge rates compared to bigger batteries. To examine the effect of thermal management, an air-cooling strategy is considered. Air-cooling is a simple cooling methodology that can be applied, and it was selected to evaluate how effective this basic cooling method is.

Chapter 3 focuses on a BEV to quantify the effect of regional climate on vehicle energy consumption, range and GHG emissions. A BEV is selected to examine the isolated effect of temperature on these issues due to two main reasons: 1) There is no excess engine heat available for cabin heating, therefore the effect of cabin heating on vehicle energy consumption is significant in BEVs. 2) Although reduced range with extreme temperatures is experienced in all vehicle technologies, only for BEVs it can cause a trip not to be completed. To address the related question, real world driving and climate data based models are used together with marginal grid emissions to make regional comparisons.

Chapter 4 aims to extend the study in Chapter 3 by comparing the BEV emissions to alternatives (PHEVs, HEVs and CVs) in terms of regional GHG emissions. Rather than focusing only on the temperature, the study presented in this chapter aims to investigate the joint effect of several different factors that might result in regional differences. For this purpose, dynamometer test data is used to estimate the relationship between energy consumption and temperature for various vehicle technologies, and average CO_2 emissions are compared based on regional differences in climate, marginal emission factors and driving patterns.

Finally, Chapter 5 turns the focus from operating factors to design decisions, and aims to find the cost minimizing battery design for different battery chemistries. A process based cost model of a NMC based battery developed in Carnegie Mellon Vehicle Electrification Group is extended to determine the optimal design for three other chemistries: LMO, NCA and LFP. The roles of various design parameters on cost and performance outcomes are discussed.

2 Plug-in Hybrid Electric Vehicle $LiFePO_4$ Battery Life Implications of Thermal Management, Driving Conditions, and Regional Climate

This chapter aims to investigate the impact of regional climate, driving conditions and thermal management on battery life, with a particular focus on an air-cooled PHEV battery. For this purpose, a mathematical model of the battery pack composed of cylindrical $LiFePO_4$/graphite cells is developed and simulations are performed using real world driving data and climate conditions. In addition, case studies are performed to test the sensitivity of the results to modeling and simulation assumptions. Results indicate that battery life estimates are sensitive to driving patterns, powertrain control strategy, pack size and battery end of life criteria. Given the base case assumptions, the use of air cooling can double battery life in a hot climate like Phoenix while extending battery life by 31% in a mild climate like San Francisco. Aggressive (US06) driving results in battery life estimates 67% shorter than drive cycles based on GPS data, suggesting significant heterogeneity of battery degradation implications across drivers.

This chapter is based on a working paper with Jeremy Michalek [26]. An early version of this work has been presented in SAE World Congress, 2012 and available as an SAE publication [27].

2.1 Background

Plug-in hybrid electric vehicles (PHEVs) have the potential to reduce operating cost, greenhouse gas (GHG) emissions, and petroleum consumption in the transportation sector. Despite these benefits, there are barriers to market penetration and high battery cost is among the most significant [1,28–30]. For many plug-in vehicles, the battery is the most expensive component [31], so if batteries need to be replaced before the vehicle's end of life (EOL), cost competitiveness suffers. Although different design choices can lead to different battery EOL criteria [32], EOL is typically defined as the time when the battery capacity drops by 20%

compared to its initial (beginning of life) value, or when 30% internal impedance growth is reached, whichever comes first.

There are two definitions that are usually used in describing battery life: Cycle life is the number of complete discharge and charge cycles that can be expected from the battery before it reaches its end of life, i.e. it is the life of the battery under active use. Calendar life on the other hand is the total life expected from the battery whether it is being actively used or not. According to the goals set by US Advanced Battery Consortium (USABC), a PHEV battery is targeted to have 15 years of calendar life and 300,000 cycles of cycle life [33]. It is also possible to define storage life (or shelf life) of the battery, which refers to the duration that a battery can be stored without being used.

Batteries degrade with time and usage, and degradation depends on the inherent characteristics of the battery such as its technology and design. Currently, PHEVs use Li-ion batteries due to superior power and energy characteristics. However, battery characteristics such as power, energy, life and safety can vary among Li-ion batteries. The main factor causing different behavior is battery chemistry, which is characterized by the materials being used in cathode and anode. The most commonly used anode material is graphite, however there are various different cathode materials being used in automobile applications. Therefore, in literature, Li-ion chemistry is often specified by cathode material. On the other hand, two batteries of the same chemistry still can show different characteristics due to their differences in design. Design parameters both in cell level (shape, electrode thickness, electrolyte material, etc.) and pack level (distance between the cells, connection elements, etc.) affect performance and life.

Apart from the specific type and design of the battery, the conditions and stress factors during storage and cycling also affect how quickly the battery will degrade. There are various factors that affect battery life such as time, charge/discharge rate, temperature, depth of discharge (DOD) and state of charge (SOC). However these factors are not independent from the design characteristics, and how much each of these factors will affect degradation will vary depending on the chemistry and design. Therefore, estimating the battery life is a complicated and challenging task, and it is not possible to obtain a generic estimation that would apply to all li-ion batteries. To obtain the exact battery life characteristics cycling and storage tests need to be performed at all possible conditions until the end of life is reached, which will require years of testing and therefore not practical because the cells will be obsolete by the time the tests are complete. For this reason, accelerated tests are performed to come up with estimates. Still, the results can be very different depending on the test conditions, even when just a single chemistry is considered.

One type of chemistry that has been extensively tested in the public literature is $LiFePO_4$ (LFP). LFP is promising due to its safety and longer life characteristics [34–36]. Table 2.1 provided a list of reviewed studies that perform accelerated tests at different temperature, discharge/charge current rates (C-rate) and depth-of-discharge (DoD) to quantify degradation and to identify the effects of these factors on degradation. Most of these studies also provide insight on the underlying degradation mechanisms and conclude that the main mechanism of degradation for LFP chemistry is shown to be usable lithium loss due SEI growth. Although SEI growth occurs during both storage and cycling, there is more capacity fade during cycling due to fresh SEI formation in the cracks that occur on the SEI layer with volume expansion and contraction during cycling [17,18]. The SEI growth usually increases with temperature and C-rate, however the degree of the increase shows variances between different studies. In addition, asymmetric cycles with different C-rates during charge and discharge can lead to different degradation behavior [15]. While Peterson et al. shows that LFP degradation is independent from DoD [37], Wang et al. and Groot et al report cycling at high DoD might create significant changes in degradation at high C-rates. Liu et al. argues that there is not a significant impedance growth in this chemistry. On the other hand Groot et al. reports up to 30% impedance growth when the cycle C-rates are different during charge and discharge. However, capacity fade is always faster than impedance growth. To sum up, various studies performed on this chemistry show differences in the results they report and there is not a generalized single model that can define the degradation.

Storage fade is dependent on temperature and the state-of-charge (SOC) level the cells are stored at. Several studies report that cells stored at higher SOC degrade at a faster [38,39]. The difference between capacity fade at two SOC levels decreases as SOC levels increase [18,40].

Table 2.1 LFP cycling fade studies reviewed

	Cell Description	Temp [^oC]	C-rate	Reported with cycles (n) or throughput (Ah)	DOD [%]	Cap. Fade	Imp. Growth
A123 Datasheet [41]	A123 26650 2.3 Ah	25,45, 60	Discharge: 1C,2.2C, Charge: 1C,1.3C	n	N/A	Yes	No
Wang et al [42]	A123 26650 2.3 Ah (paper says 2.2 Ah)	15,45, 60[2]	C/2,2C, 6C, 10C [3]	Ah	10,50,80,90 [4]	Yes	No
Peterson et al [37]	A123 26650 2.3 Ah	~25	Simulated drive cycles	both	Drive cycles corresponding to DODs between 34-97%	Yes	No
Omar et al [43]	2.3 Ah, 3.3 V No brand mentioned	-18,0, 25,40	Discharge: 1C,5C, 10C,15C Charge: 0.25C,0.5C, 1C,2C,4C	n	20,40,60, 80,100	Yes	Yes[5]
Song et al [44]	1.2 Ah 18650 No brand	25,55	N/A	n	N/A	Yes	No
Li et al [45]	11 Ah	30, 45	Discharge: 1/3C,4C Charge: 1/3C, 1.5C	n	N/A	Yes	No
Zhang et al [35]	16.4 Ah No brand	-10,0, 25,45	UDDS	n[6]	N/A	Yes	Yes
Groot et al [15]	A123 26650 2.3 Ah	Between 23 to 53	Discharge: 1C,2,3.75,4 Charge: 1,2,3.75,4	Ah	60%,100%	Yes	Yes

Among the operational factors that influence degradation, temperature is one of the most significant, because degradation increases exponentially with rise in the temperature [21,22,42]. The battery temperature should therefore be controlled and kept at certain limits in order to

[2] Document says they tested 0^oC and 25^oC as well but data is not provided
[3] Data provided only for C/2, models provided for other C-rates
[4] Not enough data for DOD dependence, it looks like it matters at high C-rates but the model does not include DOD dependence
[5] There was actually quite significant resistance growth, but capacity fade was always faster, so no model for impedance growth
[6] Capacity fade and impedance growth is measured after 300 and 600 cycles only

improve battery life. This is achieved by thermal management systems. Table 2.2 shows the classification of thermal management systems. Currently, different vehicles in the market apply different cooling strategies. Toyota Prius PHEV uses air-cooling, whereas Chevy Volt has a complex active liquid cooling strategy. Nissan Leaf does not have a thermal management system. On the other hand, Tesla Model S, an electric vehicle with almost three times energy capacity than Nissan Leaf, has an active liquid cooling system.

Table 2.2 Thermal Management Systems Classification [25]

Purpose	Heating Heating and Cooling
Cooling medium	Air Liquid
Source	Active (cooling medium pre-conditioned before entering the battery) Passive

There are many studies in literature that examine and model cell/pack level thermal behavior [46–50] and thermal management design and control for battery packs [51,52]. However, studies that examine the battery life implications of thermal management are rare. In addition, the effects of various stress factors on cell level degradation are explored considerably, however there are only a few studies that investigate the implications of these factors in real world vehicle usage conditions. Table 2.3 shows the studies that characterize the regional implications of one or more stress factors on battery life. Gross and Clark investigate the effect of thermal management on battery life using a generic battery life model, whose parameters they estimate based on the assumption that the capacity fade of the battery at the end of 15 years will be 20% when stored at 30^{o}C [53]. They then scale these parameters for other temperatures, by assuming that each 10^{o}C increase in temperature will double the fade rate. Smith et al. uses a comprehensive semi-emprical battery life model based on nickel-cobalt-aluminum (NCA) chemistry, however they do not specify a thermal management strategy in their analysis [54]. The most comprehensive analysis in this area is performed by Neubauer and Wood [55], in which they use the same battery life model as Smith et al, and compare the effect of different liquid cooling thermal management strategies on battery life.

Table 2.3 Studies that characterize the regional implications of battery life

	Regional comparison	Thermal Management	Life Model	Battery chemistry	Powertrain	Drive cycle comparison
Gross and Clark, 2011	Yes	Air vs Liquid	Function of temperature and time. Parameters estimated assuming 20% capacity fade at 30^{o}C, in 15 years, fade rate is doubled with each 10^{o}C increase	Not known	PHEV BEV	Yes
Smith et al. 2012 [54]	Yes	N/A	Function of temperature, time, number of cycles and depth of discharge. Parameters based on literature and experimental data	NCA	PHEV	Yes
Neubauer and Wood, 2014 [55]	Yes	No cooling vs liquid cooling, with three different control strategies	Function of temperature, time, number of cycles and depth of discharge. Parameters based literature and experimental data	NCA	BEV	Yes
This study	Yes	No cooling vs air cooling	Function of temperature, Ah-throughput, C-rate and time. Parameters based on literature	LFP	PHEV	Yes

In this study, we aim to asses the regional and drive cycle implications of degradation of a PHEV battery. For this purpose we construct a comprehensive and modular simulation model to address three main questions: 1) How much improvement can be obtained in a PHEV battery life with passive air-cooling? 2) How does this improvement vary across different regions and different driving and usage profiles? 3) What is the sensitivity of the results to the model parameters and assumptions? Various case scenarios are simulated for an air-cooled PHEV battery pack with LiFePO4/graphite chemistry cells.

In the following sections of this manuscript the approach of the study is described, details of each module is given with underlying assumptions, the simulations performed are explained, and finally results, limitations and future work are discussed.

2.2 Approach

To address the questions listed above, we begin by creating hypothetical scenarios for one year long of daily driving, charging and rest conditions and record the battery usage history. We use the battery usage history to estimate the degradation over years, assuming that every year the same usage profile repeats itself.

We consider a vehicle with specifications similar to a Toyota Prius and assume that this vehicle has a battery pack which has the same characteristics of a Hymotion conversion pack with ANR26650 $LiFePO_4$/Graphite cylindrical cells manufactured by A123 systems [41]. Based on these assumptions, we develop a comprehensive simulation model to estimate battery temperature, current and state of charge profiles under the hypothetical scenarios mentioned above. The model consists of three main simulation blocks: driving, charging and rest. In addition to these blocks, we have sub-models, which can be used by one or more of the simulation blocks to perform necessary calculations. These sub-models are: battery equivalent circuit model (ECM), performance model, thermal model, and battery life model. Each of these components is independent function scripts in Matlab and can be decoupled from the whole system model to perform their own calculations with the proper inputs. For the purposes of the simulations in this study, we also create a decision algorithm that decides which simulation block to run based on the travel patterns. The interactions between model components as well as the main simulation inputs are given in Figure 2.1and each model component is explained in detail in the following sections.

2.2.1 Travel Data

To estimate daily travel behavior of the vehicle, we use GPS sample data from Atlanta Regional Commission (ARC)-Regional Travel Survey with GPS Sub-Sample, available in Transportation Secure Data Center (TSDC) by National Renewable Energy Laboratory (NREL) [56]. GPS sub-sample contains data for 1653 vehicles. We filtered the data for the vehicle types and models that might be comparable to plug-in hybrid vehicles available in the market. We selected four vehicle types; Auto Sedan, Auto 2-Seat, SUVs and Station Wagons, whose models are newer than the year 2000, which decreased the total number of vehicles to 921. Each of these vehicles has 3 to 7 days of travel data information available, and the total number of travel days in this subset of data is N^{GPS} =4940. Here, it is assumed that each travel day in this dataset represents a different day of a single vehicle. For each GPS travel day k, the travel profile (φ_k^{GPS}) contains information on the number of trips the vehicle made each day (T_k^{GPS}), the onset ($t_{k\tau}^{\text{START}}$) and end times ($t_{k\tau}^{\text{START}}$) of each trip τ on travel day k and speed versus time (t) points for each trip $v_{k\tau t}^{\text{GPS}}$ as also provided in Equation (**2.1**).

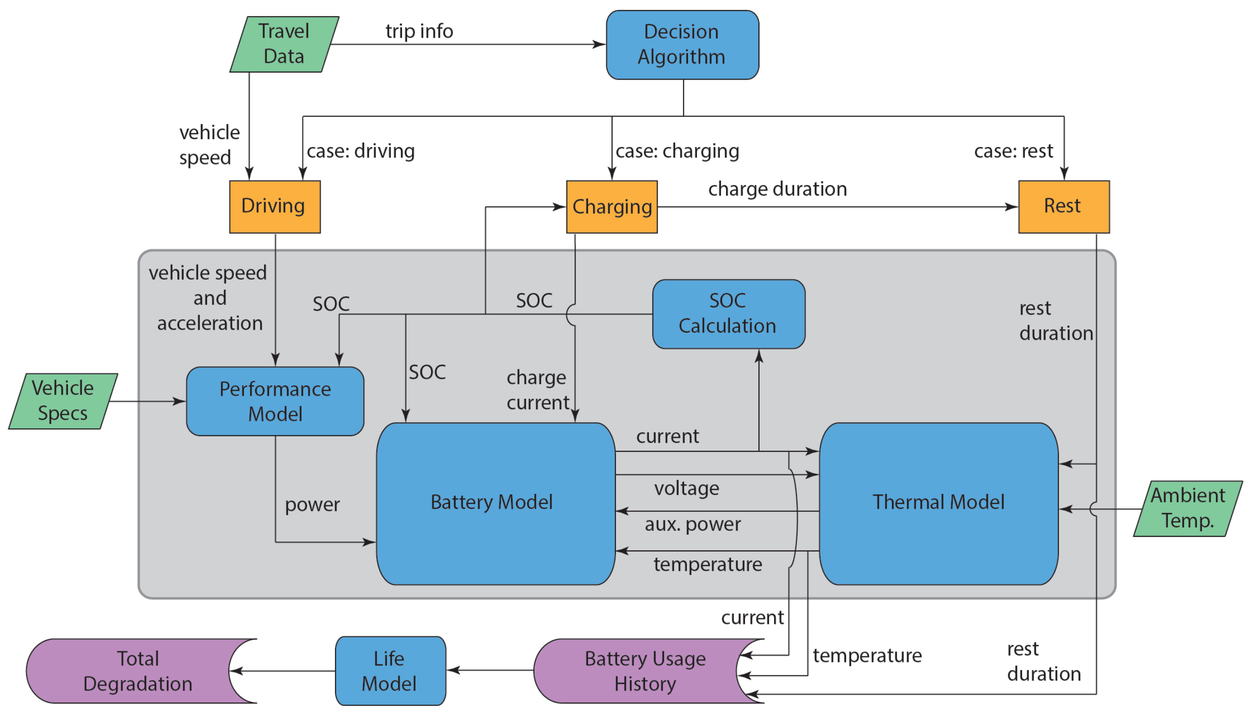

Figure 2.1 Schematic of the approach followed in the study

$$\varphi_k^{\text{GPS}} = \left\{v_{k\tau t}^{\text{GPS}}, t_{k\tau}^{\text{START}}, t_{k\tau}^{\text{END}}\right\} \quad , \quad \begin{aligned} t &= 0,1,..,t_\tau^{LENGTH} \\ t_{k\tau}^{LENGTH} &= \left(t_{k\tau}^{\text{END}} - t_{k\tau}^{\text{START}}\right), in\ seconds \\ k &= 1,2,\ldots,N^{\text{GPS}} \\ \tau &= 1,2,\ldots,T_k^{\text{GPS}} \end{aligned} \qquad (2.1)$$

To create a one year long hypothetical usage scenario, we first assume there will be no travels for 121 days [57] and the vehicle will be at rest. For the rest of the year, we pick N^{YEAR} =244 travel days from N^{GPS} =4950 available in the GPS data to represent 1 year of driving conditions. The travel days are selected randomly, such that the total miles traveled during the year is between 11,000 and 15,000 miles:

$$\varphi_d^{\mathrm{TRV}} = \{v_{d\tau t}, t_{d\tau}^{\mathrm{START}}, t_{d\tau}^{\mathrm{END}}\}$$
$$such\ that$$
$$11{,}000\ miles \leq \sum_{d=1}^{d=N^{\mathrm{TRV}}} \sum_{\tau=1}^{\tau=T_d} \sum_{t=0}^{t=t_{d\tau}^{\mathrm{LENGTH}}-1} \left(\frac{v_{d\tau t} + v_{d\tau(t+1)}}{2}\right) \leq 15{,}000\ miles \tag{2.2}$$

where φ_d^{TRV} is randomly selected travel profile for day d of the year.

To test the sensitivity of the results to drive cycle, we also perform simulations using two fuel economy test cycles by Environmental Protection Agency (EPA). The first cycle, Urban Dynamometer Driving Schedule (UDDS) represents city driving conditions [58]. The second cycle we use is US06, which refers to a high acceleration driving schedule [58]. To incorporate test cycles into the simulations, we employ two different approaches, which we describe in Section 2.3.

2.2.2 Decision Algorithm

Decision algorithm decides which block (driving, charging or rest) to run based on the travel pattern each day. If the day is a rest day, i.e. the vehicle is not driven at all, 'rest' block is simulated. If it is a travel day, each block is called in an order that is determined by onset times of the trips and duration between trips. Charging occurs right after the last trip of the day. The vehicle is assumed to be at rest in between trips and after charging until the next day's trip. The decision algorithm schematic is provided in Appendix A.

2.2.3 Simulation Procedure

In this section, a sample day of simulations with a single trip is explained. For this simulation day, it is assumed that, the driving, charging and rest blocks are simulated one after another.

Driving block takes trip speed profile $v(t)$ as an input and uses performance, battery and thermal models to estimate the dynamic current and temperature profile during the trip.

In this study we assume convenience charging, i.e. charging starts immediately after the last trip of the day. We assume a constant current charging at 4.6 A. This value is estimated based on the Hymotion battery pack specifications, in which it is mentioned that it takes 5.5 hours to charge the 25.3 Ah battery [59]. *Charging block* first decides the duration of the charging based on the remained capacity in the battery after driving. During this duration, it uses battery and thermal models to estimate the battery temperature. Charge duration is calculated as:

$$t^{\mathrm{CHG}} = \frac{(0.9)(C^{\mathrm{RATED}}) - \left(\Phi^{\mathrm{SOC}}_{t^{\mathrm{DRVEND}}}\right)(C^{\mathrm{RATED}})}{I^{\mathrm{CHG}}} \tag{2.3}$$

where t^{CHG} is the charge duration, C^{RATED} is the battery rated capacity, $\Phi^{\mathrm{SOC}}_{t^{\mathrm{DRVEND}}}$ is the SOC level at the end of driving, and I^{CHG} is the charging current.

Once charging is complete, *rest block* determines the duration the vehicle will be at rest based on the charging duration and the start of the next day's trip. Rest duration is then used as an input to the thermal model to estimate battery temperature.

2.2.4 Performance Model

The performance model calculates the power drawn from the battery to sustain a certain speed profile based on the vehicle specifications, and is then used as an input to the battery model and thermal model to estimate the current and temperature profiles. The model estimates power assuming two modes of operation: charge depleting (CD) and charge sustaining (CS) modes. We assume that PHEV we model is an extended range electric vehicle (EREV), therefore during CD mode it behaves like a battery electric vehicle, battery being the only energy source in this mode. Only the battery provides the energy required to sustain the power load until the state-of-charge (SOC) reaches a minimum preset value, which is set to be 20% in this paper. When the minimum SOC level is reached, the vehicle switches to CS mode:

$$P_t = \begin{Bmatrix} P_t^{\mathrm{CD}}(v_t, a_t, \psi^{\mathrm{VEH}}), & 0 \leq t \leq t^{\mathrm{CD,END}} \\ P_t^{\mathrm{CS}}(v_t, a_t, \psi^{\mathrm{VEH}}), & t^{\mathrm{CD,END}} < t \leq t^{\mathrm{END}} \end{Bmatrix} \tag{2.4}$$

$$t^{\mathrm{CD,END}} = min\left(t : \Phi_t^{\mathrm{SOC}} \leq 20\%\right)$$

$$\psi^{\mathrm{VEH}} = [m^{\mathrm{VEH}}, C^{\mathrm{DRAG}}, A^{\mathrm{FRONT}}, C^{\mathrm{RR}}, \eta^{\mathrm{RB}}, \eta^{\mathrm{BW}}]$$

where P_t is the power drawn from the battery at time step t, which is either equal to the power at CD mode (P_t^{CD}) or CS mode (P_t^{CS}). v_t and a_t are the vehicle speed and acceleration during the trip, Φ_t^{SOC} is the state-of-charge at time step t , and $t^{\mathrm{CD,END}}$ is the time step when $\Phi_t^{\mathrm{SOC}} \leq 20\%$ for the first time. ψ^{VEH} is a vector of constant parameters: vehicle mass (m^{VEH}), drag coefficient (C^{DRAG}), vehicle frontal area (A^{FRONT}), tire rolling resistance coefficient (C^{RR}), efficiency of power transfer from regenerative breaking to battery (η^{RB}) and efficiency of power transfer from battery to wheels (η^{BW}). The inputs-output relation of the model is illustrated in Figure 2.2.

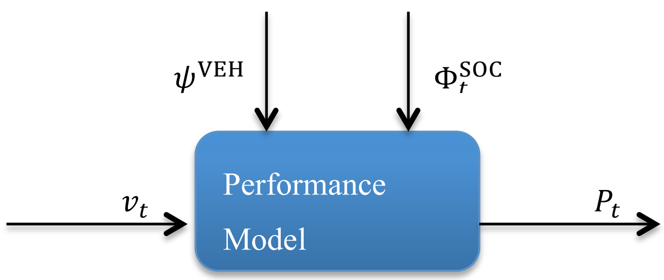

Figure 2.2 Performance model inputs and outputs at each time step

In CD mode, the power load on the battery is calculated using a similar approach presented in Peterson et al. [37]. The power P_t^{CD} drawn from the battery in CD mode can be calculated using Equation (2.5) [7].

$$P_t^{\mathrm{CD}} = \begin{cases} \eta^{\mathrm{RB}} \left(m^{\mathrm{VEH}} a_t + \frac{1}{2} \rho^{\mathrm{AIR}} v_t^2 C^{\mathrm{DRAG}} A^{\mathrm{FRONT}} + C^{\mathrm{RR}} m^{\mathrm{VEH}} g \right) v_t, & \textit{regenarative braking} \\ \dfrac{\left(m^{\mathrm{VEH}} a_t + \frac{1}{2} \rho^{\mathrm{AIR}} v_t^2 C^{\mathrm{DRAG}} A^{\mathrm{FRONT}} + C^{\mathrm{RR}} m^{\mathrm{VEH}} g \right) v_t}{\eta^{\mathrm{BW}}}, & \text{otherwise} \end{cases} \quad 2.5)$$

where g is the gravitational acceleration, and ρ^{AIR} is the air density.

When the SOC of the battery decreases to the minimum level set, the vehicle operation switches to charge sustaining (CS) mode. In CS mode, the battery SOC is kept at the target level.

[7] Hymotion battery pack does not receive any regenerative charging, however the NiMH battery in a Prius conversion does. Here, since we assume the only pack in the vehicle is Hymotion, we assume regenerative charging is accepted by this pack.

So, in order to obtain the battery current and voltage profile, it is necessary to model the power control strategy. In this study, the dynamic model of Toyota Hybrid system powertrain developed by Liu and Peng is used for this purpose [60]. The MATLAB/Simulink® based model was developed to test powertrain control strategies. It takes the vehicle specifications and the drive cycle as inputs, and evaluates the vehicle performance using mathematical models of the engine, generator, electric motor, controller, and battery. We replace the battery model in their model with an equivalent circuit model described in Section 2.2.5. We also incorporate a thermal model (Section 2.2.7). The rest of the Simulink model is treated as a black-box function that determines power load on the battery (P_t^{CS}). For more details on the Simulink model interested reader is referred to [60,61].

2.2.5 Battery Model

Battery model estimates the current and voltage profiles of the battery under a power load. The Hymotion battery pack modeled in this study consists of 14 modules, connected in series. Each module has 44 cells, and the cells are connected with a 11 parallel- 4 series configuration [62]. Pack current and voltage profiles can be estimated by evaluating each cell's electrical performance. The current drawn from each cell of the pack at each time step t is:

$$I_t = \begin{cases} \dfrac{(P_t + P_t^{\mathrm{AUX}})/N^{\mathrm{CELL,PACK}}}{V_t}, & driving \\ I^{CHG}/N^{\mathrm{CELL,PARALLEL}}, & charging \end{cases} \tag{2.6}$$

Where P_t is the power required to sustain a drive cycle, I_t is the current drawn from each cell (or recharged back to battery during regeneration braking and charging), $N^{\mathrm{CELL,PACK}}$ is the total number of cells in the battery pack, $N^{\mathrm{CELL,PARALLEL}}$ is the number of the cells connected in paralle and V_t is the cell voltage. P_t^{AUX} is power consumed by the auxiliary equipment. The main auxiliary power we consider in this study is the HVAC power consumption, which is described in Section 2.2.7.

The electrical behavior of the cells can be modeled using an equivalent circuit model (ECM). In this study, we use the ECM given in Figure 2.3.

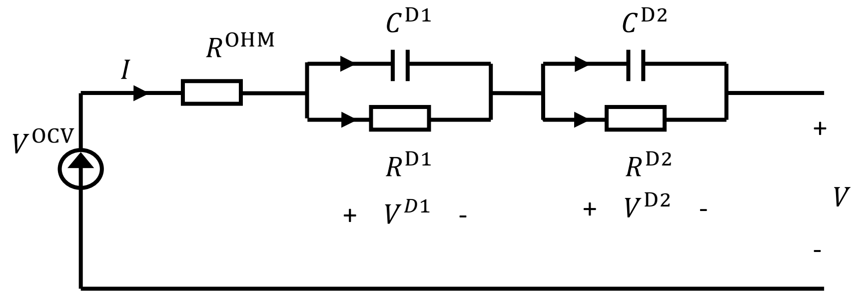

Figure 2.3 Cell equivalent circuit model

In this model, $V^{\mathrm{OCV}}$is the open circuit voltage of the battery, R^{OHM} is the ohmic resistance, and V is the battery voltage. The voltage drops V^{D1} and V^{D2} across the resistance-capacitor (RC) couples represent the dynamic voltage losses. The generic equations for this circuit model can be defined as follows:

$$V = V^{\mathrm{OCV}} - I \cdot R^{\mathrm{OHM}} - V^{\mathrm{D1}} - V^{\mathrm{D2}} \tag{2.7}$$

$$\dot{V}^{\mathrm{D1}} = -\frac{1}{R^{\mathrm{D1}}C^{\mathrm{D1}}}V^{\mathrm{D1}} + \frac{1}{C^{\mathrm{D1}}}I \tag{2.8}$$

$$\dot{V}^{\mathrm{D2}} = -\frac{1}{R^{\mathrm{D2}}C^{\mathrm{D2}}}V^{\mathrm{D2}} + \frac{1}{C^{\mathrm{D2}}}I \tag{2.9}$$

where the current I is assumed to be positive during discharge. Equations (2.8) & (2.9) are ordinary differential equations, which can be discretized for each time step:

$$V_{t+1}^{\mathrm{D1}} = V_t^{\mathrm{D1}} e^{-\frac{1}{R_t^{\mathrm{D1}}C_t^{\mathrm{D1}}}t^{\mathrm{S}}} + R_t^{\mathrm{D1}} I_t \left(1 - e^{-\frac{1}{R_t^{\mathrm{D1}}C_t^{\mathrm{D1}}}t^{\mathrm{S}}}\right) \tag{2.10}$$

where t^{S} is the sampling period (i.e. the time difference between two time steps, 1 second in our case). Then the battery voltage at each time step can be solved as:

$$V_t = V_t^{\mathrm{OCV}} - I_t \cdot R_t^{\mathrm{OHM}} - V_t^{\mathrm{D1}} - V_t^{\mathrm{D2}} \tag{2.11}$$

The ECM parameters are functions of SOC and battery temperature. Perez et al. estimate the model parameters for A123 Systems 26650 LFP/graphite cells [63] and they provide the parameters as look-up tables for each parameter, consisting of their values at 8 different temperature and 9 different SOC index points in [64]. We estimate the parameters at each time step by linear interpolation between the values provided in each look-up table. For example, ohmic resistance at each time step is:

$$R_t^{\mathrm{OHM}}\left(\Phi_t^{\mathrm{SOC}}, T_t^{\mathrm{CELL}}, \Phi^{\mathrm{SOCINDEX}}, \mathrm{T}^{\mathrm{INDEX}}\right) \tag{2.12}$$

where, Φ_t^{SOC} is the state of charge and T_t^{CELL} is the cell temperature at each time step t , and Φ^{SOCINDEX} and $\mathrm{T}^{\mathrm{INDEX}}$ are the SOC and temperature indexes of the look-up table . The look-up tables for each parameter are given in Supplemental Information.

Although some studies showed that open circuit voltage (V^{OCV}) depends on the temperature [65], many studies in literature neglect the temperature dependence of the open circuit voltage. In addition, Lam et. al. [66] showed that the deviation of V^{OCV} at different temperatures from its reference value at 25°C is less than 2mV at most temperatures. Therefore, it is safe to assume that V^{OCV} will not change with temperature; and depends only on SOC, i.e.

$$V_t^{\mathrm{OCV}}\left(\Phi_t^{\mathrm{SOC}}\right) \tag{2.13}$$

We use V^{OCV} data from Perez et. al. [63] for the simulations in this study.

2.2.6 State-of-Charge Estimation

The state-of-charge (SOC) of at each time step needs to be estimated to be used in ECM parameters interpolation as well as to decide which operation mode the vehicle is at (CD or CS). In this study, we define the SOC based on the rated capacity of the cell and approximate Φ_t^{SOC} as follows:

$$\Phi_{t+1}^{\mathrm{SOC}} = \frac{\Phi_t^{\mathrm{SOC}} C^{\mathrm{RATED}} - I_t(\frac{t^S}{3600})}{C^{\mathrm{RATED}}} \tag{2.14}$$

where C^{RATED} is the cell rated capacity in ampere-hours (Ah) and t^S is the time difference between two steps in seconds. In our simulations, assume that SOC of the battery swings between 90% and 20%, i.e. only 70% of the capacity is used.

2.2.7 Thermal Model

The thermal model approximates the battery temperature at each time step by[8]:

$$\mathrm{T}_{t+1}^{\mathrm{BAT}} = \mathrm{T}_{t}^{\mathrm{BAT}} + \frac{\dot{\mathrm{Q}}_{t}^{\mathrm{GEN,BAT}} - \dot{\mathrm{Q}}_{t}^{\mathrm{TR,BAT}}}{M^{\mathrm{BAT}}} t^{\mathrm{S}} \tag{2.15}$$

where $\mathrm{T}_{t}^{\mathrm{BAT}}$ is the battery temperature, $\dot{\mathrm{Q}}_{t}^{\mathrm{GEN}}$ is the heat generation rate inside the battery, $\dot{\mathrm{Q}}_{t}^{\mathrm{TR,BAT}}$ is the heat transferred to or from the battery, and M^{BAT} is the battery thermal mass.

In constructing this thermal model, a series of assumptions were made. First, the temperature difference across the cell is neglected. The temperature of a cylindrical cell under dynamic conditions may vary radially (core and surface temperature difference) due to different layers of materials the cell spiral consists of, as well as in longitudinal direction due to the location of tabs and connectors. What determines the cell degradation and performance is in fact cell core temperature rather than the surface temperature. There are many studies in literature that aim to model this thermal behavior of the cell [67–69], however, none of these studies provide validation since it is not always easy to measure the core temperature of the battery. Most of these studies show by modeling and simulation that, the difference between the cell core and surface temperatures is negligible under low C-rates, but may increase up to 5°C at higher C-rates. Ye et. al. [70], on the other hand, shows that, the temperature difference for a cylindrical LFP cell -with similar parameters to the cell used in this study- can reach up to 10°C under strong forced convection conditions, which might alter the final degradation profiles for the batteries. However, the possible temperature difference across the cell is assumed to be negligible in this study and further investigation of this issue is left for future work. In this study, it is also assumed that the temperature is uniform across the battery pack, i.e. there is no cell-to-cell temperature variance. We neglect any conduction between the cells as well as between cells and outer materials.

[8] Heat removed from the battery is considered positive (+) and heat transfer into the battery is negative (-).

The heat generated in the battery pack is equal to the sum of the heat generation in each cell. Since we assume the uniform temperature in the pack, heat generation can be approximated as:

$$\dot{Q}_t^{\text{GEN,BAT}} = N^{\text{CELL,PACK}} I_t \left(V_t^{\text{OCV}} - V_t\right) \tag{2.16}$$

Note that in this approximation, we consider heat generation only due to ohmic losses and neglect reversible heat generation.

The heat transfer mechanisms we consider in this study are the convection from the battery pack to cabin and ambient, and forced convection heat transfer with air cooling:

$$\dot{Q}_t^{\text{TR}} = \begin{cases} \dot{Q}_t^{\text{REM,FC}} + \dot{Q}_t^{\text{REM,NC}}, & v^{\text{AIR}} \neq 0 \\ \dot{Q}_t^{\text{REM,NC}}, & v_t^{\text{AIR}} = 0 \end{cases} \qquad 2.17)$$

where $\dot{Q}_t^{\text{TR}}$ is the total heat transfer from the battery, $\dot{Q}_t^{\text{REM,FC}}$ is the heat transfer by forced air convection, v_t^{AIR} is the speed of the air entering the battery during cooling and $\dot{Q}_t^{\text{REM,NC}}$ is the natural convection to the cabin and outside. To estimate $\dot{Q}_t^{\text{REM,FC}}$, we construct an air cooling model of the Hymotion pack. We evaluate $\dot{Q}_t^{\text{REM,NC}}$ using the thermal network model developed in NREL [55,71]. The details of these models are explained in the following sections.

2.2.7.1 Air Cooling Model

The battery pack is cooled by a fan that draws cabin air into the battery. An illustration of this cooling strategy is shown in Figure 2.4. We assume a simple on-off thermal control strategy, in which the fan is turned on and off when the battery temperature reaches and falls down to pre-determined threshold values, as given in Equation (2.19). When the fan is on, the air speed is fixed at 17 m^3/h (cubic meter per hour), which is the lowest battery fan speed for Toyota Prius Hybrid battery [72].

$$v_t^{\text{AIR}} = \begin{cases} 17\ [m^3/h], & T_t^{\text{BAT}} > 35^oC \\ 0, & otherwise \end{cases} \tag{2.18}$$

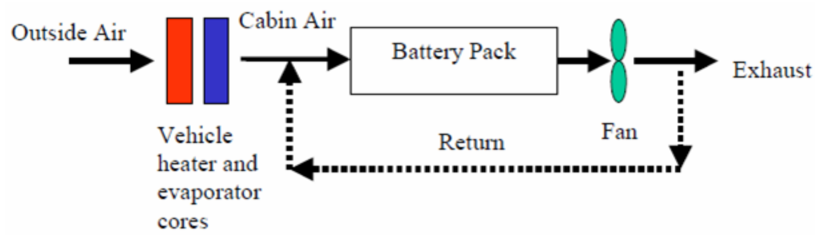

Figure 2.4 Air cooling thermal management system (Image Source: Paseran, 2001 [25])

The flow of air is divided in parallel so that same amount of air passes through each module in the pack [62]. Therefore, we only model and simulate one single module to obtain the temperature profile of the whole pack under air-cooling. A picture of the battery pack, as well as an illustration of the cell configuration inside a module is given in Figure 2.5.

Figure 2.5 (a) A123 Systems Hymotion Li-ion conversion battery pack (Image Source: A123 Hymotion Animation, [73])(b) An illustration of the cell configuration inside a single module

The heat transfer with forced air convection from cells inside the module can be estimated by :

$$\dot{Q}_t^{\mathrm{TR}} = N^{\mathrm{CELL,MODULE}} h\pi D^{\mathrm{CELL}} \Delta T_t^{\mathrm{LM}} L^{\mathrm{CELL}} \tag{2.19}$$

In this equation, h is the overall heat transfer coefficient, D^{CELL} is the cell diameter, ΔT_t^{LM} is the log mean temperature difference at each time step and L^{CELL} is the cell length. The overall heat transfer coefficient h is defined as:

$$h = N^{\mathrm{Nu}} k / D^{\mathrm{CELL}} \tag{2.20}$$

where N^{Nu} is the Nusselt number, and k is thermal conductivity of air. The cell configuration inside the pack is neither fully aligned nor fully staggered. However, it has mostly a staggered arrangement and therefore in this study the correlation in Equation (2.21) by Zhukauskas [74] for "flow across staggered bank of tubes" is used to estimate the Nusselt number.

$$N^{\mathrm{Nu}} = C(N^{\mathrm{Re,max}})^{m}(N^{\mathrm{Pr}})^{0.36}(N^{\mathrm{Pr}}/N^{\mathrm{Pr,s}})^{0.25} \tag{2.21}$$

$N^{\mathrm{Re,max}}$ is the Reynolds number calculated at maximum air velocity , C and m are constants obtained empirically and tabulated for $N^{\mathrm{Re,max}}$, and N^{Pr} is the Prandtl number. $N^{\mathrm{Re,max}}$ and N^{Pr} are calculated at the film temperature, $\mathrm{T}^{\mathrm{FILM}}$, which is defined as:

$$T^{\mathrm{FILM}} \equiv (T^{\mathrm{SURF}} + T^{\mathrm{AIR}})/2 \tag{2.22}$$

where T^{SURF} is the cell surface temperature and T^{AIR} is inlet air temperature. $N^{\mathrm{Pr,s}}$ is calculated at T^{SURF}.

In this study, we assume that air inlet temperature $\mathrm{T}^{\mathrm{AIR}}$ is equal to the cabin temperature, which is kept constant at 24°C. In addition, we assume that cell temperature is uniform radially and axially along each cylindrical cell. Therefore, cell surface temperature is actually the cell temperature overall, i.e. $T^{\mathrm{SURF}} = T^{CELL}$. Since cell temperature is time dependent, $(T^{CELL}(t))$, N^{Pr} and $N^{\mathrm{Pr,s}}$ should also vary at each time step. However, change of air Prandtl number with temperature is considerably small as given in Table 2.4, therefore we assume a constant Prandtl number N^{Pr}= $N^{\mathrm{Pr,s}}$=0.71 in this study. Therefore, a constant heat transfer coefficient h is calculated for forced air-cooling.

Table 2.4 Air Prandtl Number with temperature [75]

Temperature (°C)	Prandtl Number
20	0.713
40	0.711
60	0.709

The log mean temperature ΔT_t^{LM}difference in Equation (2.19) is defined as:

$$\Delta T_t^{\text{LM}} = \frac{\left(T_t^{\text{SURF}} - T^{\text{AIR}}\right) - \left(T_t^{\text{SURF}} - T_t^{\text{o}}\right)}{\ln\left(\dfrac{T_t^{\text{SURF}} - T^{\text{AIR}}}{T_t^{\text{SURF}} - T_t^{\text{AIROUT}}}\right)} \tag{2.23}$$

where T_t^{AIROUT} is the temperature of air leaving the battery, and can be calculated by using the relation given in Equation (2.24), which can be obtained by equating the heat transferred from the cell surfaces to air (Equation (2.19)) to the heat carried away by air.

$$\left(\frac{T_t^{\text{SURF}} - T_t^{\text{AIROUT}}}{T_t^{\text{SURF}} - T^{\text{AIR}}}\right) = exp\left(-\frac{\pi D^{\text{CELL}} N^{\text{CELL,MODULE}} h}{\rho^{\text{AIR}} v_t^{\text{AIR}} A^T c^{\text{AIR}}}\right) \tag{2.24}$$

where ρ^{AIR} is air density, v_t^{AIR} is the air speed, A^{T} is the air inlet area, and c^{AIR} is the air constant specific heat.

2.2.7.2 Thermal Network Model

We estimate the heat transfer from the battery to the ambient and to the cabin using the thermal network model shown in Figure 2.6 developed in NREL [55,71]

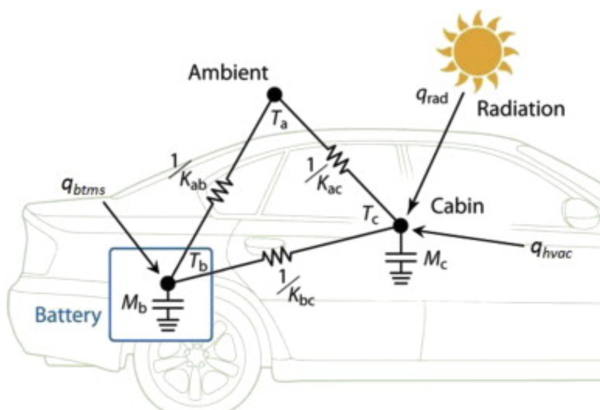

Figure 2.6 Thermal network model to predict battery temperature in various environments and under solar radiation (Image Source**:** Neubauer and Wood, 2014 [55]**)**

The heat transferred from the battery is estimated as:

$$\dot{Q}_t^{\text{TR,NC}} = K^{\text{ab}}\left(T_t^{\text{BAT}} - T_t^{\text{AMB}}\right) + K^{\text{bc}}\left(T_t^{\text{BAT}} - T_t^{\text{CAB}}\right) \tag{2.25}$$

where T_t^{AMB}, T_t^{CAB} and T_t^{BAT} are ambient, cabin and battery temperature. $1/K^{\mathrm{ac}}$ is the thermal resistance between cabin and ambient, $1/K^{\mathrm{ab}}$ is the thermal resistance between battery and ambient, and $1/\,K^{\mathrm{cb}}$ relates the battery convection to cabin. Thermal resistances were estimated by fitting values to the data collected in December 2008 in Golden, CO with a Gen 2 Toyota Prius. Cabin temperature can be estimated as:

$$T_{t+1}^{\mathrm{CAB}} = T_t^{\mathrm{CAB}} - \frac{\dot{Q}_t^{\mathrm{CAB}}}{M^{\mathrm{CAB}}} \tag{2.26}$$

where M^{CAB} is the vehicle cabin thermal mass, and $\dot{Q}_t^{\mathrm{CAB}}$ is the heat transfer rate from the cabin defined by:

$$\dot{Q}_t^{\mathrm{CAB}} = K^{\mathrm{ac}}\left(T_t^{\mathrm{CAB}} - T_t^{\mathrm{AMB}}\right) + K^{\mathrm{bc}}\left(T_t^{\mathrm{CAB}} - T_t^{\mathrm{BAT}}\right) - \dot{Q}_t^{\mathrm{RAD}} + \dot{Q}_t^{\mathrm{HVAC}} \tag{2.27}$$

where $\dot{Q}_t^{\mathrm{RAD}}$ is the radiative heat transfer and $\dot{Q}_t^{\mathrm{HVAC}}$ is the heat removal from the cabin by HVAC system. We estimate the radiative heat transfer as:

$$\dot{Q}_t^{\mathrm{RAD}} = \dot{q}_t{}^{\mathrm{SOLAR}} \varepsilon A^{\mathrm{CAR}} \tag{2.28}$$

$\dot{q}_t{}^{\mathrm{SOLAR}}$ is the global diffuse horizontal radiation per unit area that can be found in "Typical Meteorological Year" database compiled by NREL for various cities in United States [76]. ε is the surface emissivity and A^{CAR} is the car surface area. In the model, $\dot{Q}_t^{\mathrm{HVAC}}$ is estimated as:

$$\dot{Q}_t^{\mathrm{HVAC}} = \begin{array}{cc} 4500\,W, & T_t^{\mathrm{CAB}} > 25^{o}C \\ -4000\,W, & T_t^{\mathrm{CAB}} < 19^{o}C \\ 0, & otherwise \end{array} \tag{2.29}$$

The thermal model calculations with the input-output relationships are summarized in a schematic in Figure 2.7.

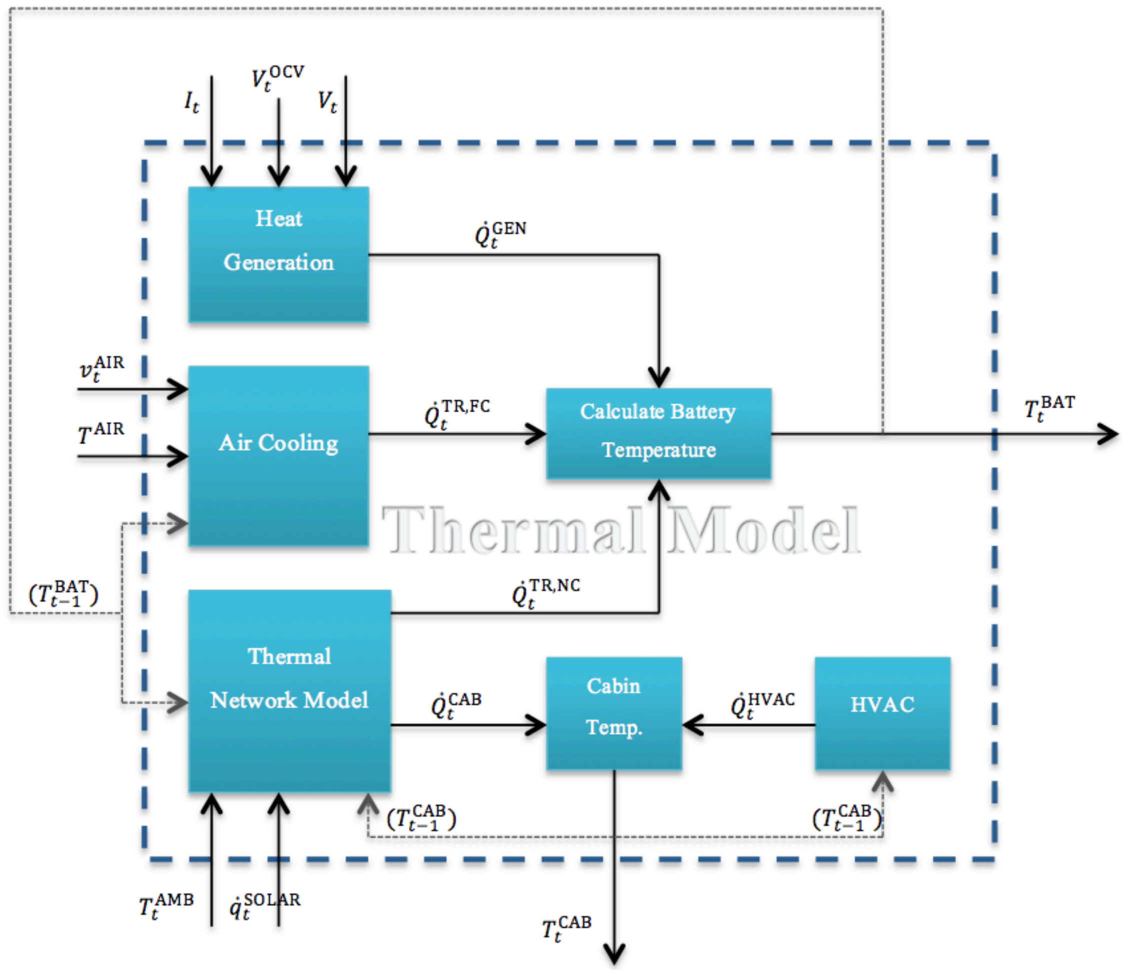

Figure 2.7 Schematic of the Thermal Model

2.2.8 Battery Degradation Model

Li-ion batteries degrade with time and usage. Degradation occurs due to various reactions and processes both in electrolyte and electrode level, and these can show differences between different chemistries.

In this study, we focus on $LiFePO_4$ (LFP) chemistry. The main reasons of this choice are: (1) the cells used in the actual Hymotion battery pack are of this chemistry, (2) due to its safety and longer life characteristic, this chemistry is a potential candidate to be used in automotive industry and extensively studied in public literature [23,35,37,42–45] , and (3) in this chemistry, the main aging is due to capacity loss rather than impedance growth [23,37], therefore the battery life model can be simplified by considering only capacity loss criteria. In LFP batteries, the main aging mechanism is the SEI growth, therefore the degradation modeling approach we follow here can be assumed to be similar in other batteries where SEI growth is the dominant factor in ageing.

Figure 2.8 shows the percent capacity fade versus Ah-processed obtained from the studies in Table 2.3 that tested A123 Systems ANR26650 cells. As can be seen from the figure, measurements and/or estimations of degradation vary a lot between studies. Therefore, it is not possible to just us model and expect an accurate result. In this study, we selected the model provided by Wang et al. [42] as our base case degradation model since it provides the most comprehensive analysis considering both temperature and C-rate as stress factors. To see the sensitivity of the results to this choice of degradation model, we also estimate the capacity loss based on manufacturer data.

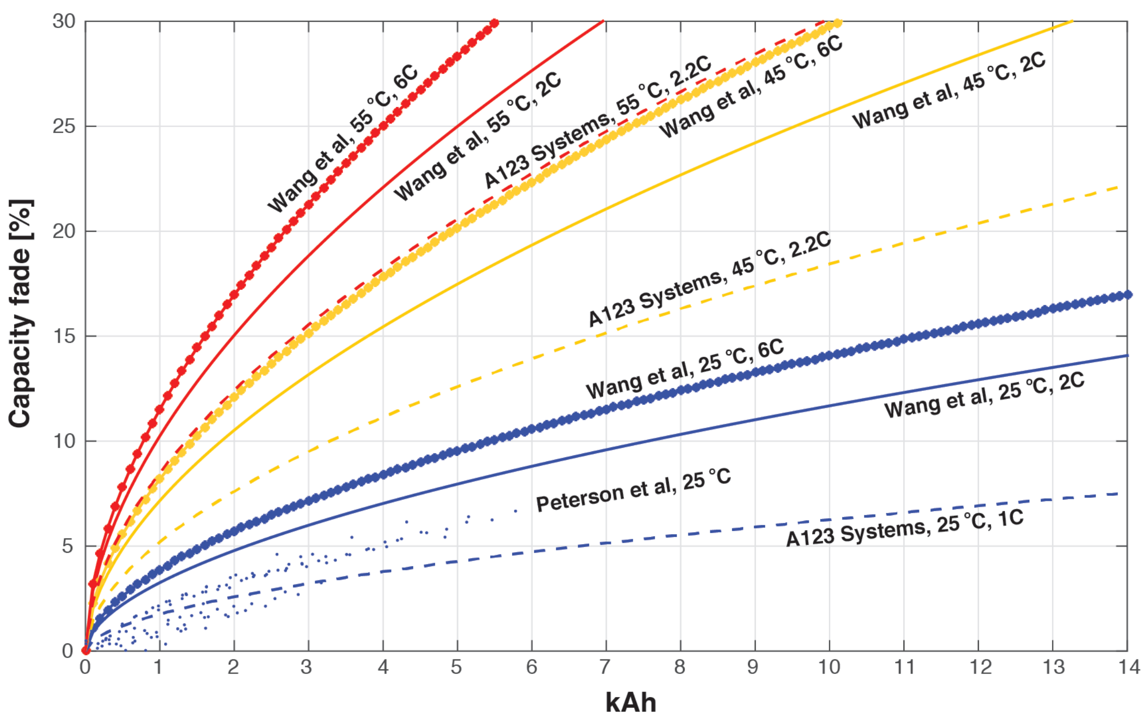

Figure 2.8 Percent capacity fade with Ah-processed during cycling of A123 Systems ANR26650 cell with 2.3 Ah capacity- comparison of results from different studies

The generic capacity loss model described in Wang et al. is given in Equation (2.30):

$$\theta^{\mathrm{CYC}} = A \cdot exp\left[\frac{-31700 + 370.3\times(I^{\mathrm{CELL}}/C^{\mathrm{CELL}})}{R^{\mathrm{GAS}} \cdot T^{\mathrm{CELL}}}\right](\phi^{\mathrm{AH,TH}})^{0.55} \quad (2.30)$$

where θ^{CYC} is the percent capacity loss with cycling, I^{CELL} is the current drawn from (or charged to) cell, C^{CELL} is the nominal cell capacity in ampere-hours (Ah), R^{GAS} is the universal gas constant, T^{CELL} is the cell temperature and ϕ^{AH} is the ampere-hour (Ah) throughput. A is a constant given at four different C-rates ($I^{\mathrm{CELL}}/C^{\mathrm{CELL}}$) in Table 2.5.

Table 2.5 Values of coefficient $\boldsymbol{A}$ in Equation (2.30) as given in Wang et al. [42]

$\mathrm{C}^{\mathrm{RATE}} = I^{\mathrm{CELL}}/C^{\mathrm{CELL}}$	1/2	2	6	10
A	31,630	21,681	12,934	15,512

The Ah- throughput in this model is defined as the energy delivered by the cell during cycling. Therefore, it does not involve the energy recharged to the cell during charging. In this study, we assume that the degradation mechanisms during the charging follow the same pattern as discharge, and we define a new parameter, Ah-processed ($\phi^{\mathrm{AH,PR}}$) as the total energy processed in a cell, i.e. summation of energy delivered to and from the cell. Therefore, replacing $\phi^{\mathrm{AH,TH}}$ with $\phi^{\mathrm{AH,PR}}/2$ in Equation (2.30), we update the model as:

$$\theta^{\mathrm{CYC}} = A \cdot exp\left[\frac{-31700 + 370.3\times(I^{\mathrm{CELL}}/C^{\mathrm{CELL}})}{R^{\mathrm{GAS}} \cdot T^{\mathrm{CELL}}}\right](0.5)^{0.55}(\phi^{\mathrm{AH,PR}})^{0.55} \quad (2.31)$$

We assume this generic model can be applied to estimate the cycling fade at each time step as follows:

$$\begin{aligned} \theta_t^{\mathrm{CYC}} &= \Gamma_t \cdot \left[\left(\frac{\theta_{t-1}^{\mathrm{CYC}}}{\Gamma_t}\right)^{\frac{1}{0.55}} + \Delta\phi_t^{\mathrm{AH,PR}}\right]^{0.55} \\ \Gamma_t &= (0.5)^{0.55} A_t \cdot exp\left[\frac{-31700 + 370.3\times C_t^{\mathrm{RATE}}}{R^{\mathrm{GAS}} T_t^{\mathrm{CELL}}}\right] \end{aligned} \quad (2.32)$$

where $\Delta\phi_t^{\mathrm{AH,PR}}$ is the ampere-hour processed between the time steps t and $t-1$:

$$\Delta\phi_t^{\mathrm{AH}} = \int_{t-1}^{t} I^{\mathrm{CELL}}(t) \cdot dt \cong \frac{1}{2}\left(\left|I_t^{\mathrm{CELL}}\right| + \left|I_{t-1}^{\mathrm{CELL}}\right|\right) \tag{2.33}$$

We estimate A_t for C_t^{RATE} by using linear interpolation between the tabulated values given in Table 2.5.

The capacity loss during storage, i.e. whenever the vehicle is at rest, is obtained by a model fitted to data provided by the cell manufacturer [38]. In the given data, the percent capacity loss was observed to vary linearly with the logarithm of time in days. Therefore, the model form given in Equation (2.34) is used to estimate the storage fade. The constant parameters given in the formula are obtained using least squares regression fit to the data.

$$\theta^{\mathrm{STO}} = \left(10^{0.0202 \cdot T^{CELL} - 5.885}\right) \cdot log10(t^{\mathrm{STO}}) \tag{2.34}$$

where t^{STO} is the storage duration in days.

Using this model for the purpose of estimating battery life in electrified vehicle applications has several limitations:

- The cycling tests were performed at static loading profiles, i.e. using constant current/discharge rates. We assume the same degradation model will be valid with under dynamic load, and that we can apply the model on second by second basis.
- The tests were performed on single cells only. We assume the degradation behavior does not change when the cells are used in connection with other cells in a pack.
- The coupled effects of stress factors are not clear. We assume the relationships observed in these tests are applicable when the model is used to estimate degradation at various other temperature and C-rate combinations.
- We assume the ageing mechanisms are exactly the same during charge and discharge. Li et al. shows that fresh SEI formation with cycling occurs only during charging and although this SEI peels off and accumulates during discharge, no new SEI formation occurs [18]. In addition, Groot et al shows that different charge/discharge current combinations can lead to different capacity loss profiles depending on the temperature [15]. As an example, their test results

indicate that for temperatures higher than 30^{o}C cycling with 1C discharge/ 3.75 C charge rates cause faster degradation than cycling with 3.75C both during charge and discharge.

- When estimating the constant parameter A_t in Equation (2.32) using Table 2.5, we assume for any C-rate lower or upper than the minimum and maximum index values given in the table, the constant A_t is equal to its value at either in the lowest or highest C-rate. Therefore, we might be underestimating degradation for C-rates higher than 10C.

All these limitations might be causing over or underestimation of degradation depending on the conditions. However, to Authors' knowledge, there is no model available in public literature that would address all these issues.

2.3 Simulations and Sensitivity Analysis

Using the procedure and models described above, we perform various simulations to see the effects of air-cooling, regional climate and drive cycle on battery life. The case studies simulated are summarized in Table 2.6.

Table 2.6 Case Studies Simulated

Test the effect of:	Options
Thermal Management	No battery thermal management Air-cooling
Region	San Francisco, CA Phoenix, AZ Miami, FL
Driving Cycle	GPS data from Atlanta EPA US06 test cycle EPA UDDS test cycle
Annual miles driven	12,400 miles 14,700 miles

Thermal management effect: To test how much air-cooling improves battery life we simulate two cases. In the first case, there is no cooling system for the battery and only the interaction between battery, ambient and cabin is considered using the thermal network model. In the second case, we assume battery is cooled with an air-cooling system described in Section 2.2.7.1.

Regional effects: We perform simulations in three different cities. Phoenix represents a region where cold hours as well as high peak temperatures can be observed. Both Miami and San Francisco show little hourly and daily fluctuations in temperature. They represent a hot and a mild climate respectively. The factors that change with region are the ambient temperature and radiation inputs to the thermal model.

Driving cycle: To test the effect of driving cycle, we follow two approaches:

Approach 1. In the first approach, the speed profiles in the GPS data are replaced by UDDS and US06 speed profiles such that the total distance driven remains the same. In doing this, we assume that the start time of each trip in the GPS data doesn't change. However, due to different speed profiles, trips can take longer or shorter with UDDS and US06, therefore trips end times are different than the GPS data. However, in particular with UDDS trips take longer since it is a low speed cycle, and the next trip start time in GPS data might be earlier than trip end time with UDDS. The algorithm does not check that, therefore this results in more than one trips to occur during the same hourly bin at certain days, which result in more driving and degradation than actual.

Approach 2. To address this issue, in the second approach we follow a different methodology and assume the same driving pattern every day throughout the year, with the same drive cycle (UDDS or US06). We divide the total annual miles driven to 244 driving days, and assume half of this distance is driven in the morning starting at 8:30 am, and the other half in the evening starting at 5:30 pm, to represent a daily commute between home and work. We assume the battery is only charged after the last trip of the day and at rest in between trips. With this approach, we aim to prevent any biases that can be introduced in the results due to different trip times.

Annual miles driven: We pick two different sets of driving days from the GPS data. The first set sums up to a total distance of 12,400 miles and the second set has an annual mileage of 14,700 miles. Note that, we make these random selections based on distance only. Therefore, the two different sets can have different driving patterns. However, the rest days and the driving days throughout the year are assumed to be the same across the two sets.

2.4 Results and Discussion

2.4.1 Annual Miles Driven:

Figure 2.9 shows the capacity fade at the end of 15 years in Phoenix when two different sets of random driving days with different annual mileages driven are selected from GPS data. The figure shows the case when there is no air-cooling employed. The capacity fade follows very similar patterns in both cases, showing only minor difference at the end of 15 years.

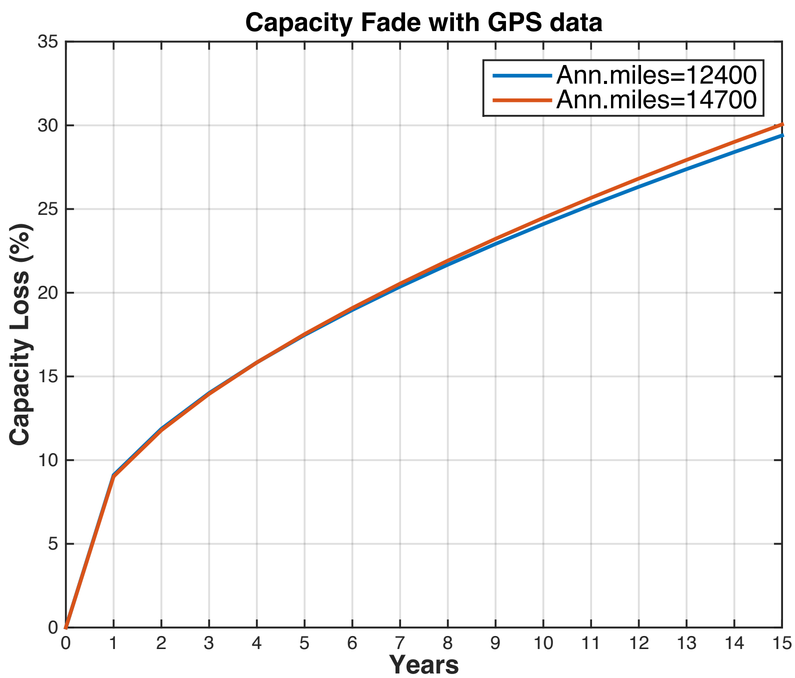

Figure 2.9 Total annual mileages comparison

Since this comparison is based on randomly selected drive cycles from GPS data, there might be differences between driving patterns and aggressiveness between two sets that would prevent analyzing isolated effect of annual miles driven. To test if that is the case, we compare the simulations performed with UDDS using approach 2, i.e. assuming same driving cycle everyday. Figure 2.10 shows this comparison. As depicted from the figure, the difference between assuming two different total annual miles traveled is bigger in this case. This might indicate that, when the driving profiles are selected randomly, driving patterns (time of driving, number of trips, duration between trips) and driving aggressiveness can dominate and effect of miles driven can become less significant.

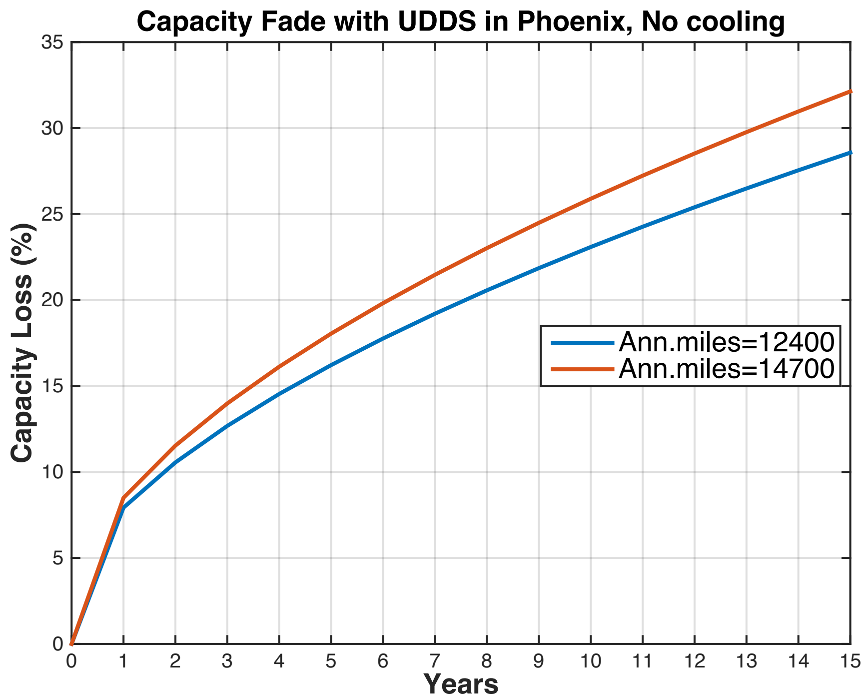

Figure 2.10 Annual mileages comparison with UDDS

2.4.2 Drive Cycle

Figure 2.11 shows the degradation profiles of assuming different driving cycles in Phoenix, in the case of no air-cooling. As expected, driving with US06 results in more degradation: battery life is halved compared to GPS when 20% capacity loss is assumed to be the end of life. UDDS results however are comparable to GPS. Furthermore, as shown in Figure 2.10, with annual mileages of 14,700 miles, UDDS might result in even higher degradation than GPS. UDDS is a milder cycle, however driving the same distances with UDDS takes considerably longer compared to GPS. Although C-rates might be lower than in the case of GPS, they might not be high enough to dominate the time effects of degradation.

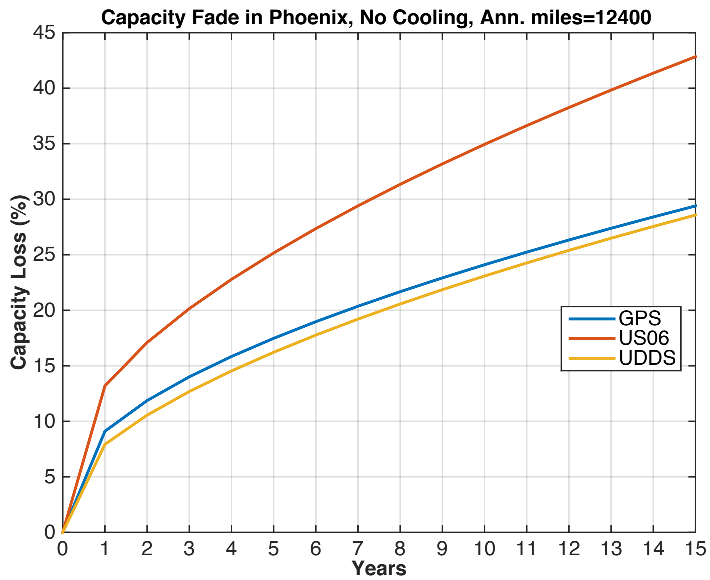

Figure 2.11 Comparison of drive cycles in Phoenix. Air-cooling is not active. Annual miles driven are 12,400 miles. UDDS and US06 results are obtained using Approach 2: assuming same driving profile and distance everyday

Figure 2.12 shows a comparison of the degradation profiles between the two approaches we use to perform simulations with US06 data. As can be seen, assuming the same driving profile everyday results in less degradation compared to replacing trips in the GPS.

In both approaches with US06, degradation is very fast and 20% capacity loss is reached in less than 3 years. To investigate this issue and test any model errors, we perform two additional case studies: In the first case, we test the effect of control strategy, and we assume a blended mode CD operation, and perform both CD and CS mode simulations using the Toyota Prius control system model in Simulink described in Section 2.2.4. In the second case, we investigate the pack size implications, and perform the simulations again assuming a pack with 5 times more modules with the same cell configurations. As expected, in both cases significant reduction in capacity fade is observed. With blended mode strategy, the battery life quadruples. In the case of a bigger pack, degradation rate is very slow and battery EOL is not reached in fifteen years. These results are consistent with the observations that degradation is much slower in big batteries, and small-battery PHEVs are typically designed as blended-operation vehicles rather than EREVs.

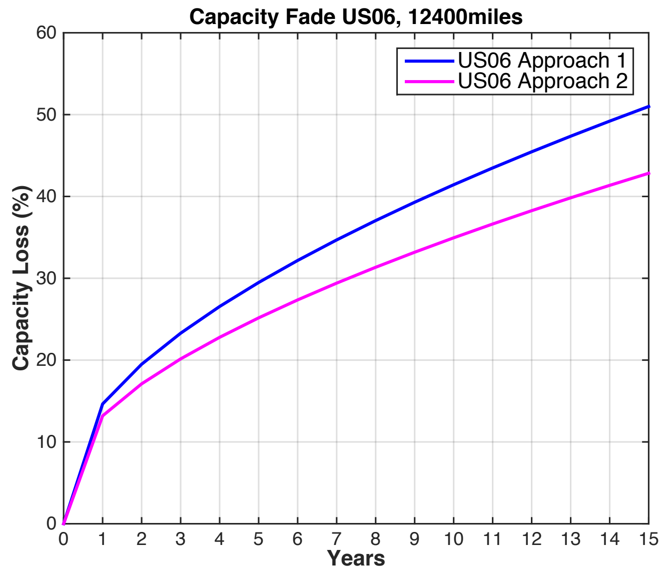

Figure 2.12 Comparison of two approaches in using US06 drive cycle. Approach 1: replace every single trip in GPS data with corresponding US06 cycles that matches the same trip distance. Approach 2: assume same miles of travel everyday and two trips, one in the morning one in the evening.

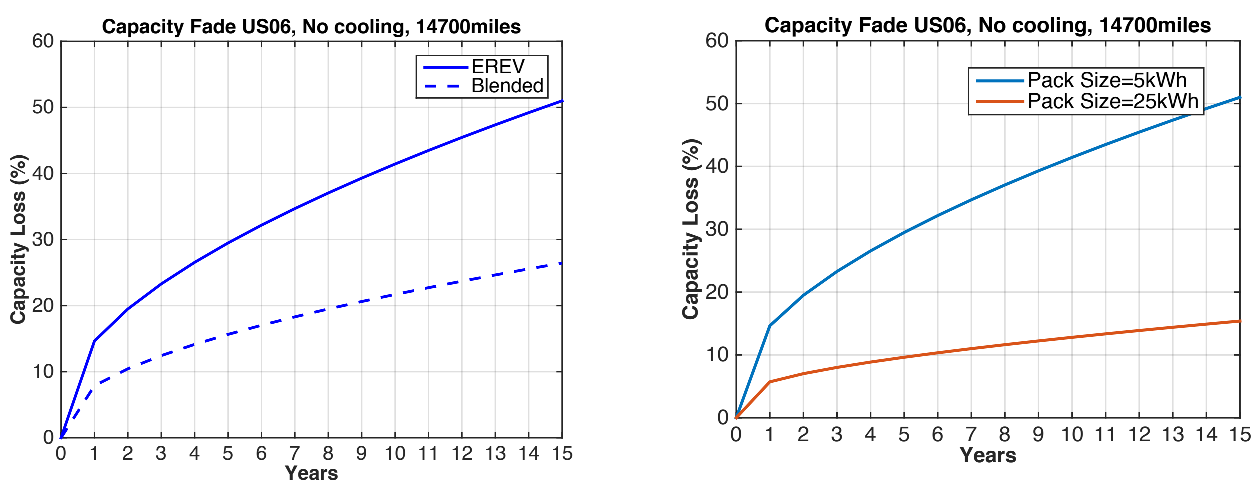

Figure 2.13 Investigation of capacity fade with US06 Left: comparison of powertrain control strategies. Right: comparison of pack size

2.4.3 Regional Effects

The comparison of capacity fade at three cities is given in Figure 2.14. It is observed that, battery life in San Francisco is 75% longer than battery life in Phoenix, mainly because less cabin thermal conditioning use in a mild climate decrease the load on the battery, therefore increasing life. In Miami battery life is one year longer than Phoenix.

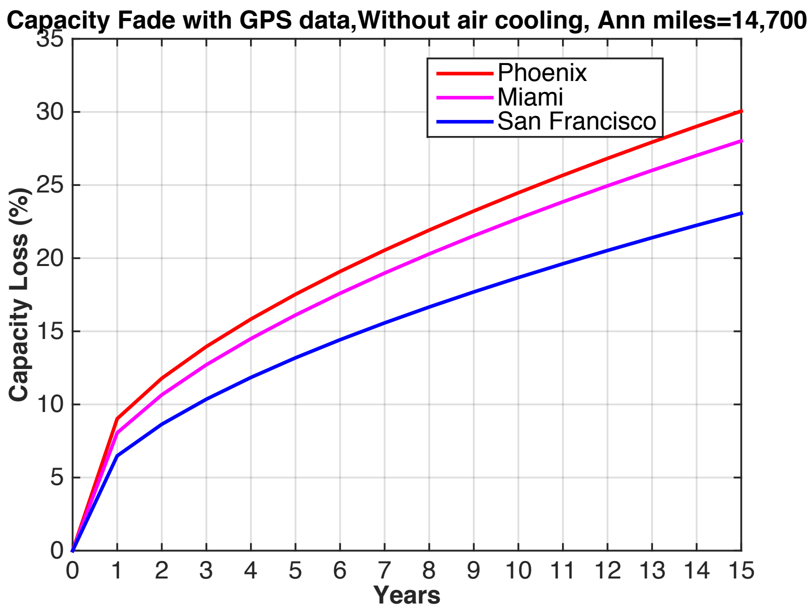

Figure 2.14 Capacity fade comparison between cities using GPS data. No air-cooling is employed and total annual miles driven is 14,700 miles

2.4.4 Effect of Thermal Management

Air-cooling can improve battery life significantly. In Phoenix, battery life doubles with GPS data, and with US06 almost 8 times longer battery life can be obtained as shown in Figure 2.15. The degree of improvement also depends on the city. As depicted in Figure 2.16, in San Francisco the improvement obtained by air-cooling is less than in Phoenix. Figure 2.17 summarizes the improvement of battery life by air-cooling for different cases simulated.

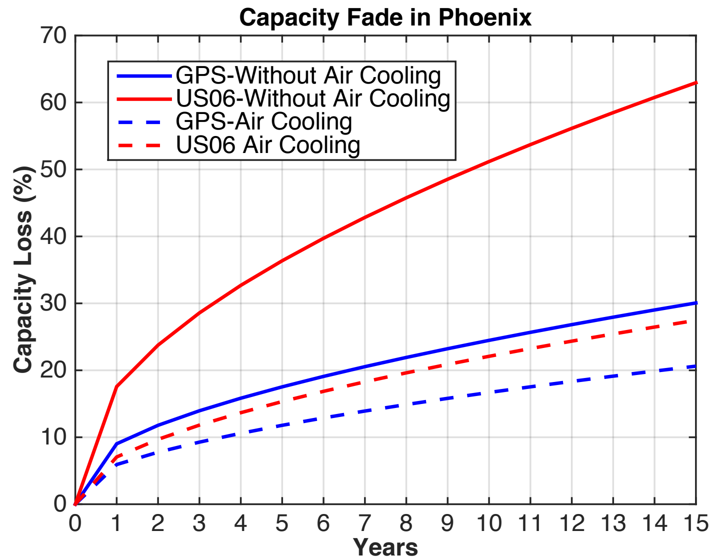

Figure 2.15 Capacity Fade in Phoenix, with annual miles driven 14,700miles. The comparison of air cooling vs no cooling for two drive cycles. US06 simulations are performed using Approach 1.

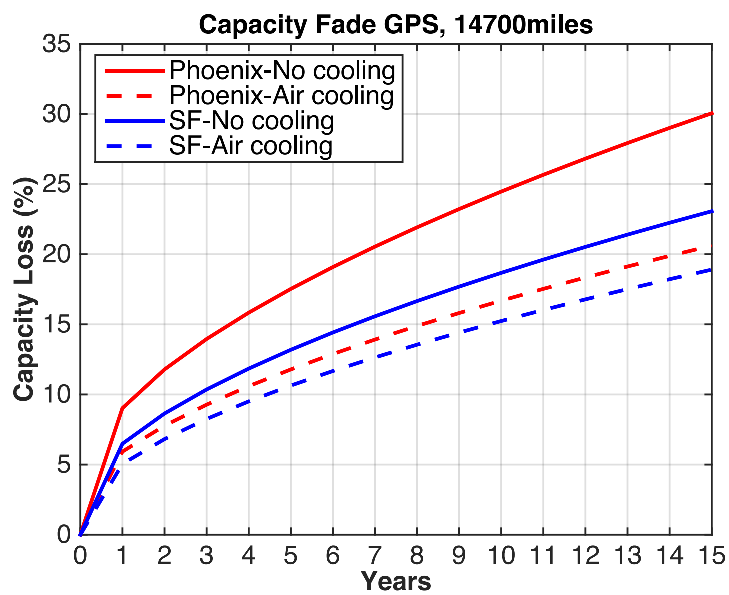

Figure 2.16 Capacity Fade in Phoenix and San Francisco, using GPS data with annual miles driven 14,700miles. The comparison of air-cooling vs. no cooling is provided for two cities

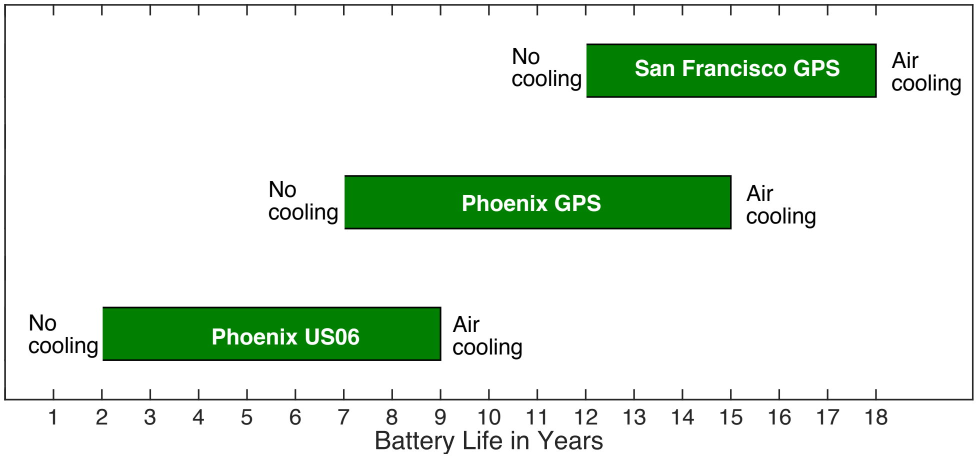

Figure 2.17 Improvement in battery life by air-cooling for different cases simulated. For all simulations, the annual miles driven=14,700 miles**.** US06 simulations were performed using Approach 1.

2.4.5 Battery End of Life Criteria

For all the results discussed so far, battery end-of-life (EOL) is assumed to be when battery loses 20% of its capacity. However, individual drivers might continue using their vehicles after this threshold. As an example, if the battery end-of-life is set to be at 30% capacity loss, in most of the cases battery life will be longer than 15 years.

The change of battery life under various cases compared to base case simulation in Phoenix is summarized in Figure 2.18. In addition, Figure 2.19 shows the comparison of different cases which were simulated with a US06 drive cycle.

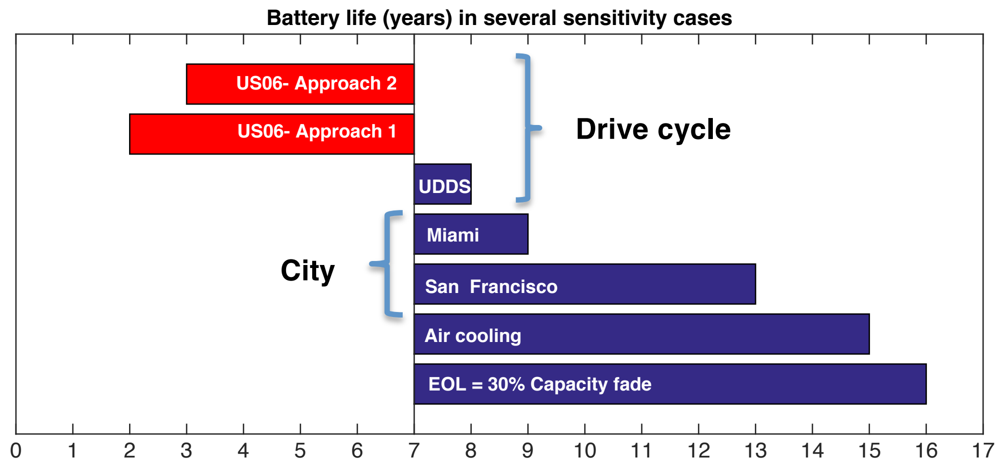

Figure 2.18 Comparison of battery life for various cases simulated. Vertical line presents the base case where; city: Phoenix, drive cyle: GPS, thermal management: none, annual miles driven=12,400 miles, battery EOL: at 20% capacity fade

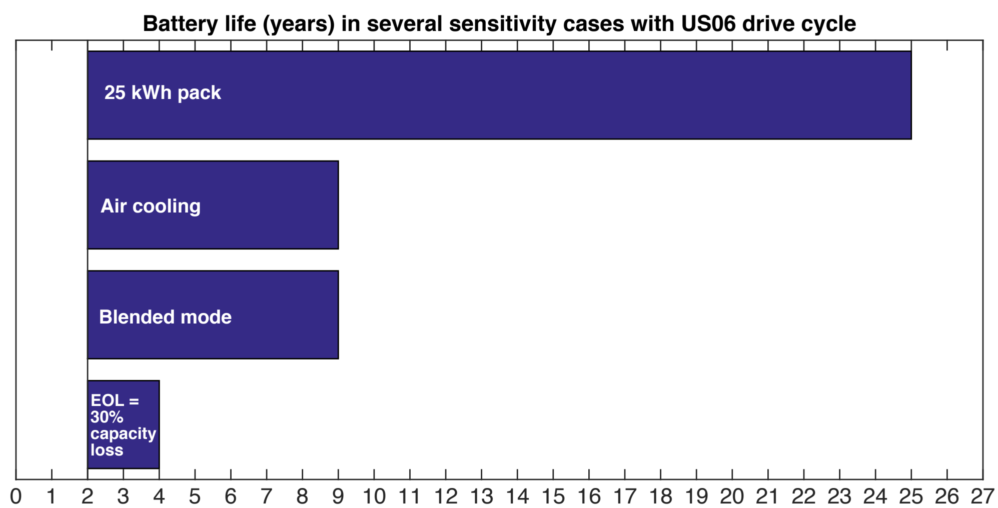

Figure 2.19 Battery life comparison change for US06 cases simulated at 14,700 miles. Vertical line presents the base case where; city: Phoenix, thermal management: none, battery EOL: at 20% capacity fade

2.5 Limitations

This study presents a comprehensive model and analysis to investigate battery life implications in PHEVs. However, several limitations in the models and simulations should be understood when interpreting our results:

Driving data. We use GPS data from Atlanta region for our base case, and assume they are representative for the whole country. However, regional variances in driving profiles can lead to different degradation profiles, which we don't consider in this study.

Battery modeling. We use an ECM parameters of which were obtained by regression based on low C-rate constant current charge/discharge tests. We assume this model can be applied for dynamic current profiles that are experienced in this study. In addition, it is not clear if the ECM can predict battery behavior at high C-rates accurately. We neglect this issue and assume the model can predict battery electrical behavior in all cases.

Thermal model. Although the thermal network model used in this study is developed based on testing a static vehicle, we assume it can be applicable in the case of a vehicle in motion. During driving, the movement of the air over the car would change the heat transfer characteristics. This is neglected. In addition, we only consider ohmic losses to model heat generation, and disregard any thermodynamic effects in heat generation. Further investigation is necessary to understand the effect of this assumption. For air-cooling, we consider a fan with a single level of cooling only and we assume airflow rate does not change. A fan with more stages can improve the cooling characteristics. Also, for cabin heating, we assume the heater will consume 4kW power, which might be larger than the typical heater power consumption in PHEVs [77].

Battery degradation modeling. The limitations of using the assumed degradation model are explained in the corresponding section (2.2.8) and won't be repeated here. To summarize, the lack of data that fully covers all aspects of degradation can result in inaccuracies in the degradation estimates.

Cold temperature effect. We don't consider any cities with extreme cold temperatures, although cold temperatures affect vehicle and battery performance. Cold temperatures can also trigger different degradation mechanisms in the battery. We don't address this issue, mainly because there is not enough data at cold temperatures for degradation modeling.

2.6 Conclusion and Future Work

We develop a comprehensive model and simulate various usage and storage scenarios to examine the battery life implications in PHEVs. Due to various uncertainties in the model described in the previous sections, we don't expect that we can predict battery life exactly, but nevertheless the model can provide initial indications of the factors that have the largest influences on battery life. Performing various simulations, we show that, battery degradation can change significantly based on drive cycle, region and thermal management. Battery life will also strongly depend on how battery end of life is defined.

There are various assumptions made in modeling and simulations, and the sensitivity of the results to these assumptions should be tested. Table 2.7 summarizes these sensitivity cases that should be addressed in future work.

Table 2.7 Sensitivity Analysis for Future Work

Sensitivity Case	Change from Base Case	Purpose
Thermal Management	Air-cooling where the fan has three stages with different on-off temperature thresholds and air-flow	Test importance of thermal management control strategy
Cabin thermal control	Assume a single constant power consumption that does not change with cabin temperature	Test the importance of HVAC use in regional temperature effects of battery life
Degradation Model	Use another set of literature data	Test importance of degradation data and model on battery life
Temperature Resolution	Use daily average ambient temperatures instead of hourly temperatures	Test importance of ambient temperature fluctuations

3 Effects of Regional Temperature on Electric Vehicle Efficiency, Range and Emissions in the United States

The efficiency of vehicles varies with ambient temperature due to changes in vehicle efficiency and extra usage of cabin climate control. This effect, however, is particularly important in BEVs since reduced efficiency will result in shorter range, and there is no other propelling device to compensate for it. This chapter therefore focuses on characterizing the effect of regional temperature differences on battery electric vehicle (BEV) efficiency, range, and use-phase CO_2 emissions in the U.S. Results indicate that annual energy consumption of BEVs can increase by an average of 15% in the Upper Midwest or in the Southwest compared to the Pacific Coast due to temperature differences. Greenhouse gas (GHG) emissions from EVs vary primarily with marginal regional grid mix – which has twice the GHG-intensity in the Upper Midwest as on the Pacific Coast. However, even within a grid region, BEV emissions vary by up to 22% due to spatial and temporal ambient temperature variation and its implications for vehicle efficiency and charging duration and timing. Cold climate regions also encounter days with substantial reduction in EV range: the average range of a Nissan Leaf on the coldest day of the year drops from 70 miles on the Pacific Coast to less than 45 miles in the Upper Midwest. These regional differences are large enough to affect adoption patterns and energy and environmental implications of BEVs relative to alternatives.

The study presented in this chapter has appeared in Environmental Science and Technology [78].

3.1 Introduction

The transportation sector is responsible for 32% of U.S. CO_2 emissions and 28% of U.S. greenhouse gas emissions [3]. In addition, 70% of U.S. petroleum demand is consumed by the transportation sector [4]. Battery electric vehicles (BEVs), which are powered by electricity alone, have potential to reduce transportation related greenhouse gas emissions as well as petroleum consumption by replacing gasoline with electricity as energy source. However, there are some barriers to large-scale adoption of these vehicles. Range anxiety is a key factor affecting consumer willingness to adopt electrified vehicles [6,7]. The driving range of a BEV depends on the energy capacity of the battery and vehicle efficiency, which are affected by design characteristics as well as some use phase factors, such as driving conditions [57],[79] and temperature [24].

Battery performance depends strongly on temperature. At cold temperatures, battery efficiency, discharge capability and available energy decreases. In addition, battery internal resistance increases, decreasing the power that can be drawn from the battery. Battery performance increases with temperature rise, but batteries also degrade faster at high temperatures[80], increasing thermal management requirements.

Ambient temperature determines initial battery temperature and thermal management loading (if the vehicle is parked outside, the battery is not thermally preconditioned, and solar radiation is negligible) as well as battery temperature and thermal management load during use. Weather conditions, therefore, have a direct impact on battery efficiency. Ambient temperature also drives use of cabin air conditioning to either heat or cool the cabin at cold and hot days respectively [55,81]. The net effect of these factors causes customers to report up to 40% decrease in their driving range on cold winter and/or hot summer days compared to the maximum range they achieve [24]. The cold temperature effect is generally larger for two main reasons: electric cabin heating consumes more power compared to cooling [77], and batteries have poorer performance at low temperatures.

Air conditioning (A/C) use during hot days is an important factor affecting the fuel economy in all types of vehicles, since A/C is the largest auxiliary load in many vehicles [82]. Cold temperatures, on the other hand, are particularly disadvantageous for BEVs, since vehicles with internal combustion engines can use engine waste heat for cabin heating, whereas in BEVs heat must be generated using limited onboard stored electrical energy. Reduced efficiency results in increased energy consumption and increased emissions from the electricity grid when BEVs charge[5,83]. The net effect on emissions varies across the country due to source of electricity generation[84] as well as the regional differences in marginal electricity grid mix[85].

Prior studies investigating the regional differences in energy consumption and emissions of electrified vehicles do not account for efficiency losses with temperature change: A 2012 report by Union of Concerned Scientists (UCS) investigates the GHG emissions of gasoline vehicles, gasoline hybrid electric vehicles (HEVs), plug-in hybrid electric vehicles (PHEVs) and BEVs in different regions of the US using constant efficiency assumptions and average electricity generation emissions in each eGRID subregion [86]. They find that in certain regions like Colorado, some HEVs have lower use-phase emissions than BEVs. Another report by Climate Central performs a similar analysis but also includes the carbon emissions from vehicle manufacturing and uses average emissions factors for electricity generation by state [87]. They conclude that in 40 states a high-efficiency hybrid vehicle like the Toyota Prius is better for the climate, and in 10 states a gasoline-powered car is the best due to the electricity generation source being dirty. However, Graff Zivin et al. (2014) point out that such average emissions factors are not appropriate for estimating the net effect of new electric vehicle load due to differences between average and marginal generation mix and substantial trade among regions. They estimate marginal emission factors in each of the eight North American Electric Reliability Corporation (NERC) regions and use results to evaluate emissions of a Chevy Volt type plug-in hybrid electric vehicle.[85] They find that in some regions, such as upper Midwest, charging from midnight to 4 am will generate more CO_2 emissions than even an average gasoline vehicle. Tamayao[88] uses the marginal emission factors proposed by Zivin et al and by Siler-Evans et al. [89] to compare various gasoline and electrified vehicle types while accounting for regional driving patterns. She finds that today's BEVs and PHEVs reduce greenhouse gas (GHG) emissions relative to their gasoline counterparts in most urban regions, but they may increase GHG emissions in the Northern Midwest, and the comparison is inconclusive in much of the country due to uncertainty in marginal grid mix estimates.

All of the analyses mentioned above assume constant efficiency for each of the vehicles they analyze, and none of them consider the ambient temperature effect. Neubauer and Wood analyze the impact of various factors, including climate, on electric vehicle miles travelled [55]. They use a vehicle performance model to estimate the change of vehicle efficiency with temperature by including a temperature dependent battery internal resistance term in their model, and they perform the analysis at three selected locations with different climates: hot, cold and mild. Their battery model (based on a nickel manganese cobalt oxide (NCA) Li-ion battery) suggests that battery resistance effects are negligible in their case, but cabin thermal conditioning can increase the per mile energy consumption by 24% percent in cold climates compared to the case when there is no heating or cooling. Kambly and Bradley also show that heating, ventilation, and air conditioning (HVAC) systems can decrease BEV range depending on the region and time of day[81,90]. Their analyses, based on a thermal comfort model of a hypothetical BEV, suggest that the vehicle range is lowest at noon when the solar load is highest, and thermally preconditioning the cabin before the trip can improve range by about 10%[90]. According to their estimates, annual HVAC energy consumption is 50% higher in Arizona than in West Virginia[81].

To the authors' knowledge, there is no study focusing on the regional benefits of BEVs due to spatial and temporal ambient temperature differences. The studies investigating regional emissions do not include the effect of ambient temperature in their analysis, and studies that examine the effect of climate do not assess regional environmental benefits. We aim to fill this gap in the literature. In this paper, we quantify the variance in driving range, electricity consumption and related emissions due to regional ambient temperature using real world energy efficiency, climate, and driving pattern data. In the following sections the data used in the analysis are introduced; the analysis method is described; results of the regional analyses are presented; and a discussion of comparisons between different regions is provided.

3.2 Data and Analysis

To estimate regional effects of temperature on electric vehicle efficiency, range and emissions, we construct models of vehicle energy consumption vs. temperature; U.S. temporal and spatial temperature variation, vehicle driving and charging patterns; and U.S. regional grid emission factors. In the following sections, we explain the data used for each aspect and our analysis approach.

3.2.1 Energy Consumption Versus Temperature

To find a relationship between energy consumption and ambient temperature we use the publicly available data collected by Canadian company FleetCarma [24]. FleetCarma provides vehicle monitoring services for fleet owners, and they collect and analyze vehicle data to determine performance under various conditions. We adopt the aggregated results from Nissan Leaf users for more than 7000 trips across North America reported as average driving range versus ambient temperature. The use of these real world data has two key advantages over the prior literature: (1) our results are based on results experienced by real drivers in actual driving conditions instead of simulation models, and (2) we include the net effect of both cabin conditioning and battery efficiency implications of ambient temperature in the analysis (as well as any other factors that may vary with temperature, such as road and driving conditions). Although these data were collected from locations across North America, we use only information about the average effect of temperature on vehicle efficiency in order to isolate the temperature effect from other location-specific factors, such as driving conditions. We convert range to energy consumption using the Nissan Leaf usable battery capacity of 21 kWh [91] applied to every data point provided in the FleetCarma dataset, and we obtain new data points for energy consumption, as given in Figure 3.1. We then fit a curve to these new data points by least squares regression using the lowest order polynomial that follows the trend of the data qualitatively and we obtain a generic functional relationship between the vehicle energy consumption per unit distance c and ambient temperature T as:

$$c(T) = \left(\sum_{n=0}^{5} a_n T^n \right) \tag{3.1}$$

where a_n's are the coefficients of the polynomial given in Wh/mi/°F^n

$$a = [0.3950 \quad -0.0022 \quad 9.1978e-05 \quad -3.9249e-06 \quad 5.2918e-08 \quad -2.0659e-10]$$

3.2.2 Spatial and Temporal Temperature Data

We use Typical Meteorological Year (TMY) Database from the National Renewable Energy Laboratory (NREL)[76] to obtain time- and location-dependent ambient temperature data. The latest database, TMY3, provides hourly values of meteorological data, including ambient temperature. These data are given for 1020 different locations in United States[92], including Guam, Puerto Rico, and US Virgin Islands, but we filter the data and exclude the latter regions, which reduces the total number of locations in our study to 1011. The temperature data in this database represent typical hourly temperatures rather than extreme cases, based on 1976 to 2005 records wherever available, and 1991-2005 records for other locations.

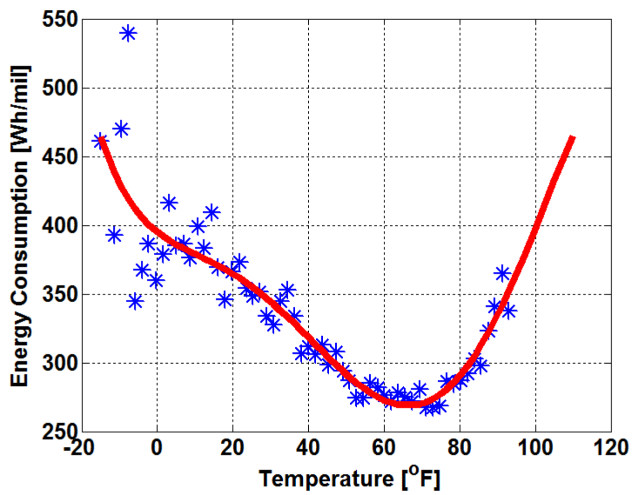

Figure 3.1 Nissan Leaf energy consumption per mile versus ambient temperature. The blue stars correspond to data points obtained by converting FleetCarma range data to energy consumption. The red curve is the polynomial fit given by Equation (3.1).

3.2.3 Driving and Charging Patterns

To obtain driving patterns, we use the National Household Travel Survey (NHTS) 2009 dataset [93]. NHTS is conducted by US Department of Transportation and is an inventory for daily household travel. It contains information on all kinds of transportation activity of a household, including walking, public transport, biking, etc. To obtain a subset of data for the purposes of this study, we filter this dataset to obtain the trips completed by private light-duty vehicles only. We also exclude the data points that are reported by the members of the household other than the driver to avoid counting the same trip by the same vehicle more than once. This reduces the total number of vehicles we include in the analysis to 87,777. The NHTS dataset has only one day of data for each vehicle. Therefore, NHTS does not provide information on day-to-day variability for a single vehicle. By averaging over each driving profile and each day of the year, we thus estimate fleet average effects, and individual vehicle owners may experience higher or lower efficiency in a given climate. In addition, we treat the full distribution of driving patterns in the NHTS data as representative of every location in the country, and we ignore any systematic regional variation in daily driving patterns in order to isolate the effect of temperature.

The data set provides start time, end time, and distance of every trip made by each vehicle on the day surveyed. We use this information to determine what time of the day and how far the vehicle is driven, and we assume charging begins upon arrival at home after the last trip of each day and continues until the battery is fully charged.

3.2.4 Grid Emission Factors

To estimate the grid emissions related to increased load with BEV electricity consumption, we need to know the marginal emissions from the power plants that are utilized to meet the extra demand. The mix of the power plants that operate on the margin, and the resulting emissions, show significant variation across regions[85,89]. Graff Zivin et al [85] estimate the marginal CO_2 emission factors by regressing the emissions in the corresponding interconnect as function of electricity consumption in each NERC region. In our analysis, we use their expected values of the seasonal time of day marginal emission factors (MEFs) for each NERC region (see supporting information). Since estimates of day to day variation of MEFs within one season are not available, we use the same MEFs for each day of the season. These MEFs estimate power plant emissions and exclude upstream emissions from feedstock supply.

3.2.5 Analysis

We start our analysis by estimating energy consumption per mile traveled every day and every hour at each location provided in the TMY3 dataset and for each vehicle driving profile in the data obtained from NHTS using the temperature-efficiency relationship extracted from the FleetCarma data. In this calculation, we apply some boundaries to the temperature values that can be used in the computation. The lower bound is equal to the minimum temperature recorded in the FleetCarma dataset. For the upper bound (i.e. high temperatures), we extrapolate the curve to the point at which the energy consumption is equal to the maximum value recorded, as shown with the curve fit in Figure 3.1.b. This results in the lower and upper ambient temperature boundaries of -15oF and 110oF, respectively. The extrapolation is necessary for fair comparison of hot vs. cold regions. The regional hourly electricity consumption per distance traveled can thus be estimated for each vehicle as follows:

$$c_{ldh}^{\text{HOUR}} = \begin{cases} \sum_{n=0}^{5} a_n \cdot (T_{ldh})^n, & -15^oF < T_{ldh} < 110°F \\ \sum_{n=0}^{5} a_n \cdot (-15)^n, & T_{ldh} \leq -15°F \\ \sum_{n=0}^{5} a_n \cdot (110)^n, & T_{ldh} \geq 110°F \end{cases} \tag{3.2}$$

where c_{ldh}^{HOUR} is the Nissan Leaf's electricity consumption per unit distance (Wh/mi) and T_{ldh} is the ambient temperature ($°F$) at location $l \in \{1,2,\dots,N_{\text{L}}\}$ day $d \in \{1,2,\dots,N_{\text{D}}\}$ and hour $h \in \{1,2,\dots,N_{\text{H}}\}$, where $N_{\text{L}} = 1011, N_{\text{D}} = 365, N_{\text{H}} = 24$. In our base case, whenever the temperature is lower or higher than the given boundaries, we assume the energy consumption will be equal to the value calculated at the boundaries.

To estimate the daily average electricity consumption per mile, we need to know how much each vehicle is driven at each hour of the day. We estimate this using the national driving patterns from the NHTS dataset. For all the vehicles in the subset of data we are using, we distribute the driving durations into hourly bins throughout the day by looking at the start and end time of each trip, and we compute Δ_{hv}^{DRV}, the amount of time (hours) each vehicle driving profile $v \in \{1,2,\dots,N_{\text{V}}\}$ spent driving during the corresponding one hour bin h (where $N_{\text{V}} = 87{,}777$ vehicle driving profiles):

$$\Delta_{hv}^{\text{DRV}} = \sum_{\tau \in \mathrm{T}_v} \begin{cases} 1 & \text{if } t_\tau^{\text{S}} \leq h-1 \text{ and } t_\tau^{\text{E}} \geq h \\ 0 & \text{if } t_\tau^{\text{S}} \geq h \text{ or } t_\tau^{\text{E}} \leq h-1 \\ \min(h, t_\tau^{\text{E}}) - \max(h-1, t_\tau^{\text{S}}) & \text{otherwise} \end{cases} \tag{3.3}$$

where t_τ^{S} and t_τ^{E} are the start and end times of each trip τ, respectively, and T_v is the set of trips for vehicle profile v in the data set.

We then use Δ_{hv}^{DRV} to obtain weighted daily average energy consumption per unit distance for each vehicle driving pattern v as follows:

$$c_{ldv}^{\mathrm{VEH}} = \frac{\sum_h \Delta_{hv}^{\mathrm{DRV}} c_{ldh}^{\mathrm{HOUR}}}{\sum_h \Delta_{hv}^{\mathrm{DRV}}}, \qquad \begin{array}{c} l = 1,2,..,N_{\mathrm{L}} \\ d = 1,2,..,N_{\mathrm{D}} \end{array} \tag{3.4}$$

where c_{ldv}^{VEH} is the daily average energy consumption per mile for vehicle driving profile v in location l and at day d (in Wh/mi).

The expected daily range in each region can be found by first calculating the range for each vehicle driving profile and then averaging over all the profiles in the dataset.

$$s_{ld} = \frac{1}{N_{\mathrm{V}}} \sum_{\mathrm{v}} \frac{C^{\mathrm{BAT}}}{c_{ldv}^{\mathrm{VEH}}} \tag{3.5}$$

where s_{ld} is the regional expected daily range averaged over all vehicles used in the analysis and C^{BAT} is the battery usable energy capacity, taken as 21 kWh for Nissan Leaf battery [91].

The distance driven by each vehicle profile on each day in each location is computed as

$$s_{ldv} = \min\left(s_v^{\mathrm{NHTS}}, \frac{C^{\mathrm{BAT}}}{c_{ldv}^{\mathrm{VEH}}}\right) \tag{3.6}$$

where s_v^{NHTS} is the distance traveled by vehicle driving profile v in the NHTS dataset. Here we assume that if the distance driven in a vehicle profile is longer than the all-electric range (AER) of the vehicle, the vehicle shortens travel on those days. We test robustness via sensitivity cases that include a larger battery (to reduce truncated trips) and a slower recharging rate (to shift charge timing).

The regional average electricity consumption per mile c_l^{REG} averaged over all vehicles and days of the year, can then be estimated as:

$$c_l^{\mathrm{REG}} = \frac{\sum_v \sum_d s_{ldv} c_{ldv}^{\mathrm{VEH}}}{\sum_v \sum_d s_{ldv}} \tag{3.7}$$

Greenhouse gas emissions vary depending on charge timing. We first determine the total charging duration for each vehicle as:

$$t_{ldv} = \frac{s_{ldv} c_{ldv}^{\mathrm{VEH}}}{r} \tag{3.8}$$

where s_{ldv} is total daily distance traveled by vehicle profile v, t_{ldv} is the total charging duration in hours, r is the constant battery charging rate, which is 6.6 kW for Nissan Leaf battery[94]. Then we distribute the total charging duration into hourly bins assuming charging starts right after the last trip of the day ends

$$\Delta_{ldhv}^{\mathrm{CHG}} = \sum_{\tau \in L_v} \begin{cases} 1 & \text{if } t_\tau^{\mathrm{E}} \leq h-1 \text{ and } t_\tau^{\mathrm{E}} + t_{ldv} \geq h \\ 0 & \text{if } t_\tau^{\mathrm{E}} \geq h \text{ or } t_\tau^{\mathrm{E}} + t_{ldv} \leq h-1 \\ \min(h, t_\tau^{\mathrm{E}} + t_{ldv}) - \max(h-1, t_\tau^{\mathrm{E}}) & \text{otherwise} \end{cases} \tag{3.9}$$

where L_v is the last trip of the day for vehicle profile v, and we obtain $\Delta_{ldhv}^{\mathrm{CHG}}$ which gives the charging duration that falls into hourly bin h. Using this information, CO_2 emissions can be estimated as:

$$\Gamma_{ldhv} = \frac{r \Delta_{ldhv}^{\mathrm{CHG}} M_{ldh}^{\mathrm{MEF}}}{\eta}, \qquad v = 1, .., N_{\mathrm{V}} \tag{3.10}$$

where Γ_{ldhv} is the CO_2 emissions in grams from charging vehicle v at hour h of day d in location l, M_{ldh}^{MEF} is the expected value of the regional seasonal time of day marginal emission factors in grams/kWh, and η is the charging efficiency taken as 87%[95]. Note that, 87% represents the on-board charger + electric vehicle supply equipment (EVSE) efficiency. In other words, 87% of the energy delivered from grid is can be charged into battery. We neglect any losses that might occur between the onboard charger and the battery, therefore the efficiency value used here does not affect charging duration. We account here only for power plant emissions and ignore upstream emissions associated with feedstock supply.

Regional average CO_2 emissions in grams/mile, γ_l, (averaged over all vehicle profiles and days of the year) are then found by:

$$\gamma_l = \frac{\sum_d \sum_h \sum_v \Gamma_{ldhv}}{\sum_v \sum_d s_{ldv}} \tag{3.11}$$

3.3 Results And Discussion

The variation of daily average driving range in selected cities is shown in

Figure **3.2**. In three of the cities, the median of the daily averages is around 70 miles (112 km). In San Francisco the median is 76 miles (122 km) and the driving range is greater than 70 miles 99% of the time. As the location changes to cities where more hot or cold extremes might be observed, we see a wider spread of vehicle range throughout the year. In Phoenix, where the daily average temperature can be as high as 105^{o}F (41^{o}C), the range can drop as low as 49 miles (78 km) – a 29% decrease from the median value of 69 miles (111 km). In cold climates, such as Rochester, MN, the decrease in the range compared to the median can be as high as 36%.

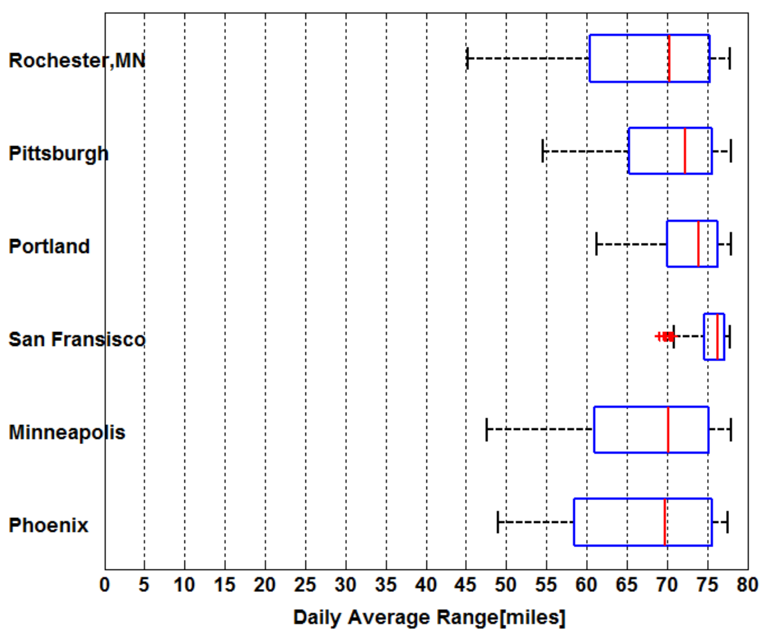

Figure 3.2 Box plot of daily driving range distributions for selected cities. Red lines indicate median range; blue boxes capture the 2nd and 3rd quartiles across days of the year, the whiskers

extend to the most extreme data points that are not considered outliers, and the red + symbols indicate outlier days.

As mentioned before, the temperature limits used in computations are -15 and 110°F (-26 and 43°C), and we do not know exactly how the range or vehicle efficiency changes in excess of these values. In **Figure 3.3** the locations where the temperature is outside the limits at least one hour on the worst day of the year are marked, indicating that actual range on the worst day of the year may be lower than estimated here. For comparison, we also make the same calculation by extrapolating the curve for a wider range of temperature values in the supporting information, and overall trends are robust.

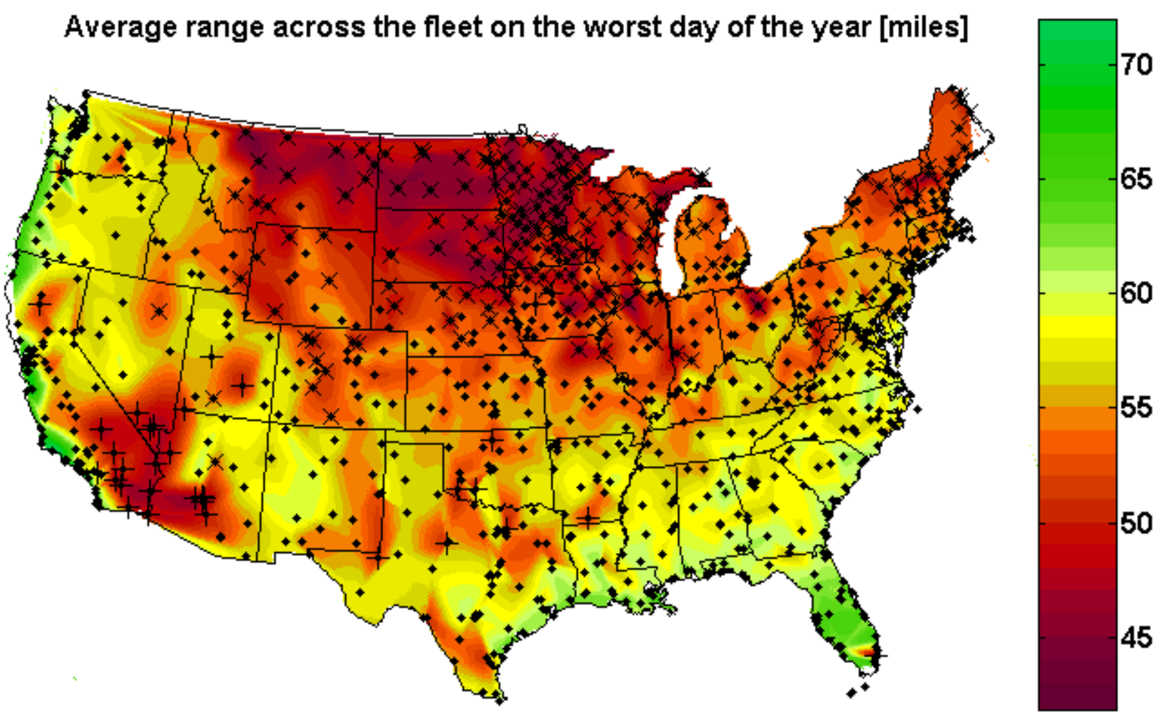

Figure 3.3 Average range across the fleet on the worst day of the year (day with the lowest predicted EV range). In the figure, dots (•) represent the locations given in the TMY3 dataset, crosses (×) represent locations with temperatures colder than the minimum data point at least one time during the year, and plus signs (+) represent locations with temperature warmer than our imposed upper limit of extrapolation at least one time during the year.

Similar to the change in driving range, Figure 3.4 shows that the average energy consumption per mile can increase by 15% from 273 Wh/mi (170 Wh/km) along Pacific Coast or at certain parts of South Florida to 315 Wh/mi (196 Wh/km) in the Upper Midwest. It is also possible to observe that the energy consumption can vary inside the same state because of the temperature differences of different locations. In Southeast California, the average energy consumption is 323 Wh/mi (201 Wh/km), 18% higher than the coast.

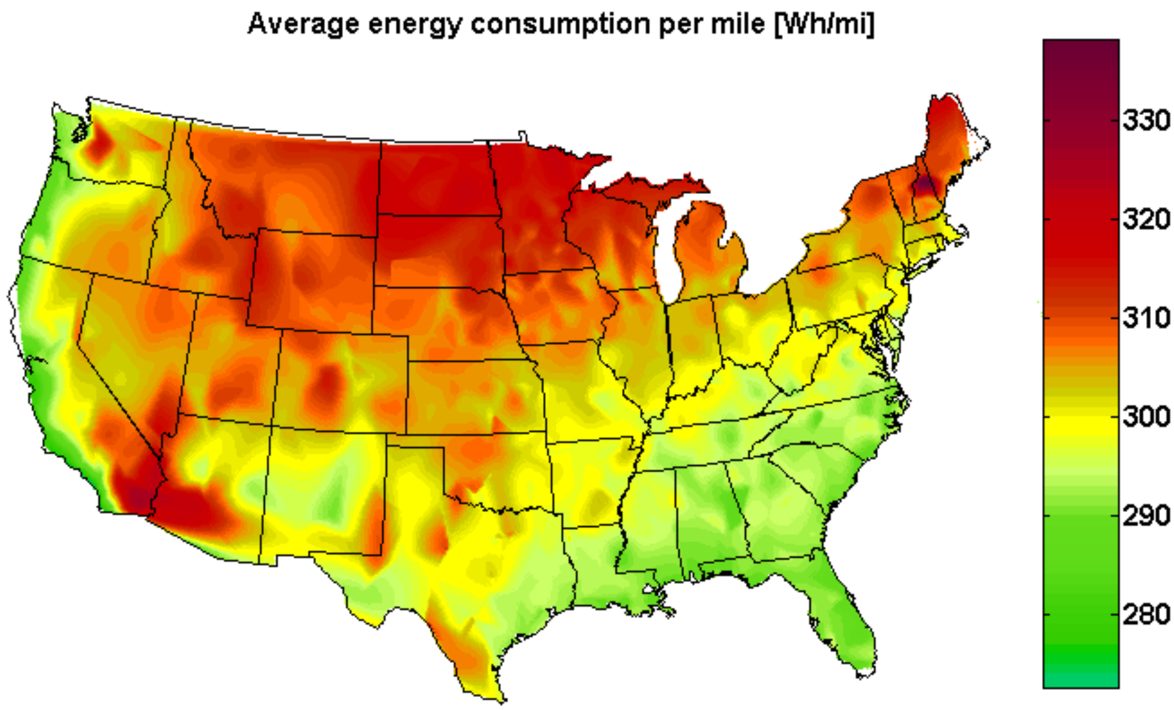

Figure 3.4 Energy consumption per mile averaged across the fleet over a full year (Wh/mi)

As depicted in Figure 3.5, the most significant factor affecting the regional differences in emissions is the grid mix. The worst region in terms of CO2 emissions is MRO, where both the marginal emission factors and the energy consumption per mile are high. WECC, with the cleanest grid, has the lowest emissions – especially on the coast where energy consumption is lowest. When the mean value of average emissions in MRO is compared to the mean value in WECC, there is a 186% increase due primarily to grid mix. Within the WECC region, the emission rates can increase from 100 g/mi(62 g/km)up to 122 g/mi (76 g/km), a 22% increase inside the same NERC region due to ambient temperature. Note that this happens mainly because of two reasons: energy consumption changes with temperature, but also as energy consumption changes so does the charging duration. This creates an impact on emissions, too, since marginal emission factors vary depending on the time of the day when the vehicle is being charged. For reference, tailpipe CO_2 emissions for a Toyota Prius hybrid electric vehicle is reported as 179 g/mi (111 g/km)[96]; however, gasoline vehicle emissions rates also vary with temperature.

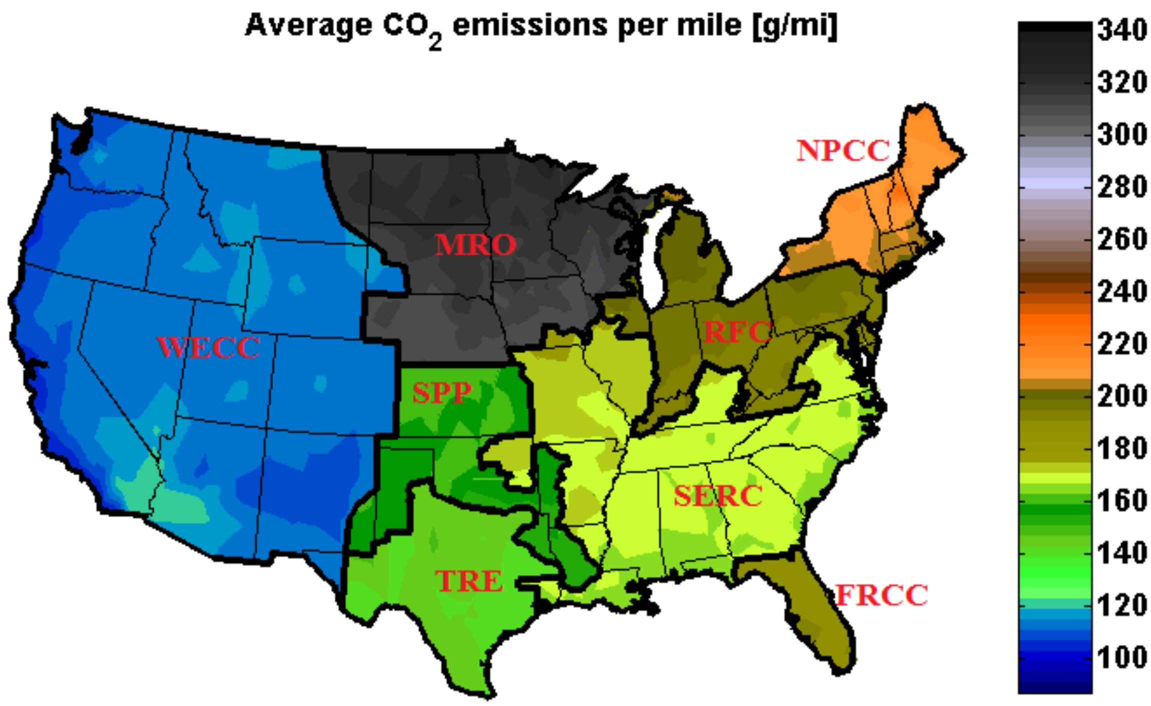

Figure 3.5 CO_2 emissions per mile in eight NERC regions averaged across the fleet and over the year (g/mi)

Since the main source of difference in the regional emissions is the grid mix, as the grid becomes cleaner for most of the country, as targeted by the Environmental Protection Agency's Clean Power Plan [97] , the impact of location on the environmental benefits of electric vehicles will be reduced. However ambient temperature will remain a source of variation in EV benefits across the US.

To see the sensitivity of these results to some of our assumptions, such as battery capacity and charging rate, we run two other cases: 1) with an increased battery capacity of 85 kWh and 2) with a lower charge rate of 3.3 kW. Both of these assumptions can change emissions estimates up to 4%. Details are available in the Supporting Information.

3.4 Limitations and Assumptions

In this study, we use data only for a particular electric vehicle, the Nissan Leaf. Other electric vehicles differ in vehicle efficiency, HVAC efficiency, battery technology, and thermal management and may therefore have different temperature-specific range and emissions implications. Nevertheless, the trends observed here are fairly general because 1) heater and A/C use increases BEV energy consumption, and 2) electrochemical reactions in batteries are temperature dependent. With improvements in battery technology and with the use of more energy efficient vehicle thermal conditioning systems, it might be possible to see a reduced effect of ambient temperature in the future.

The driving range versus temperature dataset we use in this study is collected from real world trips. It therefore contains some effects due to different driving styles, trip conditions such as congestion on the road, driver preferences on climate control, vehicle differences such as the model year, and other weather elements, such as precipitation and humidity. We attribute the entire efficiency effect to temperature, which could introduce bias if temperature is correlated but not perfectly correlated with these other factors. In addition, the FleetCarma dataset reports average driving range observed across the fleet. Therefore, the results shown in Figure 2 do not show the worst range that can be experienced but rather the fleet average range on the worst day of the year. Some drivers may experience shorter range. In particular, the Nissan Leaf drivers observed in the data are early adopters and may have different behaviors than mainstream consumers (for example, with respect to HVAC use or driving style). Also, we assume the range at temperatures below -15°F or above 110°F are equal to the estimated range at the corresponding limit. The results using extended extrapolation are also provided in the supporting information, resulting in similar trends but increased magnitude in the hottest and coldest regions.

The NHTS dataset provides information on the trips taken by each surveyed U.S. vehicle on a single survey day and does not include day to day variability for each vehicle. In this study we average over the vehicle profiles to assess implications for average driving distances and assume these daily distances are identical spatially and seasonally. Individual drivers may experience different range and efficiency, and any correlations between driving distance and location or weather could influence results.

We only consider convenience charging in this study. However, time of charging could have a significant effect on emissions. For example, delayed nighttime charging may avoid adding demand during peak times and reduce costs while increasing marginal emission rates in many areas because coal fired power plants tend to be on the margin at times of low demand[85]. In addition, we assume charging rate is constant during charging, and we neglect the effect of temperature on charging efficiency and duration.

Finally, we use point estimates for marginal emission factors and for the curve fit in Equation (3.1). Uncertainty in marginal emission factors and vehicle efficiency implies uncertainty in implications of electric vehicle charging. Further, we attribute the estimated marginal emissions within each NERC region to every location in that NERC region. In practice, marginal emissions vary by location within each NERC region, but due to substantial interregional trade, differences of marginal emission rates at sub-NERC-region resolution are not known. Large penetration of electric vehicles could also have grid effects that are beyond marginal. Additionally, we estimate only power plant emissions associated with electric vehicle charging and do not consider the full life cycle (e.g.: including upstream emissions from feedstock supply or temperature-specific repair and maintenance), and we characterize only CO^2 emissions and do not estimate implications of other air emissions from electric vehicle charging.

4 Variation of Electric Vehicle Life Cycle Greenhouse Gas Reduction Potential across U.S. Counties due to Regional Electricity Sources, Driving Patterns, and Climate

Chapter 3 focused on examining the effect of regional temperature differences on BEV efficiency and emissions, and showed that the effect can be large enough to affect environmental implications of BEVs relative to alternatives. This chapter aims to investigate this further and expands the focus by considering various other regional factors and vehicle technologies. The differences in life cycle greenhouse gas (GHG) emissions of gasoline and plug-in vehicles across U.S. counties are characterized by accounting for heterogeneity due to regional marginal grid mix, ambient temperature, patterns of vehicle miles traveled, and assumed driving conditions (city vs. highway). The potential of plug-in vehicles to decrease transportation related CO_2 emissions depends strongly on the region and vehicle type. Results indicate that PEV benefits vary substantially by vehicle model and region: The Nissan Leaf battery electric vehicle creates lower GHG emissions than the most efficient gasoline vehicle (the Toyota Prius) in Texas, Florida, the southwestern US, and urban counties of the western US and New England; whereas the Leaf has higher emissions in most of the rest of the country, especially the Midwest and the South. The Chevrolet Volt plug-in hybrid electric vehicle has higher emissions than the Prius everywhere, though both vehicles are lower emitting than most other vehicles. Regional grid mix, temperature, driving patterns, and vehicle model all have significant implications on the relative benefits of PEVs versus gasoline vehicles.

This study is a working paper with coauthors Mili-Ann M. Tamayao, Chris Hendrickson, Ines Azevedo, and Jeremy J. Michalek [98].

4.1 Introduction

The greenhouse gas (GHG) emissions implications of plug-in electric vehicles (PEVs) vary regionally in the United States. Table 4.1 summarizes studies that aim to characterize regional differences and their assumptions about life cycle scope, electricity grid emissions, driving patterns, and climate:

- **Life Cycle:** While some studies use a life cycle scope that includes vehicle and battery manufacturing; petroleum extraction, processing, transportation, and combustion; power plant and fuel feedstock production and transportation; and end of life emissions, several examine only use-phase or only tailpipe and power plant emissions, making incomplete comparisons of emissions implications among alternative vehicle technologies. Several life cycle suggest that emissions implications from sources other than tailpipe and power plant emissions can comprise more than one third of life cycle GHG implications.
- **Electricity Grid:** Critical to assessing life cycle emissions of PEVs is the mix of electricity sources used to generate electricity to charge the vehicle. While early studies used an attributional approach, assigning to the PEV the average emission rates for power plants in the same state or power grid region where it is charged, recent studies have taken a consequential scope, estimating the change in grid emissions resulting from new PEV charging in a region. Tamayao et al. (2015) show that differences between average vs. marginal emissions can affect whether PEVs are estimated to be higher or lower emitting than efficient gasoline vehicle models [99].
- **Driving Patterns:** Most regional US PEV GHG studies ignore regional differences in driving distance distributions and driving conditions that affect vehicle efficiency. Karabasoglu and Michalek show that driving conditions (drive cycle) can affect economic and environmental benefits of electrified vehicles substantially[79].
- **Climate:** Most regional US PEV GHG studies ignore the effect of regional temperature. But regional temperature has a significant effect on vehicle efficiency due to heating, ventilation, and air conditioning (HVAC) use and temperature-related battery efficiency effects. Compared to mild climate tests without HVAC use, Yuksel and Michalek [78] estimate that BEVs can consume an average of 15% more energy in hot and cold regions of the US; Neubauer and Wood [100] estimate that HVAC use can increase energy consumption by 24% in cold climates; Kambly and Bradley [81,90] note that HVAC use can decrease BEV range depending on the region and time of day; and Meyer et al.[101] observe a 60% drop in range in -20^{o}C lab tests with maximum climate control use.

Despite interest in understanding regional variation of life cycle PEV GHG emissions, no study has accounted for regional differences in consequential grid emissions, driving patterns, and climate to assess regionally-specific life cycle implications of PEVs in the U.S. We construct a model to integrate these effects with a comprehensive life cycle scope to characterize regional differences in PEV GHG benefits relative to gasoline vehicles.

Table 4.1 Studies that characterize regional variation in US PEV GHG emissions

Study	Life cycle	Electricity grid	Driving patterns	Climate
EPRI-NRDC, 2007	Yes	**Consequential** Bottom-up modeled emissions	**Homogeneous** Federal Urban Driving Schedule (FUDS)	Ignored
Anair and Mahmassani, 2012	Yes	Attributional Average emissions rate in eGRID subregion	Homogeneous EPA combined city/highway; Volt 64% eVMT	Ignored
MacPherson et al., 2012	Yes	?	?	?
Thomas 2012	Yes	**Consequential** Average marginal emissions from Hadley and Tsvetkova (2009)	**Homogeneous** EPA combined driving cycle	Ignored
Yawitz et al., 2013	Yes	Attributional Avg emissions rate in state	Homogeneous	Ignored
Graff Zivin et al., 2014	No Tailpipe and power plant emissions only	Consequential Interconnect emissions due to marginal load in each NERC region	Homogeneous EPA combined city/highway (verify); 35 mi/day	Ignored
Onat et al, 2015	Yes	Consequential Marginal emissions from ORNL	Homogeneous EPA combined (verify), NHTS (check how they use it)	Ignored
Tamayao et al., 2015	Yes	Consequential Compares Graff Zivin et al. (2014) and Siler-Evans et al. (2012) marginal emission factors by NERC region.	Homogeneous EPA combined	Ignored
Yuksel and Michalek, 2015	No Use-phase only	Consequential Compares Graff Zivin et al. (2014) and Siler-Evans et al. (2012) marginal emission factors by NERC region.	Homogeneous Efficiency based on FleetCarma on-road data; US NHTS driving distance distribution	Regional Based on FleetCarma data for Nissan Leaf and regional temperature data
This Study	Yes	Consequential Compares Graff Zivin et al. (2014) and Siler-Evans et al. (2012) marginal emission factors by NERC region.	Regional city / hwy / combined based on county urbanization level; NHTS driving distance distribution from same state / urbanization level	Regional Based on ANL laboratory test data at different temperatures and regional temperature data.

4.2 Data and Approach

We compare 5 existing vehicle models given in Table 4.2 to represent conventional vehicles (CVs), hybrid electric vehicles (HEVs), plug-in hybrid electric vehicles (PHEVs), and battery electric vehicles (BEVs). These models were chosen based on availability of Argonne National Laboratory vehicle test efficiency data at high, low, and moderate test chamber temperatures

Table 4.2 Vehicle Types and Models Considered

Brand	Type	Model Year	Battery Energy Capacity	
			Nominal (kWh)	Usable (kWh)
Nissan Leaf	BEV	2013	24	21
Chevy Volt	PHEV (EREV)	2013	16.5	10.8
Toyota Prius PHEV	PHEV	2013	4.4	2.7
Toyota Prius	HEV	2010		
Mazda iLoop	CV	2014	N/A	N/A

We use county-level data where possible and use regional data where we lack county-level resolution. In particular, for our base case we assume the following:

- **Power Grid:** We adopt regional 2011 marginal emission factors from Siler-Evans et al. [89] based on regressions of empirical, historical changes in power plant emissions with respect to changes in load within each North American Electric Reliability Corporation (NERC) region, and we estimate upstream feedstock-related emissions based on the marginal mix of fuel types. Lacking resolution to estimate county-level marginal emissions factors, we assume that new demand in each county within a NERC region has the same marginal emissions implications.
- **Driving Patterns:** Daily trip length and timing for each county is drawn from the distribution of trips in the National Household Travel Survey (NHTS)[93] from all counties from the same state. For urban counties we use the urban dynamometer driving schedule (UDDS) test results, for rural counties we use the Highway Fuel Economy Test

(HWFET) cycle results, and for outlying (suburban) counties we use the combined results to represent the dominant driving conditions in each case. Of course, individual drivers within each county observe a diverse set of driving conditions.

Temperature: We use data from the National Renewable Energy Laboratory (NREL) of over 1000 data points in the contiguous US and interpolate temperature at the center of each county hourly for a typical meteorological year, and we interpolate vehicle efficiency as a function of temperature using Argonne lab test data.

Figure 4.1 summarizes the analysis, and the following sections provide detail on the data we use and our calculations for the base case simulations. We also perform sensitivity analysis to test implications of several factors and assumptions and to test robustness of our results. Additional detail is provided in the Supplemental Information.

4.2.1 Data:

Vehicle Energy Efficiency. For each vehicle model we consider in this study, we first estimate how vehicle energy efficiency changes with driving cycle and temperature. For this purpose, we use the Downloadable Dynamometer Database (D^3) by Argonne National Laboratory Advanced Powertrain Research Facility[102], which provides dynamometer test data for several vehicle models. The vehicles are tested at three different temperatures (20, 72 and 95F), and EPA defined driving cycles UDDS, US06 and HWFET[58]. During the tests at 20 and 95F, the air conditioner is set to keep the cabin temperature at 72F. We only use the results from UDDS and HWFET tests to represent city and highway driving respectively, and we take their weighted average to represent combined drive cycle. Total gasoline and/or electricity consumption is reported at the end of each test, as well as the distance of the drive cycle, which provides us the vehicle gasoline/electricity consumption per mile driven at different temperatures and driving cycles.

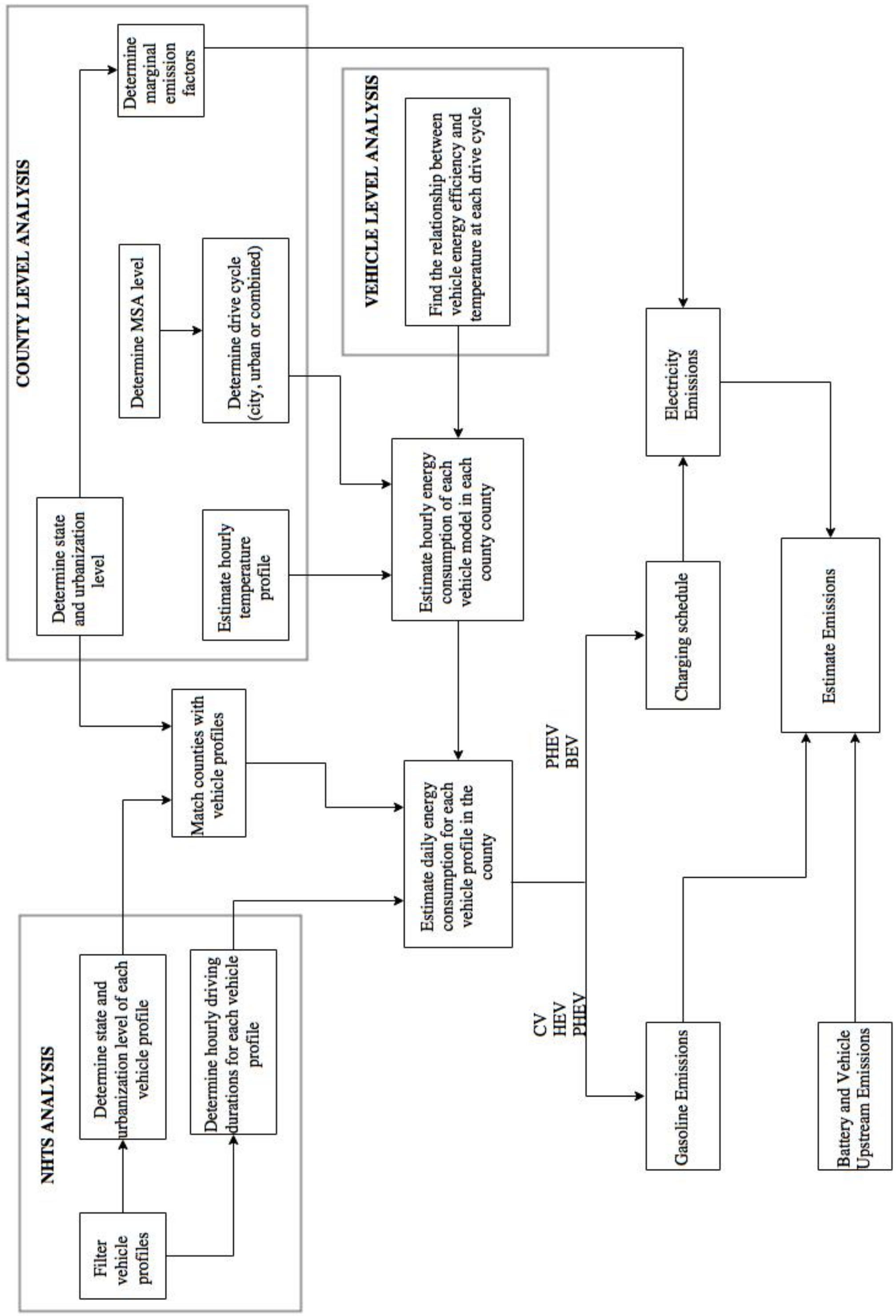

Figure 4.1 Analysis Schematic

$$c(T,\phi) = \begin{cases} m_1(\phi)\cdot(T-72) + c^{\mathrm{DYNO}}(72,\phi), & 20 \le T \le 72 \\ m_2(\phi)\cdot(T-72) + c^{\mathrm{DYNO}}(72,\phi), & 72 < T \le 95 \\ c^{\mathrm{DYNO}}(20,\phi), & T < 20 \\ c^{\mathrm{DYNO}}(95,\phi), & T > 95 \end{cases} \quad \phi \in \{\mathrm{UDDS}, \mathrm{HWFET}\} \tag{4.1}$$

where $c(T,\phi)$ is the energy consumption per mile at temperature T and drive cycle ϕ. $c^{\mathrm{DYNO}}(T,\phi)$ refers to dynamometer test results at $T = [20,72,95]$. m_1 and m_2 are the slopes of the piecewise linear curves defined as:

$$\begin{aligned} m_1(\phi) &= \frac{c^{\mathrm{DYNO}}(20,\phi) - c^{\mathrm{DYNO}}(72,\phi)}{72-20} \\ m_2(\phi) &= \frac{c^{\mathrm{DYNO}}(95,\phi) - c^{\mathrm{DYNO}}(72,\phi)}{95-72} \end{aligned} \tag{4.2}$$

County Geographic Information. We adopt county geographical information (such as latitude, longitude, state, etc.) from a United States County Map shape file in ArcGIS. We use the MSA levels to determine the driving cycle (city, highway or combined) in each county, which is described in more detail in the following sections.

Temperature Data. We use Typical Meteorological Year (TMY) Database from the National Renewable Energy Laboratory (NREL) [76] to obtain time- and location-dependent ambient temperature data . The temperature data in this database represent typical hourly temperatures rather than extreme cases. The latest database, TMY3, provides hourly values of meteorological data, including ambient temperature. These data are given for 1020 different locations in United States, including Guam, Puerto Rico, and US Virgin Islands, but we filter the data and exclude these regions, which reduces the total number of locations to 1011. We then perform a spatial interpolation to find the temperature profiles at the center of each of the 3109 counties in the continental US.

NHTS Analysis. To obtain vehicle driving profiles, we use National Household Travel Survey (NHTS) 2009 dataset [93]. NHTS is conducted by US Department of Transportation and is an inventory for daily household travel. We filter the dataset considering trips completed by private light-duty vehicles only. We also exclude the data points that are reported by the members of the household other than the driver to avoid counting the same trip by the same vehicle more than once. This reduces the total number of vehicles we include in the analysis to 76,149. The vehicle driving profiles provide start time, end time, and distance of every trip made by each vehicle profile on the day surveyed. We use this information to determine what time of the day and how far each vehicle profile is driven. Although the dataset doesn't give exact location of vehicle profiles, it reports the state and urbanization level of their locations. For our base case simulations, we match the vehicle profiles to counties based on the states only. In other words, we assume that the driving distance profiles in all the counties across one state are the same.

Emission Factors. For grid emissions associated with PEV charging, we use marginal emission factors estimated by Siler-Evans et al [89] for 2011 in our base case simulations, since this is the most recent year available. The marginal emissions in some regions may have changed since 2011, given ongoing plant construction and retirement as well as changes in energy prices. However, consequential emissions from charging PEVs are primarily produced from fossil fuels in the US, since low-emitting generators like nuclear, wind, solar, and hydroelectric power plants typically will not produce any more or less energy in the presence versus absence of PEV load. Thus, regional differences in consequential grid emissions are primarily due to the portion of coal versus natural gas power plants on the margin, and the amount of change in current or future marginal grid mixes is thus practically bounded by coal and natural gas emissions rates (at least unless and until so much low-emitting capacity is installed that it would be curtailed in the absence of PEVs). We also use the marginal grid mix to compute upstream emissions using average emissions rate for production of coal and natural gas.

For gasoline emissions, we use estimates for GHG emissions per gallon of gasoline combusted from and upstream oil production, transportation, and refining emissions estimates from Tamayao et al. [99].

Finally, we adopt vehicle and battery manufacturing emissions estimates from the Tamayao et al. [99].

4.2.2 Calculations:

Energy consumption. We start our analysis by estimating energy consumption per mile traveled every day and every hour at each county for each vehicle profile from NHTS, and for each vehicle model. The regional hourly electricity consumption per distance traveled then can be estimated as follows:

$$c_{ildhk}^{\text{HOUR}}(T_{ldh}, \phi_l) = \begin{cases} m_{1ik}(\phi_l) \cdot (T_{ldh} - 72) + c_{ik}^{\text{DYNO}}(72, \phi_l), & 20 \le T_{ldh} \le 72 \\ m_{2ik}(\phi_l) \cdot (T_{ldh} - 72) + c_{ik}^{\text{DYNO}}(72, \phi_l), & 72 < T_{ldh} \le 95 \\ c_{ik}^{\text{DYNO}}(20, \phi_l), & T_{ldh} < 20 \\ c_{ik}^{\text{DYNO}}(95, \phi_l), & T_{ldh} > 20 \end{cases} \tag{4.3}$$

c_{ildhk}^{HOUR} is either the electricity or gasoline consumption of the vehicle model $i \in \{1 = \text{BEV}, 2 = \text{PHEV}, 3 = \text{HEV}, 4 = \text{CV}\}$ per unit distance (Wh/mi) at location $l \in \{1,2,\dots,N_L\}$, day $d \in \{1,2,\dots,N_D\}$, and hour $h \in \{1,2,\dots,N_H\}$, where $N_L = 3109$, $N_D = 365$, and $N_H = 24$. $k = 1$ and $k = 2$ represents driving modes of charge depleting (CD) and charge sustaining (CS) in PHEVs. $k = 0$ for all other vehicle types, meaning CD and CS modes are not applicable for those. Energy consumption per unit distance depends on the driving cycle the vehicle is driven at, and ϕ_l represents the driving cycle applicable in the county l which is determined based on county's MSA level. We use the classification by the U.S. Census Bureau, which classifies counties as nonmetropolitan, central and outlying, with MSA Levels 0, 1 and 2 respectively. Here we assume the driving profiles corresponding to each of these classifications can be represented by highway, city and combined driving cycles, respectively. Then, ϕ_l can be defined as:

$$\phi_l = \begin{cases} \phi^{\text{HW}}, & \beta_l^{\text{MSA}} = 0 \\ \phi^{\text{CITY}}, & \beta_l^{\text{MSA}} = 1 \\ \phi^{\text{COMBINED}}, & \beta_l^{\text{MSA}} = 2 \end{cases} \tag{4.4}$$

Where β_l^{MSA} is the MSA level of each county l. The energy consumption per mile at highway and city driving conditions can be obtained by using the dynamometer test results with HWFET and UDDS driving cycles respectively. The energy consumption at combined drive cycle is a weighed average of highway and city energy consumptions which is estimated as follows:

$$c_{ildhk}^{\text{HOUR}}\left(T_{ldh}, \phi^{\text{COMBINED}}\right) = 0.55 \cdot c_{ildhk}^{\text{HOUR}}\left(T_{ldh}, \phi^{\text{CITY}}\right) + 0.45 \cdot c_{ildhk}^{\text{HOUR}}\left(T_{ldh}, \phi^{\text{HW}}\right) \tag{4.5}$$

To estimate the daily average electricity consumption per mile, we need to know how much each vehicle is driven at each hour of the day. We estimate this using the driving patterns from the NHTS dataset. For all the vehicles in the subset of data we are using, we distribute the driving durations into hourly bins throughout the day by looking at the start and end time of each trip, and we compute Δ_{hv}^{DRV}, the amount of time (hours) each vehicle driving profile $v \in \{1,2,\ldots,N_{\text{V}}\}$ spent driving during the corresponding one hour bin h (where $N_{\text{V}} = 76{,}149$ vehicle driving profiles):

$$\Delta_{hv}^{\text{DRV}} = \sum_{\tau \in \mathrm{T}_v} \begin{cases} 1 & \text{if } t_\tau^{\text{S}} \leq h-1 \text{ and } t_\tau^{\text{E}} \geq h \\ 0 & \text{if } t_\tau^{\text{S}} \geq h \text{ or } t_\tau^{\text{E}} \leq h-1 \\ \min\left(h, t_\tau^{\text{E}}\right) - \max\left(h-1, t_\tau^{\text{S}}\right) & \text{otherwise} \end{cases} \tag{4.6}$$

where t_τ^{S} and t_τ^{E} are the start and end times of each trip τ, respectively, and T_v is the set of trips for vehicle profile v in the data set.

We then use the Δ_{hv}^{DRV} to obtain the daily weighted average energy consumption per unit distance (Wh/mi):

$$c_{ildvk}^{\text{VEH}} = \frac{\sum_h \Delta_{hv}^{\text{DRV}} \cdot c_{ildhk}^{\text{HOUR}}}{\sum_h \Delta_{hv}^{\text{DRV}}}, \qquad \begin{matrix} i = 1,..4 & l = 1,2,..N_L & v = 1,2,..,N_V \\ k = 0,1,2 & d = 1,2,..,N_D & \square = 1,2,..,\square_{\square} \end{matrix} \tag{4.7}$$

where c_{ildvk}^{VEH} is the daily average electricity consumption ($c_{ildvk}^{\text{VEH,ELEC}}$) in Wh/mi or daily average gasoline consumption ($c_{ildvk}^{\text{VEH,GAS}}$) in gal/mi for each vehicle type i, at location l and day d, for vehicle profile v from NHTS and driving mode k. c_{ildvk}^{VEH} is used to estimate the all-electric range (AER) for BEVs and PHEVs as follows:

$$s_{ildv}^{\text{ELEC}} = \begin{cases} C_i^{\text{BAT}} / c_{ildvk}^{\text{VEH,ELEC}}, & i = 1,2 \\ 0, & i = 3,4 \end{cases} \tag{4.8}$$
$$l = 1,2,..N_L \quad d = 1,2,..,N_D \quad v = 1,2,..,N_V \quad k = 0$$

where s_{ildv}^{ELEC} is AER and C_i^{BAT} is battery usable capacity

To estimate the total daily average energy consumption in Wh, we need to determine the daily distance traveled by each vehicle profile. For all vehicle types except BEVs, daily distance traveled is equal to the distance provided for each vehicle profile in NHTS. For BEVs, we assume that if the distance driven in a vehicle profile is longer than the AER of the BEV, the vehicle shortens travel on those days. Then, the daily driving distance, s_{ildv}^{DAY}, is defined as:

$$s_{ildv}^{\mathrm{DAY}} = \begin{cases} min\left(s_{ildv}^{\mathrm{ELEC}}, s_{lv}^{\mathrm{NHTS}}\right), & i = 1 \\ s_{lv}^{\mathrm{NHTS}}, & i = 2,3,4 \end{cases} \tag{4.9}$$

where s_{lv}^{NHTS} is the daily vehicle miles traveled from NHTS for location l and vehicle profile v.

Then, daily average electricity consumption C_{ildv}^{ELEC} in Wh and gasoline consumption C_{ildv}^{GAS} in gal for each vehicle type and vehicle profile can be estimated as:

$$C_{ildv}^{\mathrm{ELEC}} = \begin{cases} s_{ildv}^{\mathrm{DAY}} \cdot c_{ildvk}^{\mathrm{VEH,ELEC}}, & i = 1,2 \\ 0, & i = 3,4 \end{cases} \tag{4.10}$$
$$l = 1,2,..N_L \quad d = 1,2,..,N_D \quad v = 1,2,..,N_V \quad k = 0$$

$$C_{ildv}^{\mathrm{GAS}} = \begin{cases} 0, \\ c_{ildv1}^{\mathrm{VEH,GAS}} \cdot min\left(s_{ildv}^{\mathrm{ELEC}}, s_{lv}^{\mathrm{NHTS}}\right) + \left(s_{ildv}^{\mathrm{ELEC}} < s_{lv}^{\mathrm{NHTS}}\right) \cdot \left(s_{lv}^{\mathrm{NHTS}} - s_{ildv}^{\mathrm{ELEC}}\right) \cdot c_{ildv2}^{\mathrm{VEH,GAS}}, \\ s_{ildv}^{\mathrm{DAY}} \cdot c_{ildv0}^{\mathrm{VEH,GAS}}, \end{cases} \quad 4.11)$$

Electricity emissions. CO_2 emissions due to electricity consumption vary depending on charge timing. We first determine the total charging duration for each vehicle as:

$$t_{ildv} = \frac{C_{ildv}^{\mathrm{ELEC}}}{\eta_i \cdot r_i}, \quad i = 1,2 \tag{4.12}$$

where t_{ildv} is the total charging duration in hours, and r_i is the constant battery charging rate. η_i is the efficiency between the charger and the battery. In this study, we neglect the efficiency loss between the EVSE equipment and the charger, since it is much lower compared to the losses between charger and the battery.

Then we distribute the total charging duration into hourly bins assuming convenience charging for our base case simulations (i.e. charging starts right after the last trip of the day ends)

$$\Delta_{ildhv}^{\mathrm{CHG}} = \sum_{\tau \in L_v} \begin{cases} 1 & \text{if } t_\tau^{\mathrm{E}} \le h-1 \text{ and } t_\tau^{\mathrm{E}} + t_{ldv} \ge h \\ 0 & \text{if } t_\tau^{\mathrm{E}} \ge h \text{ or } t_\tau^{\mathrm{E}} + t_{ldv} \le h-1 \\ \min(h, t_\tau^{\mathrm{E}} + t_{ldv}) - \max(h-1, t_\tau^{\mathrm{E}}) & \text{otherwise} \end{cases} \tag{4.13}$$

where L_v is the last trip of the day for vehicle profile v, and we obtain $\Delta_{ildhv}^{\mathrm{CHG}}$ which gives the charging duration that falls into hourly bin h. To test the effect of charging scheme on the results, we also run a case where we assume delayed charging instead of convenience charging, which is assumed to start at midnight. We then find the CO_2 emissions as:

$$\Gamma_{ildhv}^{\mathrm{ELEC}} = r_i \cdot \Delta_{ildhv}^{\mathrm{CHG}} \cdot \left(E_{ldh}^{\mathrm{MEF}} + E_{ldh}^{\mathrm{UPST}}\right), \qquad i = 1,2 \tag{4.14}$$

where $\Gamma_{ildhv}^{\mathrm{ELEC}}$ is the CO_2 emissions in grams from charging vehicle v at hour h of day d in location l. E_{ldh}^{MEF} is the expected value of the regional time of day marginal emission factors in grams/kWh, and $E_{ldh}^{\mathrm{UPST}}$is the expected value of the regional time of day electricity upstream emissions in grams/kWh.

Regional average CO_2 emissions due to electricity consumption in grams/mile, $\gamma_{il}^{\mathrm{ELEC}}$, (averaged over all vehicle profiles and days of the year) are then found by:

$$\gamma_{il}^{\mathrm{ELEC}} = \frac{\sum_d \sum_h \sum_v \Gamma_{ildhv}^{\mathrm{ELEC}}}{\sum_v \sum_d s_{ildv}^{\mathrm{DAY}}}, \quad i = 1,2 \tag{4.15}$$

Gasoline emissions. Total gasoline emissions due to combustion and gasoline upstream can be found by:

$$\Gamma_{ildv}^{\mathrm{GAS}} = C_{ildv}^{\mathrm{GAS}} \cdot \left(G_{ldh}^{\mathrm{COMB}} + G_{ldh}^{\mathrm{UPST}}\right) \tag{4.16}$$

where $\Gamma_{ildv}^{\mathrm{GAS}}$ is the CO_2 emissions in grams due to gasoline consumption, G_{ldh}^{COMB} is the expected value of the gasoline combustion emissions factor in g/gal, and G_{ldh}^{UPST} is expected value of the gasoline upstream emissions factor in g/gal.

Regional average CO_2 emissions due to gasoline consumption in grams/mile, $\gamma_{il}^{\mathrm{GAS}}$, (averaged over all vehicle profiles and days of the year) are then found by:

$$\gamma_{il}^{\mathrm{GAS}} = \frac{\sum_d \sum_v \Gamma_{ildv}^{\mathrm{GAS}}}{\sum_v \sum_d s_{ildv}^{\mathrm{DAY}}}, \quad i = 2,3,4 \tag{4.17}$$

Total average emissions are then defined as :

$$\gamma_{il} = \begin{cases} \gamma_{il}^{\mathrm{ELEC}}, & i = 1 \\ \gamma_{il}^{\mathrm{ELEC}} + \gamma_{il}^{\mathrm{GAS}}, & i = 2,3 \\ \gamma_{il}^{\mathrm{GAS}}, & i = 4 \end{cases} \tag{4.18}$$

4.3 Results and Discussion

Figure 4.2 summarizes the increase or decrease in life cycle GHG emissions from owning and operating a 2013 Nissan Leaf BEV, 2013 Chevrolet Volt PHEV, and 2013 Prius PHEV relative to the most efficient gasoline vehicle: the HEV Prius (modeled here using data from a 2010 Prius). Relative to the HEV Prius:

- the Leaf reduces emissions across most of the US but increases emissions for rural highway drivers of the Midwest and the South;
- the Volt increases emissions everywhere; and
- the PHEV Prius reduces emissions in Texas, Florida, and the southwestern US as well as for most urban drivers, and it increases emissions for many rural highway drivers, especially in the Northern Midwest.

Figure Figure 4.2d also shows county urbanization levels, for reference.

Similarly Figure 4.3 summarizes the increase or decrease in life cycle GHG emissions from owning an operating the same three vehicles relative to an efficient conventional gasoline vehicle with EPA-rated combined (5-cycle) fuel efficiency of 32 mpg: the 2014 Mazda 3 iLoop (the iLoop is an energy recovery braking system intended to capture a portion of the benefits that HEVs and PEVs capture in regenerative braking to displace accessory load without a full hybrid system). Relative to the CV Mazda 3:

- the Leaf reduces emissions across most of the US but increases emissions for rural highway drivers of the Midwest.

- the Volt similarly reduces emissions across most of the US but increases emissions for rural highway drivers of the Midwest and the South.
- the PHEV Prius reduces emissions everywhere

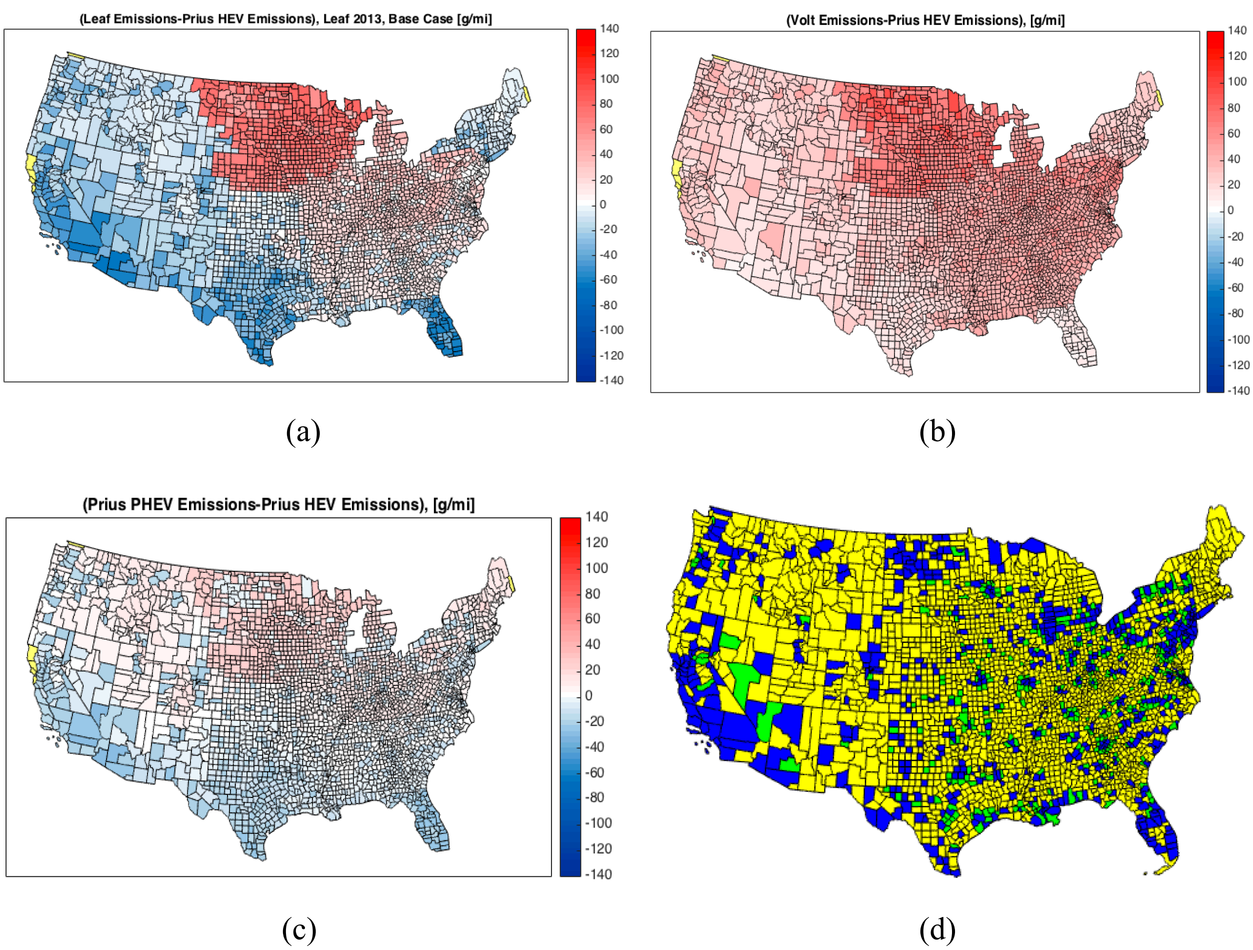

Figure 4.2 Estimated difference in life cycle GHG emissions (gCO_2 eq/mi) relative to a 2010 Toyota Prius (base case assumptions) (a) 2013 Nissan Leaf, (b) 2013 Chevrolet Volt, (c) 2013 Prius PHEV, and (d) US counties color-coded with respect to their MSA levels. yellow: nonmetropolitan (highway driving), blue: central (city driving), green: outlying (combined driving)

Figure 4.4 shows the breakdown of use-phase CO_2 emissions for each vehicle in three selected counties: Alameda, CA, which includes the cities of Berkeley and Oakland, represents a mild climate region with a clean electricity grid; Maricopa, AZ, which includes the city of

Phoenix, represents a hot climate with a clean electricity grid; and Olmstead, MN, which includes the city of Rochester, represents a cold climate region with a coal-heavy electricity grid. The figure also shows that all vehicles are higher emitting in Minnesota, a colder state. However, the biggest effect is observed with the BEV, followed by the PHEVs. Batteries are less efficient when cold, and so are engines, but gasoline vehicles are able to use waste heat from the engine to heat the cabin, while BEVs and EREV PHEVs need to draw energy from the battery to heat the cabin.

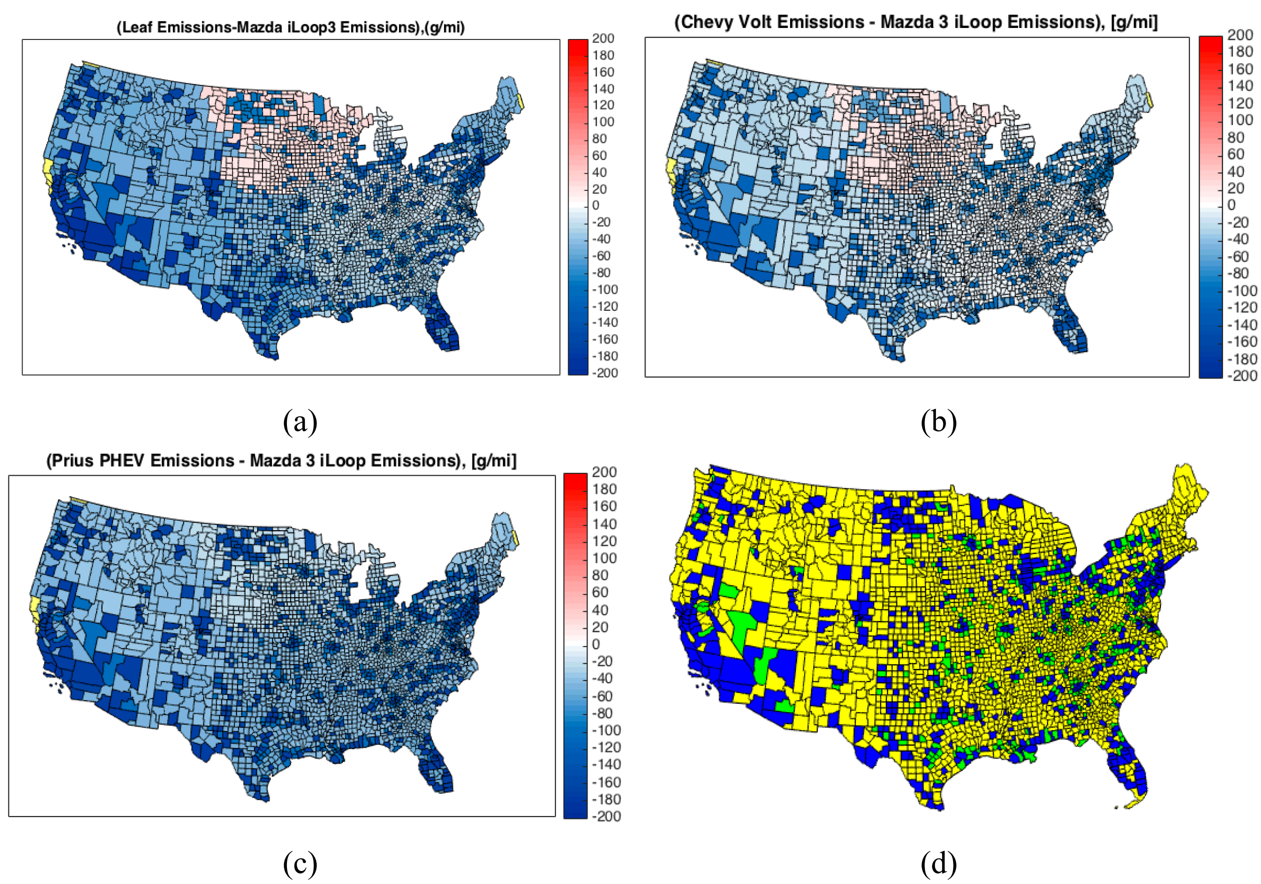

Figure 4.3 Estimated difference in life cycle GHG emissions (gCO_2 eq/mi) relative to a 2014 Mazda 3 iLoop (base case assumptions) (a) 2013 Nissan Leaf, (b) 2013 Chevrolet Volt, (c) 2013 Prius PHEV, and (d) US counties color-coded with respect to their MSA levels. yellow: nonmetropolitan (highway driving), blue: central (city driving), green: outlying (combined driving)

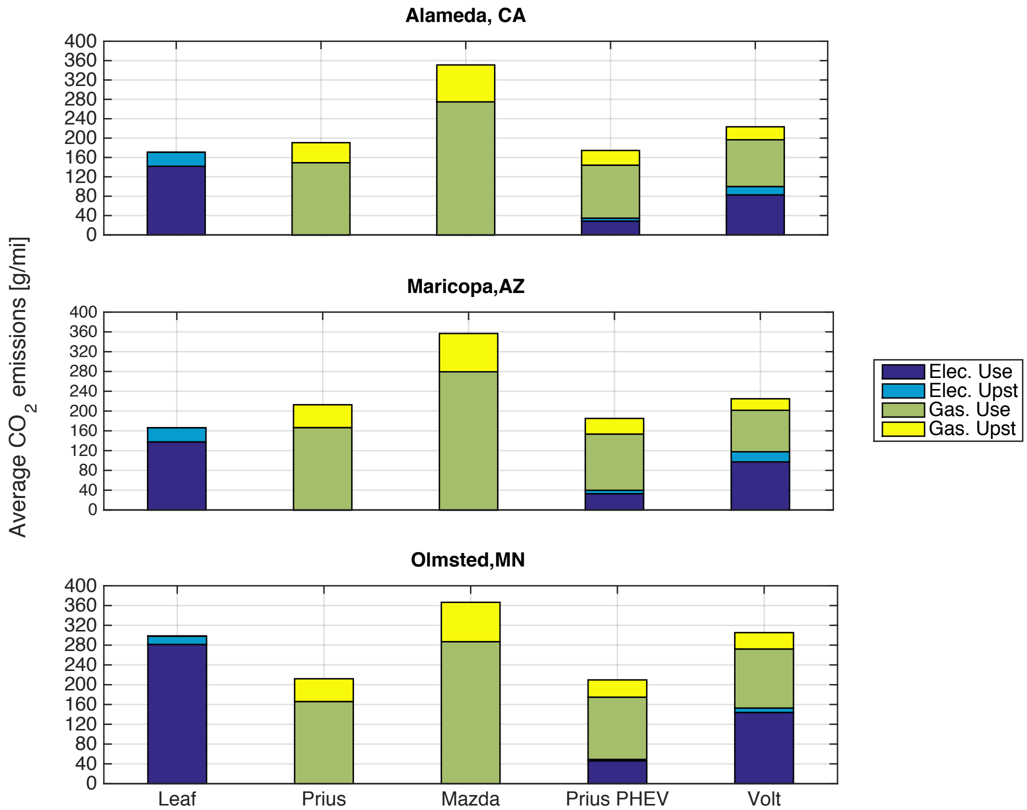

Figure 4.4 CO_2 emissions in g/mi in selected counties from three different states

4.4 Sensitivity Analysis

We perform sensitivity analysis to test assumptions, assess robustness, and isolate various effects. Details can be found in the Supplemental Information, but Table 4.3 summarizes key findings. Overall, we find that regionally specific temperature effects and driving patterns have significant effects on outcomes; delayed charging increases PEV GHG emissions in most regions and makes them less competitive with gasoline vehicles.

Table 4.3 Summary of findings from sensitivity analysis

Sensitivity Case	Change from Base Case	Purpose	Finding
No Temperature	Vehicle efficiency at 72ºF used for all counties all year	Test importance of temperature effect	Temperature effect can change comparison results for northern states
MSA level VMT	Each county's VMT distribution is drawn from all NHTS data from the same state and urbanization level	Test importance of differences in urban/rural driving distance	No significant change in the results observed
Delayed Charging	Each PEV's charging schedule begins at midnight, rather than upon arrival at home	Test importance of charge timing	Delayed charging increases GHG emissions of PEVs in most of the country and reduces competitiveness with the HEV
Homogeneous Driving Conditions	Vehicle efficiency on combined UDDS/HWFET used for all counties	Test importance of drive cycle	Drive cycle affects the relative benefits of PEVs versus HEVs (and especially versus CVs). Without differentiated drive cycles, urban counties are not distinct from nearby rural counties.

4.5 Limitations

Our analysis represents the most recent data available at the highest resolution available to account for regional grid emissions, driving patterns, and temperature effects on life cycle GHG emissions of PEVs and gasoline vehicles. However, several limitations in the available data should be understood when interpreting our results:

- **Regional Grid Emissions:** Our marginal emissions estimates are historical and do not capture the current grid, a future grid, or changes in the grid that may occur during the vehicle's life. Because marginal emissions come primarily from fossil fuel plants, the mix of natural gas versus coal on the margin determines the consequential emissions of PEV charging. If coal-heavy regions switch to more natural gas generation on the margin, comparisons in those regions will begin to look more like the cleaner regions in our analysis. Also, while we discuss county-level differences, we assume that in each NERC region all counties have identical marginal emission factors because we lack data sufficient to estimate high resolution marginal emission factors. In practice, it may be the case that adding PEV load in some areas of a NERC region could have different emission implications than adding the same load in a different area of the same NERC region.

- **Driving Patterns:** Our summary maps assign the UDDS test results to urban counties and the HWFET test results to rural counties, but in practice driving conditions are heterogeneous in all counties. Further, on-road driving conditions differ from these two laboratory tests, which are known to produce optimistic fuel efficiency estimates due to their relatively mild drive cycle demands. Driving distances also may vary for different urban counties in a state, but we lump counties together when estimating driving distance distributions because we lack data resolution to identify driving distance distributions for individual counties. The NHTS data set provides information on the trips taken by each surveyed U.S. vehicle on a single survey day and does not include day-to-day variability for each vehicle. In this study, we average over the vehicle profiles to assess implications for average driving distances and we assume these daily profiles are identical across the year.
- **Temperature:** We treat temperature as the only factor affecting vehicle efficiency on a particular drive cycle, but in practice other regional factors, such as humidity, could affect HVAC use, and regional road conditions such as terrain, traffic, and wind can also affect efficiency. Our efficiency estimates are based on linear interpolation using test results at three temperatures for each drive cycle. Yuksel and Michalek[78] suggest that this captures the general trend well but coarsely. We also avoid extrapolation beyond the range of temperatures tested and therefore likely make conservative estimates of vehicle efficiency loss in extreme weather regions.
- **Vehicles:** We examine only five specific vehicle models for which we have access to test data. Other vehicle models, including more recent model years of the vehicles examined, could have different performance characteristics, temperature sensitivity, etc.

5 Optimization of Li-ion Batteries for Vehicle Electrification: A Case Study to Compare Chemistries

Chapters 2 through 4 focused mainly on operational factors that would affect benefits of vehicle electrification. One significant barrier to widespread adoption of electrified vehicles is battery cost since battery is one of the most expensive components of electrified vehicles. The purchase cost of the battery depends on the optimal design that would satisfy the power and energy requirements of the vehicle. The battery chemistry is also important in determining the cost. The study in this chapter is a case study that builds up on a processed based cost model developed by Sakti et al [31]. This study extends the original model and finds the optimum battery design that minimizes the production cost of the battery pack for four different plug-in vehicles with different battery energy and power capacities, and for four different chemistries that are in use in vehicle electrification.

This chapter is based on a working paper with coauthors Darshit Mehta and Jeremy Michalek.

5.1 Introduction

Battery is one of the most expensive components in an electrified vehicle. Battery cost depends on the cell level design parameters such as electrode thickness and cell surface area, as well as pack level design decisions like number of cells and modules. In addition, cost depends on the chemistry of the cells, which is mainly identified by the cathode material used.

There are various studies in literature estimating li-ion battery cost. However, publicly available bottom-up models that estimate the cost and performance of a battery design are rare. Argonne National Laboratory (ANL) cost model BatPaC is a pioneer in addressing this issue [12]. The process based cost model (PBCM) introduced by Sakti et al. builds up on BatPaC [31]. The major improvement introduced by PBCM is that, it estimates resource requirements at process-step-level by considering yield rates at each step, therefore accounts for any discrete resource investments at each step to realize changes in production model. Sakti et al. uses this cost model to optimize the battery design for minimum cost assuming the power and energy requirements of 4 different vehicle types: PHEV10, PHEV30, PHEV60 and BEV200. The study shows the optimal design based on cells with NMC333 chemistry, and investigates cathode thickness and power-to-energy ratio implications.

The study presented in this chapter builds on the study by Sakti et al. and aims to carry it further by introducing two improvements to the study scope: 1) PBCM created in Sakti et al. is a model based on Microsoft Excel and the cost minimization problem is solved by evaluating the battery cost over a grid of values and using linear interpolation to estimate the cost of intermediate designs. In this study, the model is replicated in Matlab, which allows using the cost function directly in optimization and solving the problem using optimization techniques. This increases the precision of the solution. In addition, the speed of the approach is enhanced which enables fast study of more cases. 2) Using this replicated model, this study identifies the optimal battery design with 3 other chemistries also: NCA, LMO and LFP. By classifying the design across various chemistries, a significant component of battery cost is addressed.

5.1.1 Optimization Problem

The following optimization problem is introduced by Sakti et al.:

$$\begin{gathered} min.\ C(\boldsymbol{x}) \\ w.r.t\quad \boldsymbol{x} = [x^{\mathrm{T}}, x^{\mathrm{W}}, x^{\mathrm{B}}, x^{\mathrm{N}}, x^{\mathrm{M}}] \\ s.t.\quad P^{\mathrm{PEAK}} - P(\boldsymbol{x}) \leq 0 \\ E^{\mathrm{AER}} - E(\boldsymbol{x}) \leq 0 \\ c^{\mathrm{MIN}} \leq c(\boldsymbol{x}) \leq c^{\mathrm{MAX}} \\ \boldsymbol{x}^{\mathrm{MIN}} \leq \boldsymbol{x} \leq \boldsymbol{x}^{\mathrm{MAX}} \\ x^{\mathrm{T}}, x^{\mathrm{W}} \in \mathbb{R} \\ x^{\mathrm{B}}, x^{\mathrm{N}}, x^{\mathrm{M}} \in \mathbb{Z} \end{gathered}$$

Minimize battery cost
with respect to cathode thickness, cell width, number of bi-cell layers, number of cells per module and number of modules
Such that:

- Power capability of the battery should be bigger than the peak power required
- Energy capacity should satisfy the energy required
- Cell capacity and design variables should be within their bounds
- Cathode thickness and cell width are continuous, number of bicell layers, number of modules and cells are integer variables

where $C(\boldsymbol{x})$ is the battery pack cost estimated by the PBCM that is explained in the following sections. x^{T} is the cathode thickness, x^{W} is the cell width, x^{B} is the number of bi-cell layers, x^{N} is the number of modules cells per module, x^{M} is the number modules and $c(\boldsymbol{x})$ is the cell capacity in Ah. The minimum and maximum bounds for the design variables ($\boldsymbol{x}^{\mathrm{MIN}}$ and $\boldsymbol{x}^{\mathrm{MAX}}$), as well as for the cell capacity (c^{MIN} and c^{MAX}) are given in Table 5.1 and calculation of $c(\boldsymbol{x})$ is provided in the following sections.

Table 5.1 Minimum and max values used for design variables and cell capacity. Values obtained from [31]

	x^{T}	x^{W}	x^{B}	x^{N}	x^{M}	$c(\boldsymbol{x})$
Min.	25	1	1	1	1	10
Max	125	1000	1000	1000	1000	60

$P(\boldsymbol{x})$ is the power capability of the battery and $E(\boldsymbol{x})$ is the pack's energy capacity. P^{PEAK} and E^{AER} represent the power and energy requirement of the vehicle respectively. These values are provided for 4 different vehicle types in Table 5.2. where the PHEVs considered are extended range electric vehicles.

Table 5.2 Peak power and energy requirements. Values obtained from [31].

		PHEV10	PHEV30	PHEV60	BEV200
Peak power requirement (kW)	P^{PEAK}	48.6	44	47.9	80
Energy requirement (kWh)	E^{AER}	3.6	8	16.5	48

5.1.2 Battery Energy and Power Calculations

5.1.2.1 Cell Capacity and Pack Energy

Cell capacity $c(\boldsymbol{x})$ is defined as:

$$c(\boldsymbol{x}) = \frac{x^{\mathrm{T}} A^{\mathrm{P}} s^{\mathrm{PAM}} m^{\mathrm{FR}} \rho^{\mathrm{P}}}{10^9} \tag{5.1}$$

where A^{P} it the cathode surface area, s^{PAM} is the specific capacity of the cathode active material, m^{FR} is the mass fraction of the active material in the cathode (89%), and ρ^{P} is the cathode density. A^{P} is can be defined as :

$$A^{\mathrm{P}} = 2x^{\mathrm{B}}r(x^{W})^{2} \tag{5.2}$$

where r is the cell aspect ratio (length/width, assumed to be 3 in this study).

Using cell capacity, pack energy can be calculated as:

$$E(\boldsymbol{x}) = x^{\mathrm{M}}x^{\mathrm{N}}V^{\mathrm{NOM}}c(\boldsymbol{x}) \tag{5.3}$$

where V^{NOM} is the cell nominal voltage.

5.1.2.2 Pack Power Capability

Sakti et al. defines power capability by using hybrid pulse power characterization (HPPC) test results from Battery Design Studio (BDS) simulation software. HPPC test gives 10-s power capabilities of the cell in 10% DOD (depth-of-discharge increments). They perform the tests for 48 different cell designs that vary with cathode thickness and cell capacity, and fit a curve to the results to obtain the following relation for $P(\boldsymbol{x})$:

$$P(\boldsymbol{x}) = x^{N}x^{M}\left(\frac{x^{\mathrm{T}}c(\boldsymbol{x})}{\beta_1 + \beta_2 \cdot (x^{\mathrm{T}})^{\beta_3}} - \beta_4 x^{\mathrm{T}}c(\boldsymbol{x})\right) \tag{5.4}$$

where $\beta_1 = 149$, $\beta_2 = 0.281$, $\beta_3 = 2$, and $\beta_4 = 8.98\times10^{-6}$ are the constants obtained through regression. In this study, a different approach is followed for power calculation and the following relation from ANL's BatPaC 2.1 is employed:

$$P(\boldsymbol{x}) = \frac{x^{\mathrm{N}}x^{\mathrm{M}}V^{\mathrm{OCV,P}}\,V^{\mathrm{OCV,FR}}(1 - V^{\mathrm{OCV,FR}})A^{\mathrm{P}}(\boldsymbol{x})}{R^{\mathrm{ASI}}(x^{\mathrm{T}})} \tag{5.5}$$

where R^{ASI} is the area specific impedance (ohm-cm^2), x^{N} is the number of cells per module, x^{M} is the number of modules, $V^{\mathrm{OCV,P}}$ is the open circuit voltage at the SOC for rated power (20% SOC for PHEVs and EVs), and $V^{\mathrm{OCV,FR}}$ is the fraction of the open circuit voltage at which the designed power is achieved (0.8 default in BatPaC).

Area specific impedance is a function of various parameters, however for simplicity for it is simplified as:

$$R^{\mathrm{ASI}} = R^{\mathrm{Const}} + R^{\mathrm{POS}} + R^{\mathrm{NEG}} + R^{\mathrm{CC}} + R^{\mathrm{CellTerm}} + \frac{R^{\mathrm{CNCT}} A^{\mathrm{P}}}{x^{\mathrm{N}} x^{\mathrm{M}}} \tag{5.6}$$

where R^{Const} is a lumped parameter used to define any resistance that are not defined with the other parameters in the equation, R^{POS} and R^{NEG} are interfacial impedance for positive and negative electrode respectively, R^{CC} is the current collector foil impedance, R^{CellTerm} is the impedance of cell terminals, and R^{CNCT} is the summation of resistances for cell terminals, module terminals, module interconnects and battery terminals. Gallagher et al. introduce this relation as a simplified calculation of the area specific impedance for battery design [103]. We further simplify this relation by neglecting the last three terms in Equation (5.6). This is just for simplicity purposes since the last three terms are estimated by a combination of various relations that require tracking down various variables and functions in the BatPaC model. Based on quick estimations in BatPaC, neglecting these terms results in less than 1% decrease in the total area specific impedance for a small battery. However, in large batteries, this decrease can be up to 10% based on chemistry. This would result in an increase in the power capability calculated. The investigation of this issue has been left as future work and the area specific impedance is estimated by considering only the first three terms:

$$R^{\mathrm{ASI}} = R^{\mathrm{Const}} + R^{\mathrm{POS}} + R^{\mathrm{NEG}} \tag{5.7}$$

R^{Const} is provided for the four chemistries inspected in Table **5**.3. Impedance for negative electrode is given as:

$$R^{\mathrm{NEG}} = \frac{R^{\mathrm{GAS}} T}{i_o a^{\mathrm{NEG}} L^{\mathrm{NEG}} F} \tag{5.8}$$

L^{NEG} is the negative electrode thickness, defined as:

$$L^{\mathrm{NEG}} = r^{\mathrm{NP}} \frac{s^{\mathrm{NAM}} \rho^{\mathrm{N}}}{s^{\mathrm{PAM}} \rho^{\mathrm{P}}} \tag{5.9}$$

The definition and values of the parameters used in equations (5.8) and (5.9) are provided in Table **5**.3.

Table 5.**3** Parameter used in power and energy relations. Values obtained from ANL's BatPaC [12]

			NMC333-G	NCA-G	LFP-G	LMO-G
$V^{\mathrm{OCV,P}}$	OCV at 20% SOC	Volts	3.516	3.551	3.246	3.826
V^{NOM}	Nominal Voltage	Volts	3.671	3.680	3.282	3.954
R^{Const}	Lumped constant impedance	$ohm \cdot cm^2$	33	27	30.5	23
R^{GAS}	Universal gas constant	$Wh/mol \cdot K$	2.3x10^{-4}	2.3x10^{-4}	2.3x10^{-4}	2.3x10^{-4}
T	Absolute temperature	K	297	297	297	297
i_o	Exchange current density	$Ampere/cm^2$	0.00015	0.00015	0.00015	0.00015
a^{NEG}	Ratio of interfacial area to (-) electrode volume	cm^2/cm^3	74000	74000	74000	74000
r^{NP}	Negative to positive ratio after formation		1.25	1.25	1.2	1.2
F	Faraday's constant	Ah/mol	26.801	26.801	26.801	26.801
s^{PAM}	(+) electrode active material capacity	mAh/g	150	160	150	100
ρ^{P}	(+) electrode density	g/cm^3				
s^{NAM}	(-) electrode active material capacity	mAh/g	150	160	150	100
ρ^{N}	(-) electrode density	g/cm^3				
a^{POS}	Ratio of interfacial area to (+) electrode volume	cm^2/cm^3	8900	8900	420000	49200
I^{IONLIM}	Limiting ionic current for lithium cation transport through seperator	$Ampere/Ah$	120	120	120	120
I^{MAX}	C-rate at full power	$Ampere/Ah$	5	5	5	5
I^{C}	Maximum current density at full power	mA/cm^2	20	20	20	20
I^{CLIM}	Limiting current densitiy	mA/cm^2	85	85	85	85

Impedance for positive electrode is given as:

$$R^{\mathrm{POS}} = \frac{R^{\mathrm{GAS}}T}{i_o a^{\mathrm{POS}} x^{\mathrm{T}} F}\left\{\left(1 - \frac{I^{\mathrm{MAX}}}{I^{IONLIM}}\right)\left[1 - \left(\frac{I^{\mathrm{C}}}{I^{\mathrm{CLIM}}}\right)^2\right]\right\}^{0.5} \tag{5.10}$$

The comparison of the power capabilities obtained from two different calculations is provided in Figure 5.1 for NMC chemistry at different cell capacities. As depicted from the figure, the power capability obtained from BatPac model is lower compared to BDS results. This can be explained by the fact that BatPac model designs the battery to allow for degradation and resistance growth so that required power rating from the battery is also satisfied at end of life. The further investigation of this issue is left as future work and for the optimization described in this study the power capability is calculated using Equation (5.5).

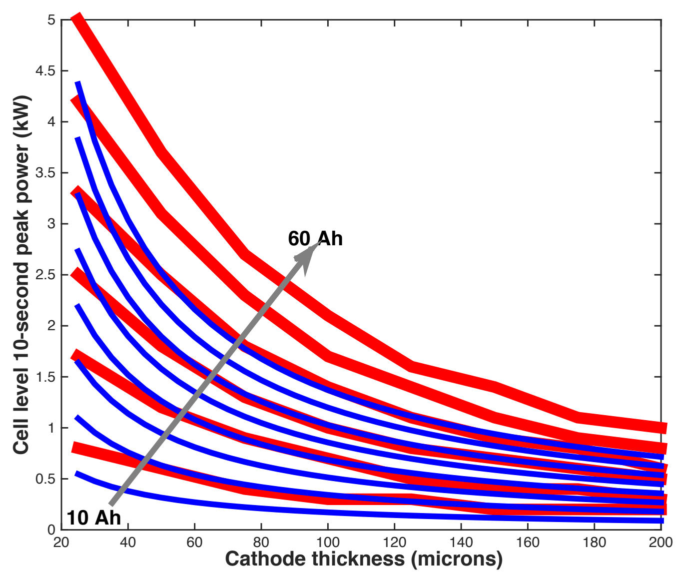

Figure 5.1 Power capability calculation: Comparison of two approaches. Red: Power calculation using BDS HPPC test results as presented in Sakti et al. and given in Equation **(5.4)**. Blue: calculation using the relation from BatPac given in Equation **(5.5)**. Each of the 6 lines in each color represent the results between 10Ah and 60 Ah cell capacity with 10 Ah increments.

5.1.3 Battery Cost Model

Using the PBCM, the unit battery production cost can be obtained by considering the annual production cost at each process step:

$$C(\boldsymbol{x}) = \frac{C^{\mathrm{MTL}}(\boldsymbol{x}) + C^{\mathrm{EQP}}(\boldsymbol{x}) + C^{\mathrm{BLD}}(\boldsymbol{x}) + C^{\mathrm{LBR}}(\boldsymbol{x}) + C^{\mathrm{ERG}}(\boldsymbol{x}) + C^{\mathrm{AUX}}(\boldsymbol{x}) + C^{\mathrm{MNT}}(\boldsymbol{x}) + C^{\mathrm{OH}}(\boldsymbol{x})}{V^{\mathrm{ANN}}} \tag{5.11}$$

where the cost terms in the numerator refers to annual material, equipment, labor, building, energy, auxiliary equipment, maintenance and overhead costs, respectively. V^{ANN} is the annual production volume. In this study, we assume the annual production volume is fixed at $V^{\mathrm{ANN}} = 20{,}000$ packs. More details on each cost parameter are available at Sakti et al.

According to the BatPac and the PBCM, the differences that occur between different chemistries are due to differences in cell level design and cost parameters. All processes and equipment requirements are assumed to be the same for all chemistries.

5.1.4 Optimization

The optimization problem is introduced in section 5.1.1 is a non-convex mixed integer non-linear program (MINLP) This problem is solved using a branch and bound method that uses a randomized multi-start at each node. The optimization problem at each node is solved using a sequential quadratic programming algorithm.

5.2 Results and Discussion

Optimal design variables for each chemistry are tabulated in Table 5.4. Figure 5.2 shows the comparison of battery specific cost with vehicle range and for each chemistry, and Figure 5.3 shows the cathode thickness at optimal design.

In general, the lowest cost is obtained by using the thickest cathode thickness possible to satisfy the constraints of the problem. The specific cost of the battery decreases with pack size since packaging, thermal management and battery control systems costs are spread over a larger energy capacity. In addition, specific cost decreases as cathode thickness increases since thicker electrodes allow the designer to use less inactive material. Furthermore, for PHEV10 and PHEV30 a general trend of adding more cells to modules instead of increasing the number of modules is observed. This is expected since additional modules result in more module regulation costs, primarily from state-of-charge regulators [31]. However, as the energy requirement increases with PHEV60 and BEV200, the number of modules increases as well. Further investigation is necessary to ensure global solution and to understand the causes of this trend.

LMO is the cheapest option for all vehicle types, and LFP is the most expensive except for PHEV10. The positive active material cost of LMO is cheapest among the alternatives. In addition, high power to energy ratio of LMO allows for bigger cathode thickness in PHEV10 small battery applications and this decrease the cost. Similarly, LFP allows for thicker cathode thickness for PHEV10 and cost of LFP for this vehicle is lower than NMC and NCA Figure 5.4 gives the comparison of the power capabilities of the 4 different chemistries considered. Both LFP and LMO uses the maximum cathode thickness allowable starting from PHEV30. This might be explained by the lower energy capabilities of these cathodes. For all chemistries, starting from PHEV60, optimum design is obtained at maximum allowable cathode thickness.

LFP is a high cost option as the power-to-energy ratio decreases, i.e. energy requirement increases. Although active material capacity and cost are comparable to other chemistries, the energy capacity is lower. To satisfy the energy requirement, bigger surface area and increased number of cells are needed with this chemistry, which increases the unit and specific cost. These trends of comparison between chemistries are consistent with what is reported in literature [104].

Figure 5.5 shows that for PHEV10, the optimum is obtained at the intersection of power and energy constraint. As pack energy requirement increases, the upper capacity bound becomes active. As shown in Figure 5.6, with PHEV60 relaxing the upper bound on the capacity will improve the cost.

Table 5.4 Optimum design variables and cost for each chemistry and vehicle type.

	Cathode Thickness (μm)	# of bi-cell layers	Cathode width (mm)	# of cells per module	# of modules	Cell capacity (Ah)	Pack cost ($)	Pack specific cost ($/kWh)
NMC								
PHEV10	28.5	106.0	87.6	9.0	2.0	54.5	2274.4	631.8
PHEV30	83.4	38.0	87.8	19.0	2.0	57.3	2771.6	346.4
PHEV60	125.0	23.0	94.2	25.0	3.0	59.9	4247.9	257.4
BEV200	125.0	14.0	120.2	44.0	5.0	59.4	10640.3	221.7
NCA								
PHEV10	29.1	105.0	86.9	9.0	2.0	54.3	2281.8	633.8
PHEV30	85.0	40.0	83.5	13.0	3.0	55.7	2827.3	353.4
PHEV60	125.0	23.0	94.1	25.0	3.0	59.8	4374.6	265.1
BEV200	125.0	14.0	120.1	44.0	5.0	59.3	11007.9	229.3
LFP								
PHEV10	59.2	79.0	96.7	10.0	2.0	54.8	2345.0	651.4
PHEV30	125.0	37.0	100.0	14.0	3.0	58.0	3107.4	388.4
PHEV60	125.0	30.0	112.9	21.0	4.0	60.0	5393.1	326.9
BEV200	125.0	23.0	128.6	35.0	7.0	59.7	13694.0	285.4
LMO								
PHEV10	83.4	69.0	86.0	8.0	2.0	56.9	1886.9	524.1
PHEV30	125.0	36.0	99.4	17.0	2.0	59.5	2630.0	328.8
PHEV60	125.0	33.0	104.0	14.0	5.0	59.6	4292.9	260.2
BEV200	125.0	24.0	122.1	29.0	7.0	59.8	10793.7	224.9

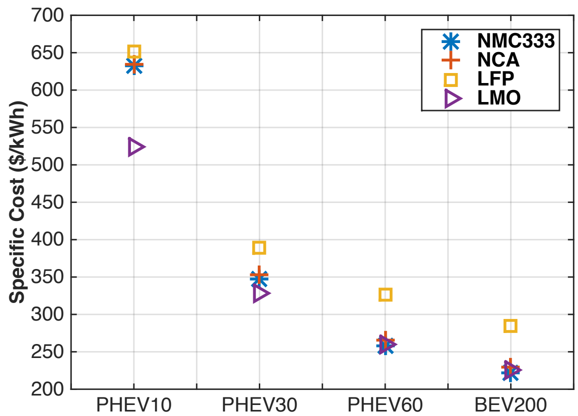

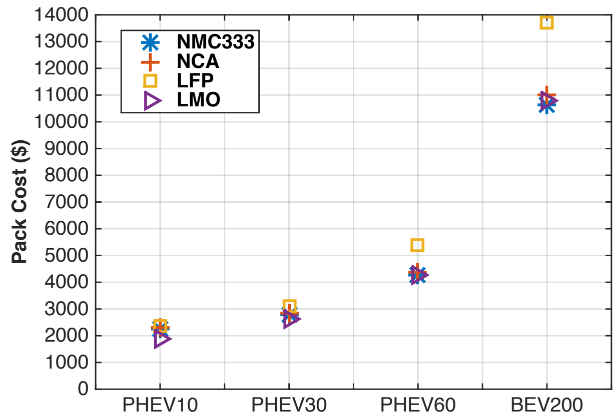

Figure 5.2 Battery cost comparison with 4 different cathode materials for 4 vehicle types. Left: specific cost (cost per kWh energy). Right: Pack cost

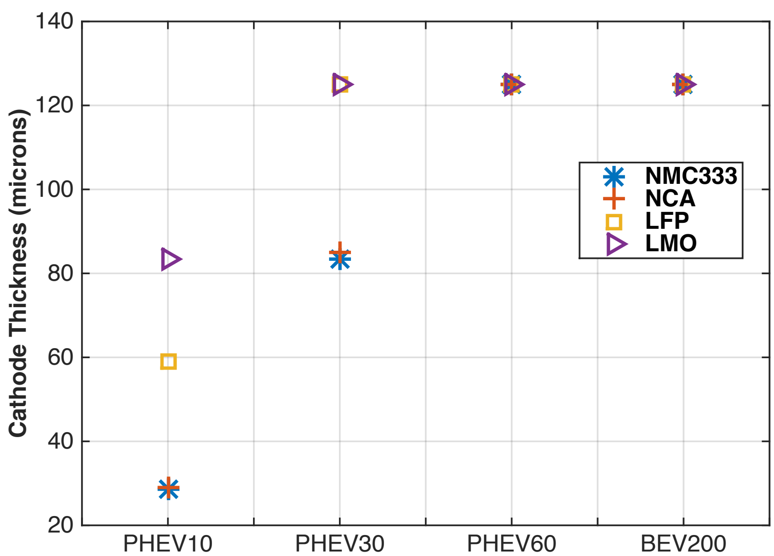

Figure 5.3 Cathode thickness at optimal design

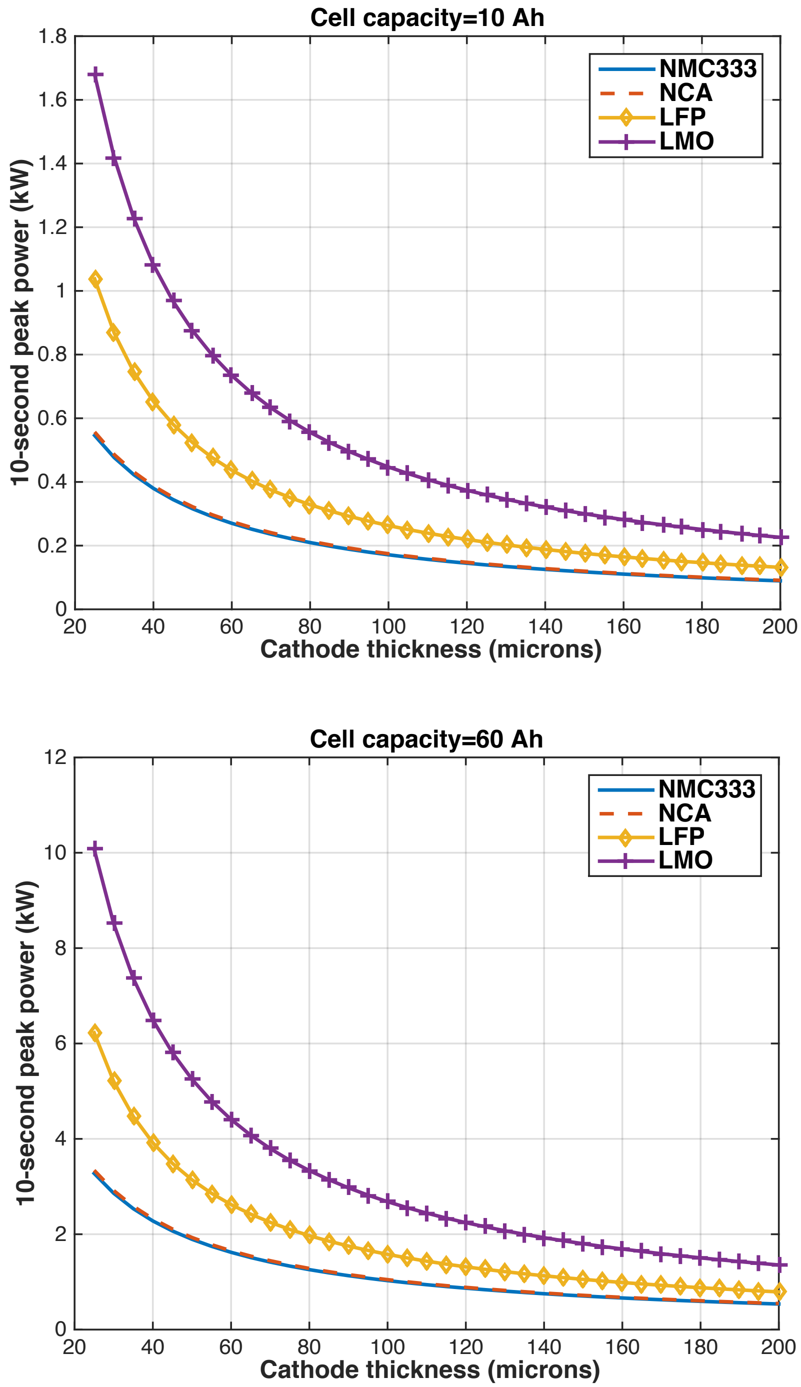

Figure 5.4 Comparison of power capabilities of cells with different cathode materials

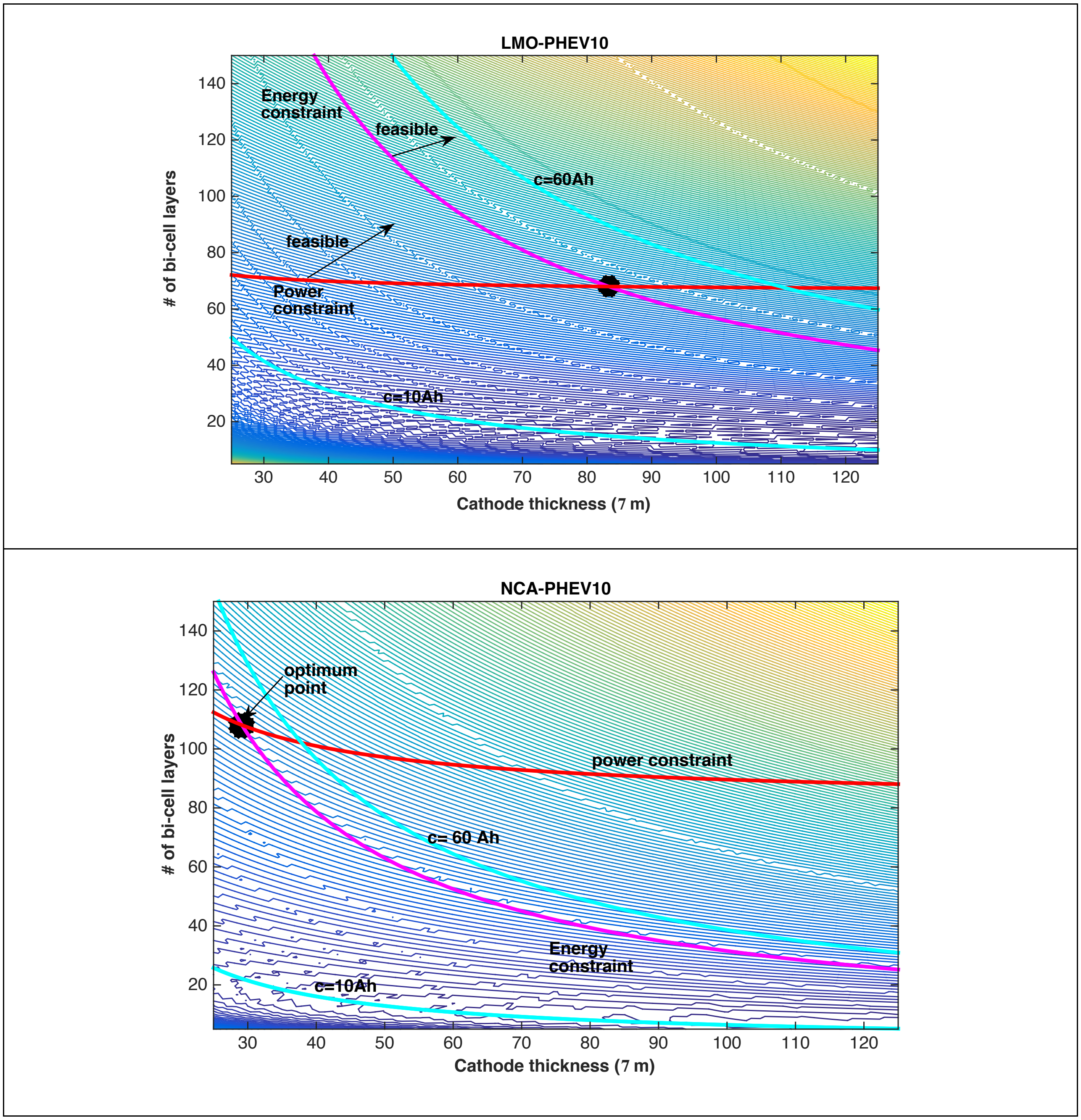

Figure 5.5 Contour plot of cost function with cathode thickness and # of bi-cell layers for the optimal PHEV10 design: Comparison of NCA and LMO. The feasible domain for both power and energy constraint is above the constraint line.

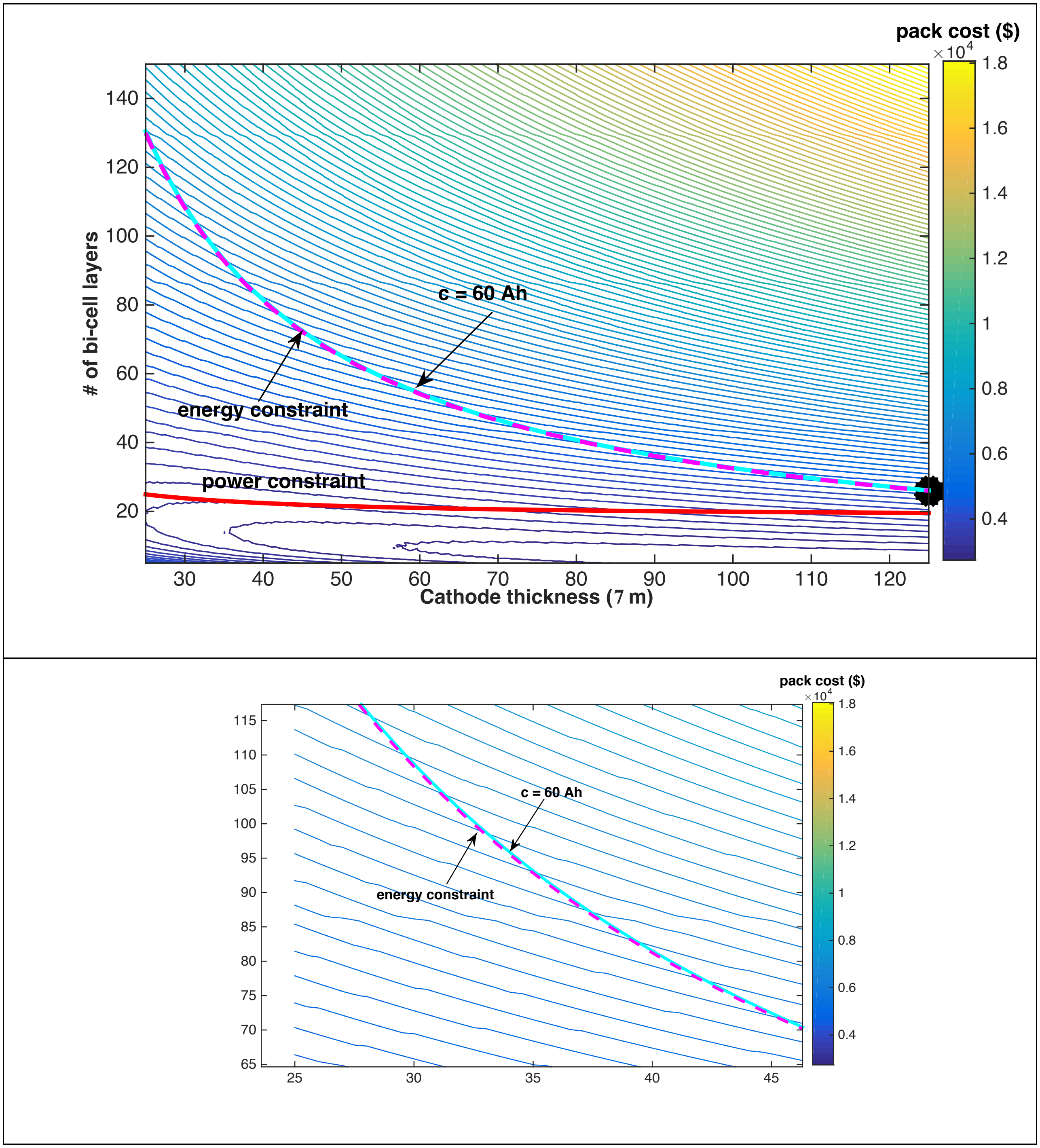

Figure 5.6 Contour plot of cost function with cathode thickness and # of bicell layers for the optimal PHEV60 design: NCA chemistry. The feasible domain for both power and energy constraint is above the constraint line.

5.3 Sensitivity Analysis

Most of the boundaries introduced in Table 5.1 are arbitrary for modeling purposes. However, there can still be restrictions to the minimum and maximum values of the variables. Sakti et al. discusses that, although manufacturers are able to produce cathode thicknesses up to 125 microns, thicker electrodes might generate defects and form cracks during drying. Too thin cells might be difficult to manufacture, and larger capacity cells are more prone to yield loss because more bi-cell layers must be stacked and wired [31]. Nelson et al. state that cell capacities of 200 Ah or larger are currently available for certain chemistries. However, it is not clear if a battery designer would select to combine smaller cells with parallel connections due to availability. They also argue that, it is not clear what will be the largest capacity cell in the near future [12]. All these in mind, we relax the boundaries upper bounds of the cathode thickness and cell capacity to repeat the optimization to see the effect of these bounds on the results. Table 5.5 shows the new relaxed boundaries and Table 5.6 shows the new optimum design variables and cost. For PHEV10, the optimum cathode thickness with relaxed boundaries remains the same as the original case whereas the number of modules decreases since the cell capacity increases. As the pack energy increases, the cathode thickness hits the upper bound again however the upper bound on the cell capacity is not active anymore for most of the cases. Figure 5.7 shows how the specific cost of the pack changes across different vehicles and chemistries with relaxed boundaries compared to the original case. The biggest reduction in cost occurs with BEV200.

Table 5.5 Relaxed boundaries for sensitivity analysis

	x^T	x^W	x^B	x^N	x^M	$c(\boldsymbol{x})$
Min.	25	1	1	1	1	10
Max	200	1000	1000	1000	1000	200

Table 5.6 LMO Optimal design variables and cost, after relaxed boundaries

	Cathode Thickness (μm)	# of bi-cell layers	Cathode width (mm)	# of cells per module	# of modules	Cell capacity (Ah)	Pack cost ($)	Pack specific cost ($/kWh)
NMC								
PHEV10	28.5	167.0	93.7	5.0	2.0	98.1	2241.5	622.6
PHEV30	83.4	94.0	99.3	6.0	2.0	181.6	2626.4	328.3
PHEV60	166.3	45.0	103.2	8.0	3.0	187.3	3709.4	224.8
BEV200	200.0	29.0	120.6	11.0	6.0	198.1	8513.0	177.4
NCA								
PHEV10	29.1	165.0	93.1	5.0	2.0	97.9	2249.6	624.9
PHEV30	85.0	92.0	99.3	6.0	2.0	181.2	2677.2	334.6
PHEV60	169.4	44.0	103.3	8.0	3.0	186.8	3828.6	232.0
BEV200	200.0	29.0	120.4	11.0	6.0	197.6	8889.6	185.2
LFP								
PHEV10	59.2	134.0	105.0	5.0	2.0	109.7	2306.2	640.6
PHEV30	145.9	73.0	110.2	5.0	3.0	162.5	2850.5	356.3
PHEV60	200.0	45.0	128.4	9.0	3.0	186.2	4330.1	262.4
BEV200	200.0	33.0	153.4	15.0	5.0	195.0	10512.7	219.0
LMO								
PHEV10	83.4	118.0	93.0	4.0	2.0	113.8	1852.1	514.5
PHEV30	200.0	63.0	100.0	4.0	3.0	168.6	2290.7	286.3
PHEV60	200.0	51.0	120.9	7.0	3.0	199.3	3553.3	215.4
BEV200	200.0	34.0	143.3	13.0	5.0	186.8	8273.8	172.4

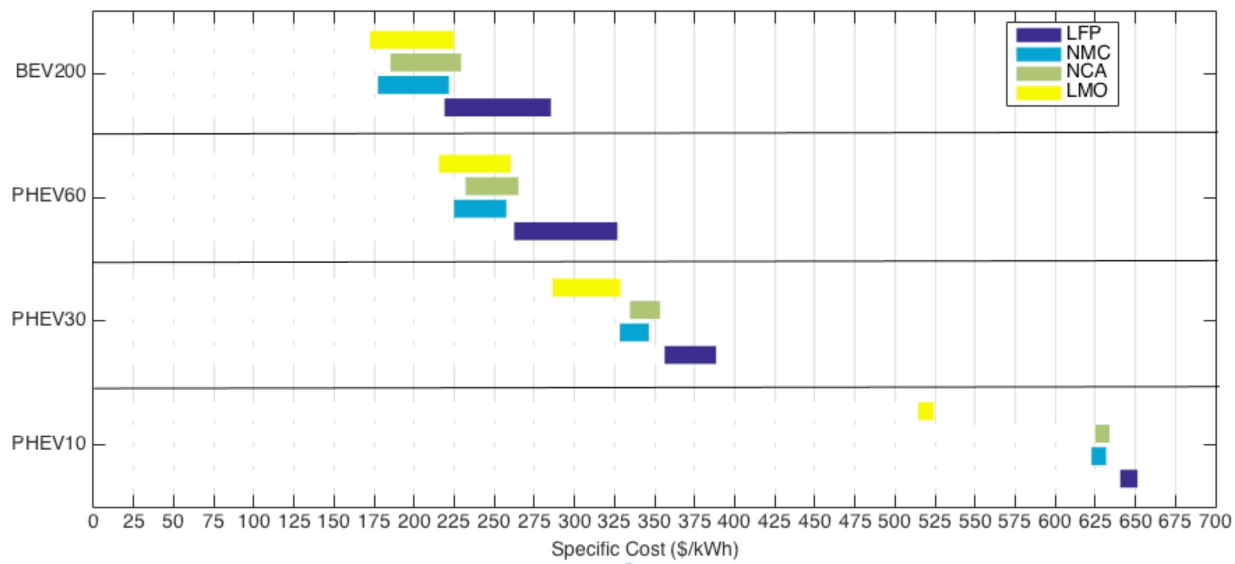

Figure 5.7 Specific cost change with relaxed upper boundaries. Left side of each bar represent the cost with relaxed boundaries and right side shows the cost with original boundaries

5.4 Limitations and Conclusion

This study introduces the optimal design problem for minimizing the cost of plug-in vehicle battery considering the design parameters cathode thickness, cell width, bi-cell layers, number of cells per module and number of modules, and the cell chemistry.

Results show that among different chemistries, LMO is the cheapest option, showing it as a good candidate. However, this study does not examine any other possible implications that might stem from chemistry choice. LMO has issues with Mn solubility, which affects cycle life, therefore it is not favorable for future electric vehicle applications [105].

For small batteries where high power-to-energy ratio is required, the optimum design occurs at the intersection of power and energy constraints. This point can shift based on the formulation used for power capability calculations. As energy requirement from the pack increases, the energy constraint becomes more dominant. Relaxing the capacity upper bound improves the results for bigger batteries. In addition, production volume might have different applications for different chemistries. Further investigation and case studies are necessary to examine the implications of : 1) lower and upper boundaries on design variables and capacity, 2) the model to estimate the power capability of the battery, 3) production volume.

Finally, in this study we assume cells and modules are connected in series only. Parallel connections can change the cell capacity requirement. In addition, parallel connections create additional costs due to increased number of cell terminals and interconnects and formation cycling units in the manufacturing facility [12].

6 Conclusions

In this thesis, a series of studies were presented to investigate battery life, range and emission benefits with a particular focus on the effect of temperature on these outcomes. In addition, driving cycle, thermal management and battery chemistry effects are examined in portion to understand these challenges. This chapter summarizes the contributions of the presented work, and makes suggestions for future research in the area.

6.1 Contributions

6.1.1 Methodological Contributions

The methodological contribution from Chapter 2 is introducing a method for modeling the interactions between powertrain operations, battery performance, vehicle and battery thermal behavior and battery degradation, to be used for estimating temperature effect on battery life.

Chapters 3 & 4 introduce a method to estimate regional variation in electrified vehicle range, efficiency and emissions by bringing together real world and test data for vehicle efficiency, climate, driving patterns and marginal emission factors.

The methodological contribution of Chapter 5 is the solution of the MINLP problem of optimizing battery design that minimizes the production cost by using a branch-and-bound algorithm.

6.1.2 Applicative Contributions

Applicative contributions from Chapter 2 include comparison of temperature and various usage scenarios in terms of their effects on battery life and quantification the improvement by use of air-cooling as battery thermal management. Results suggest that, aggressive driving can decrease battery life by ~70% compared to real world driving profiles obtained from GPS data. This decrease in battery life with aggressive driving drops to 40% when air cooling is employed, indicating that the effect of temperature increase is reduced by conditioning the battery however the charge/discharge rates during driving can still cause significant difference. Regional climate will have a noteworthy effect on battery life if thermal management is not used. Battery life in Phoenix is 25% lower than life in San Francisco, however use of thermal management reduces this difference.

The applicative contribution of the study introduced in Chapter is the quantification of the effect of regional temperature variances on BEV range, efficiency and emissions. In climates with hot temperature peaks, or in cold climates, the range can drop by 29-36%. Average vehicle energy consumption in Upper Midwest can increase by 15% compared to Pacific Coast or Florida. The main factor that affects regional differences in emissions is the grid mix, however temperature can still create up to 22% difference.

Applicative contributions from Chapter 4 include comparison of light-duty vehicle technologies for personal use in terms of their average GHG emissions and investigating the factors that affect this comparison. Results suggest that compared to Toyota Prius, Nissan Leaf reduces emissions across most of the US except for rural highway drivers of Midwest and South. While Prius PHEV decreases emissions everywhere when compared to Toyota Prius, Volt on the other hand increases emissions everywhere. Charging in the midnight rather than upon arrival at time increases GHG emissions of PEVs. Temperature and driving cycles affect the relative benefits of PEVs over HEVs.

Finally, the applicative contribution of the study presented in Chapter 5 is identifying and comparing the cost minimizing design variables for different chemistries. Results indicate that LMO is the cheapest option for all cases investigated and LFP is the most expensive option except for PHEV10. Increasing the cathode thickness decreases the cost for all chemistries.

6.2 Open Questions and Suggestions for Future Work

Limitations and future work suggestions for each individual study are provided at the end of the corresponding chapter. There are still many open questions that remain beyond the scope of this dissertation that need to be investigated to fully address the research questions proposed in the beginning. Table 6.1 aims to summarize the portions of the questions addressed in this dissertation, as well as some other areas that can be investigated.

Hot temperatures are found to be significantly important both for life and range, efficiency and emissions benefits. Battery life analysis has been performed for a PHEV, and a case study with a bigger pack size showed that, the effect might not be as significant for BEVs. However, the study in Chapter 3 showed that cold temperatures can cause significant reduction in BEV efficiency, because battery load increases due to cabin heating requirements. This extra load at extreme cold temperatures won't be significant enough to create significant degradation differences in BEVs and in PHEVs, the heating load will be lower due to available excess engine heat. However, cold temperatures can affect battery life since they can create different degradation mechanisms. Although it is not clear if the degree of this effect will be as high as it is at hot temperatures, it is worth investigating for a complete regional assessment of climate. In addition, although not explicitly shown in Table 6.1, battery life and range and emission benefits are related, since as battery experiences capacity and power fade, the efficiency will decrease, affecting the range and emissions benefits. This issue should be taken into account for a complete picture of temperature effect. The lifetime cost of operating electrified vehicles under the temperature effect should also be incorporated.

Air-cooling is shown to play an important role in increasing battery life in small pack PHEVs. However, the improvement should also be investigated for higher pack batteries. Furthermore, to fully understand thermal management benefit more needs to be done. Liquid cooling option should also be examined. In addition, heating the batteries might be a good solution for the efficiency loss problem in the cold temperatures that needs to be considered in the analyses. The trade-off between the benefits and cost advantages/disadvantages of employing different strategies remains a significant open question. For example, liquid cooling might provide better cooling characteristics, however it is more expensive and it adds more load on the battery, increasing the operational costs. In addition, this tradeoff can also change with vehicle technology and battery chemistry. A full trade-off analysis should cover all these issues.

Chapter 2 focuses on a LFP chemistry PHEV pack with 5 kWh capacity to investigate life benefits, and Chapter 5 shows that LFP is a moderate cost alternative for a PHEV10 with a 3.6 kWh battery. In the context of the studies performed, selection of the LFP in battery life study is not inconsistent with the cost benefits. However, LMO is still a cheaper option in terms of production cost. Furthermore, for all other vehicles considered in Chapter 5, LFP is the highest cost option. On the other hand, LFP shows good battery life characteristics as shown in

Chapter 2 unless it is used with very aggressive driving without cooling. Therefore, it is still possible that LFP lifetime cost might be better compared to alternatives. To determine this, the battery life studies can be performed for other chemistries as well, and the study in Chapter 5 can be extended to estimate lifetime cost rather than the production cost.

Different chemistries might cause the temperature effect on EV range and emissions benefits to vary as well. Although the battery efficiency loss is a smaller portion of range loss at cold temperatures compared to heater use, different chemistries can show different performance characteristics with temperature, which might worth considering.

In the end, this dissertation accomplishes to address only a small portion of the challenges in further adoption of electrified vehicles by creating models and comparing various scenarios. It is author's hope that this dissertation can provide necessary knowledge and guidance in literature for the future research towards overcoming challenges in electrification of transportation.

Table 6.1 Summary of key findings and open areas for further investigation

	Battery Life	Range/Efficiency/ Emissions	Cost	
			Production Cost	Lifetime Cost
Regional Climate				
Hot temperature	☑ In hot climates battery life can decrease by 46% for batteries with LFP chemistry	☑ Range can drop by 29% in hot regions and by 36% in cold regions compared to mild climates. Overall, energy consumption and emissions can increase by 15 and 22% respectively based on regional climate.		☐
Cold Temperature	☐			☐
Thermal Management				
Air Cooling	☑ Air-cooling can improve battery life by 2 to 8 times depending on region and drive cycle.	☐	☐	☐
Liquid Cooling	☐	☐	☑	☐
Heating	☐	☐	☐	☐
Battery Chemistry				
LFP	More than 15 years of life can be obtained if thermally controlled. For aggressive driving, the battery life can be much shorter.	☐	For a BEV200 specific cost range: 219 – 285 $/kWh	☐
NCA	☐	☐	185-229 $/kWh	☐
LMO	☐	☐	172-225 $/kWh	☐
NMC	☐	☐	177-235 $/kWh	☐

References

[1] J.J. Michalek, M. Chester, P. Jaramillo, C. Samaras, C.-S.N. Shiau, L.B. Lave, Valuation of plug-in vehicle life-cycle air emissions and oil displacement benefits., Proc. Natl. Acad. Sci. U. S. A. 108 (2011) 16554–8. doi:10.1073/pnas.1104473108.

[2] T.R. Hawkins, O.M. Gausen, A.H. Strømman, Environmental impacts of hybrid and electric vehicles—a review, Int. J. Life Cycle Assess. 17 (2012) 997–1014. doi:10.1007/s11367-012-0440-9.

[3] U.S. Environmental Protection Agency, Inventory of U.S. Greenhouse Gas Emissions and Sinks: 1990-2012, Washington, DC, 2014.

[4] C. Knittel, Reducing petroleum consumption from transportation, J. Econ. Perspect. 26 (2012) 93–118. doi:10.1257/jep.26.1.93.

[5] J.J. Michalek, M. Chester, P. Jaramillo, C. Samaras, C.-S.N. Shiau, L.B. Lave, Valuation of plug-in vehicle life-cycle air emissions and oil displacement benefits., Proc. Natl. Acad. Sci. U. S. A. 108 (2011) 16554–8. doi:10.1073/pnas.1104473108.

[6] J. Axsen, K. Kurani, The Early U.S. Market for PHEVs: Anticipating Consumer Awareness, Recharge Potential, Design Priorities and Energy Impacts, 2008.

[7] J.P. Helveston, Y. Liu, E.M. Feit, E. Fuchs, E. Klampfl, J. Michalek, Will Subsidies Drive Electric Vehicle Adoption? Measuring Consumer Preferences in the U.S. and China, n.d.

[8] J. Neubauer, A. Brooker, E. Wood, Sensitivity of battery electric vehicle economics to drive patterns, vehicle range, and charge strategies, J. Power Sources. 209 (2012) 269–277. doi:10.1016/j.jpowsour.2012.02.107.

[9] S. Plotkin, M. Singh, Multi-path transportation futures study: vehicle characterization and scenario analyses., 2009. http://www.osti.gov/bridge/product.biblio.jsp?osti_id=968962 (accessed May 29, 2014).

[10] Hernandez E., 48 kWh LEAF in your future?, 2013. http://livingleaf.info/2013/10/48-kwh-leaf-in-your-future/ (accessed July 1, 2015)

[11] D. Linden, T.B. Reddy, Handbook of Batteries, 2001. doi:10.1016/0378-7753(86)80059-3.

[12] P. a. Nelson, K.G. Gallagher, I. Bloom, D.W. Dees, Modeling the Performance and Cost of Lithium-Ion Batteries for Electric-Drive Vehicles Chemical Sciences and Engineering Division, (2012).

[13] A. Barré, B. Deguilhem, S. Grolleau, M. Gérard, F. Suard, D. Riu, A review on lithium-ion battery ageing mechanisms and estimations for automotive applications, J. Power Sources. 241 (2013) 680–689. doi:10.1016/j.jpowsour.2013.05.040.

[14] J. Vetter, P. Novák, M.R. Wagner, C. Veit, K.-C. Möller, J.O. Besenhard, et al., Ageing mechanisms in lithium-ion batteries, J. Power Sources. 147 (2005) 269–281. doi:10.1016/j.jpowsour.2005.01.006.

[15] J. Groot, M. Swierczynski, A.I. Stan, S.K. Kær, On the complex ageing characteristics of high-power LiFePO4/graphite battery cells cycled with high charge and discharge currents, J. Power Sources. 286 (2015) 475–487. doi:10.1016/j.jpowsour.2015.04.001.

[16] M.B. Pinson, M.Z. Bazant, Theory of SEI Formation in Rechargeable Batteries: Capacity Fade, Accelerated Aging and Lifetime Prediction, J. Electrochem. Soc. 160 (2012) A243–A250. doi:10.1149/2.044302jes.

[17] R. Deshpande, M. Verbrugge, Y.-T. Cheng, J. Wang, P. Liu, Battery Cycle Life Prediction with Coupled Chemical Degradation and Fatigue Mechanics, J. Electrochem. Soc. 159 (2012) A1730–A1738. doi:10.1149/2.049210jes.

[18] D. Li, D. Danilov, Z. Zhang, H. Chen, Y. Yang, P.H.L. Notten, Modeling the SEI-Formation on Graphite Electrodes in LiFePO4 Batteries, J. Electrochem. Soc. 162 (2015) A858–A869. doi:10.1149/2.0161506jes.

[19] USABC Electric Vehicle Battery Test Procedures Manual, Revision 2, 1996, http://avt.inl.gov/battery/pdf/usabc_manual_rev2.pdf

[20] S. Saxena, C. Le Floch, J. MacDonald, S. Moura, Quantifying EV battery end-of-life through analysis of travel needs with vehicle powertrain models, J. Power Sources. 282 (2015) 265–276. doi:10.1016/j.jpowsour.2015.01.072.

[21] M. Broussely, S. Herreyre, P. Biensan, Aging mechanism in Li ion cells and calendar life predictions, J. Power …. 98 (2001) 13–21. http://www.sciencedirect.com/science/article/pii/S0378775301007224 (accessed December 12, 2012).

[22] E. Thomas, I. Bloom, J. Christophersen, V. Battaglia, Statistical methodology for predicting the life of lithium-ion cells via accelerated degradation testing, J. Power Sources. 184 (2008) 312–317. doi:10.1016/j.jpowsour.2008.06.017.

[23] P. Liu, J. Wang, J. Hicks-Garner, E. Sherman, S. Soukiazian, M. Verbrugge, et al., Aging Mechanisms of LiFePO[sub 4] Batteries Deduced by Electrochemical and Structural Analyses, J. Electrochem. Soc. 157 (2010) A499. doi:10.1149/1.3294790.

[24] M. Allen, Electric Range for the Nissan Leaf & Chevrolet Volt in Cold Weather, http://news.fleetcarma.com/2013/12/16/nissan-Leaf-Chevrolet-Volt-Cold-Weather-Range-Loss-Electric-Vehicle/. (2013). http://news.fleetcarma.com/2013/12/16/nissan-leaf-chevrolet-volt-cold-weather-range-loss-electric-vehicle/ (accessed April 15, 2014).

[25] A.A. Pesaran, Battery Thermal Management In Ev And Hevs: Issues And Solutions, Batter. Man. 43 (2001) 34–49. http://www.nrel.gov/vehiclesandfuels/energystorage/pdfs/aabc_lv.pdf (accessed December 12, 2012).

[26] T. Yuksel, J.J. Michalek, Electric Vehicle LiFePO4 Battery Life Implications of Thermal Management, Driving Conditions, and Regional Climate, 2015 (working paper).

[27] T. Yuksel, J. Michalek, Development of a Simulation Model to Analyze the Effect of Thermal Management on Battery Life, SAE Tech. Pap. (2012). doi:10.4271/2012-01-0671.

[28] J. Axsen, A.. Burke, K.S. Kurani, Batteries for PHEVs: Comparing Goals and State of Technology, in: G. Pistoia (Ed.), Electr. Hybrid Veh. Sources, Model. Infrastruct. Mark., Elsevier, 2010: pp. 405–427.

[29] M. Delucchi, T. Lipman, Lifetime cost of battery, fuel-cell, and plug-in hybrid electric vehicles, in: Electr. Hybrid Veh. Sources, Model. Infrastruct. Mark., 2010: pp. 19–60.

[30] T. Markel, A. Brooker, J. Gonder, M.O. Keefe, A. Simpson, M. Thornton, Plug-In Hybrid Vehicle Analysis Plug-In Hybrid Vehicle Analysis, 2006.

[31] A. Sakti, J.J. Michalek, E.R.H. Fuchs, J.F. Whitacre, A techno-economic analysis and optimization of Li-ion batteries for personal vehicle electrification, n.d.

[32] C.-S.N. Shiau, N. Kaushal, C.T. Hendrickson, S.B. Peterson, J.F. Whitacre, J.J. Michalek, Optimal Plug-In Hybrid Electric Vehicle Design and Allocation for Minimum Life Cycle Cost, Petroleum Consumption, and Greenhouse Gas Emissions, J. Mech. Des. 132 (2010) 091013. doi:10.1115/1.4002194.

[33] A. Pesaran, T. Markel, H. Tataria, D. Howell, Battery Requirements for Plug-in Hybrid Electric Vehicles--analysis and Rationale, 2009. http://www.nrel.gov/docs/fy09osti/42240.pdf (accessed December 12, 2012).

[34] M. Broussely, Battery Requirements for HEVs, PHEVs, and EVs: An Overview, in: Electr. Hybrid Veh. Sources, Model. Infrastruct. Mark., 2010: pp. 305–347.

[35] Y. Zhang, C.-Y. Wang, X. Tang, Cycling degradation of an automotive LiFePO4 lithium-ion battery, J. Power Sources. 196 (2011) 1513–1520. doi:10.1016/j.jpowsour.2010.08.070.

[36] K. Amine, J. Liu, I. Belharouak, High-temperature storage and cycling of C-LiFePO/graphite Li-ion cells, Electrochem. Commun. 7 (2005) 669–673. doi:10.1016/j.elecom.2005.04.018.

[37] S.B. Peterson, J. Apt, J.F. Whitacre, Lithium-ion battery cell degradation resulting from realistic vehicle and vehicle-to-grid utilization, J. Power Sources. 195 (2010) 2385–2392. doi:10.1016/j.jpowsour.2009.10.010.

[38] A123 Systems Inc., Development of Battery Packs for Space Applications About A123Systems, NASA Aerospace Battery Workshop, November 27-29, 2007.

[39] S. Grolleau, A. Delaille, H. Gualous, P. Gyan, R. Revel, J. Bernard, et al., Calendar aging of commercial graphite/LiFePO4 cell – Predicting capacity fade under time dependent storage conditions, J. Power Sources. (2013). doi:10.1016/j.jpowsour.2013.11.098.

[40] Y. Zheng, Y.-B. He, K. Qian, B. Li, X. Wang, J. Li, et al., Effects of state of charge on the degradation of LiFePO4/graphite batteries during accelerated storage test, J. Alloys Compd. 639 (2015) 406–414. doi:10.1016/j.jallcom.2015.03.169.

[41] A123 Systems Inc., High Power Lithium Ion ANR26650M1A, 2010.

[42] J. Wang, P. Liu, J. Hicks-Garner, E. Sherman, S. Soukiazian, M. Verbrugge, et al., Cycle-life model for graphite-LiFePO4 cells, J. Power Sources. 196 (2011) 3942–3948. doi:10.1016/j.jpowsour.2010.11.134.

[43] N. Omar, M.A. Monem, Y. Firouz, J. Salminen, J. Smekens, O. Hegazy, et al., Lithium iron phosphate based battery – Assessment of the aging parameters and development of cycle life model, Appl. Energy. 113 (2014) 1575–1585. doi:10.1016/j.apenergy.2013.09.003.

[44] H. Song, Z. Cao, X. Chen, H. Lu, M. Jia, Z. Zhang, et al., Capacity fade of LiFePO4/graphite cell at elevated temperature, J. Solid State Electrochem. 17 (2012) 599–605. doi:10.1007/s10008-012-1893-2.

[45] Z. Li, L. Lu, M. Ouyang, Y. Xiao, Modeling the capacity degradation of LiFePO4/graphite batteries based on stress coupling analysis, J. Power Sources. 196 (2011) 9757–9766. doi:10.1016/j.jpowsour.2011.07.080.

[46] S. Chen, C. Wan, Y. Wang, Thermal analysis of lithium-ion batteries, J. Power Sources. 140 (2005) 111–124. doi:10.1016/j.jpowsour.2004.05.064.

[47] C. Forgez, D. Vinh Do, G. Friedrich, M. Morcrette, C. Delacourt, Thermal modeling of a cylindrical LiFePO4/graphite lithium-ion battery, J. Power Sources. 195 (2010) 2961–2968. doi:10.1016/j.jpowsour.2009.10.105.

[48] U. Iraola, I. Aizpuru, J.M. Canales, a Etxeberria, I. Gil, Methodology for thermal modelling of lithium- ion batteries, (2013) 6750–6755.

[49] A. Tourani, P. White, P. Ivey, A multi scale multi-dimensional thermo electrochemical modelling of high capacity lithium-ion cells, J. Power Sources. 255 (2014) 360–367. doi:10.1016/j.jpowsour.2014.01.030.

[50] X. Zhang, Thermal analysis of a cylindrical lithium-ion battery, Electrochim. Acta. 56 (2011) 1246–1255. doi:10.1016/j.electacta.2010.10.054.

[51] K. Buford, J. Williams, M. Simonini, Determining Most Energy Efficient Cooling Control Strategy of a Rechargeable Energy Storage System, (2011). doi:10.4271/2011-01-0893.

[52] J. Bakker, Pack level design optimization for electric vehicle thermal management systems minimizing, (2013), Master of Science Thesis.

[53] O. Gross, S. Clark, Optimizing Electric Vehicle Battery Life through Battery Thermal Management, Gener. J. Am. Soc. Aging. (2011). doi:10.4271/2011-01-1370.

[54] K. Smith, M. Earleywine, E. Wood, Comparison of Plug-In Hybrid Electric Vehicle Battery Life Across Geographies and Drive Cycles, SAE Technical Paper (2012). http://www.nrel.gov/vehiclesandfuels/energystorage/pdfs/53817.pdf (accessed December 15, 2012).

[55] J. Neubauer, E. Wood, Thru-life impacts of driver aggression, climate, cabin thermal management, and battery thermal management on battery electric vehicle utility, J. Power Sources. 259 (2014) 262–275. doi:10.1016/j.jpowsour.2014.02.083.

[56] NREL: Vehicles and Fuels Research - Secure Transportation Data Center, http://www.nrel.gov/vehiclesandfuels/secure_transportation_data.html.

[57] E. Traut, C. Hendrickson, E. Klampfl, Y. Liu, J.J. Michalek, Optimal design and allocation of electrified vehicles and dedicated charging infrastructure for minimum life cycle greenhouse gas emissions and cost, Energy Policy. 51 (2012) 524–534. doi:10.1016/j.enpol.2012.08.061.

[58] U. EPA, Dynamometer Drive Schedules | Testing and Measuring Emissions | US EPA, http://www.epa.gov/nvfel/testing/dynamometer.htm (accessed December 29, 2013).

[59] Hymotion L5 Plug-in Conversion Module Spec Sheet, 2009, http://www.proauto1.com/pdf/L5_SpecSheet.pdf (accessed September 2011)

[60] J. Liu, H. Peng, Modeling and Control of a Power-Split, 16 (2008) 1242–1251.

[61] J. Liu, H. Peng, Z. Filipi, Modeling and Analysis of the Toyota Hybrid System, (2005) 24–28.

[62] Y. Ma, H. Teng, M. Thelliez, Electro-Thermal Modeling of a Lithium-ion Battery System, SAE Int. J. Engines. 3 (2010) 306–317.

[63] H.E. Perez, J.B. Siegel, X. Lin, A.G. Stefanopoulou, Y. Ding, M.P. Castanier, Parameterization and Validation of an Integrated Electro-Thermal Cylindrical LFP Battery Model, Vol. 3 Renew. Energy Syst. Robot. Robust Control. Single Track Veh. Dyn. Control. Stoch. Model. Control Algorithms Robot. Struct. Dyn. Smart Struct. (2012) 41–50. doi:10.1115/DSCC2012-MOVIC2012-8782.

[64] http://deepblue.lib.umich.edu/handle/2027.42/97341, (accessed January 2014)

[65] R.C. Kroeze, P.T. Krein, Electrical battery model for use in dynamic electric vehicle simulations, 2008 IEEE Power Electron. Spec. Conf. (2008) 1336–1342. doi:10.1109/PESC.2008.4592119.

[66] L. Lam, P. Bauer, E. Kelder, A practical circuit-based model for Li-ion battery cells in electric vehicle applications, 2011 IEEE 33rd Int. Telecommun. Energy Conf. (2011) 1–9. doi:10.1109/INTLEC.2011.6099803.

[67] H.E. Perez, J.B. Siegel, A.G. Stefanopoulou, JSME 2012 11th Motion and Vibration Conference ELECTRO-THERMAL CYLINDRICAL LFP BATTERY MODEL, in: 2012: pp. 1–10.

[68] M. Muratori, N. Ma, M. Canova, Y. Guezennec, A 1+1D THERMAL DYNAMIC MODEL OF A LI-ION BATTERY CELL, in: Proc. ASME Dyn. Syst. Control Conf., Cambridge, Massachusetts, 2010: pp. 625–631.

[69] G. Zhang, L. Cao, S. Ge, C. Wang, In Situ Measurement of Li-Ion Battery Internal Temperature, Meet. Abstr. 536 (2013) 2013. https://ecs.confex.com/ecs/224/webprogram/Abstract/Paper25308/B3-0538.pdf (accessed January 13, 2014).

[70] Y. Ye, Y. Shi, L.H. Saw, A. a. O. Tay, An electro-thermal model and its application on a spiral-wound lithium ion battery with porous current collectors, Electrochim. Acta. (2014). doi:10.1016/j.electacta.2013.12.122.

[71] K. Smith, A. Le, L. Chaney, NREL_PriusThermModel_xEV, 2012, personal communication.

[72] M. Zolot, A. Pesaran, M. Mihalic, Thermal Evaluation of Toyota Prius Battery Pack, in: Futur. Conf., 2002. http://www.nrel.gov/vehiclesandfuels/energystorage/pdfs/2a_2002_01_1962.pdf (accessed December 12, 2012).

[73] A123 Hymotion Animation, (2010). https://www.youtube.com/watch?v=5APr9sM3fVw.

[74] F.P. Incropera, D.P. DeWitt, Fundamentals of Heat and Mass Transfer, 1996.

[75] Dry Air Properties, http://www.engineeringtoolbox.com/dry-air-properties-d_973.html (accessed July 15, 2015).

[76] National Solar Radiation Data Base: 1991- 2005 Update: TMY3, (n.d.). http://rredc.nrel.gov/solar/old_data/nsrdb/1991-2005/tmy3/ (accessed April 16, 2014).

[77] R. Barnitt, A. Brooker, L. Ramroth, J. Rugh, K.A. Smith, Analysis of off-board powered thermal preconditioning in electric drive vehicles, in: 25th World Batter. Hybrid Fuel Cell Electr. Veh. Symp. Exhib., Shenzhen, China, 2010. http://www.nrel.gov/docs/fy11osti/49252.pdf (accessed August 1, 2014).

[78] T. Yuksel, J.J. Michalek, Effects of Regional Temperature on Electric Vehicle Efficiency, Range, and Emissions in the United States, Environ. Sci. Technol. 49 (2015) 3974–3980. doi:10.1021/es505621s.

[79] O. Karabasoglu, J. Michalek, Influence of driving patterns on life cycle cost and emissions of hybrid and plug-in electric vehicle powertrains, Energy Policy. 60 (2013) 445–461. doi:10.1016/j.enpol.2013.03.047.

[80] T. Reddy, Linden's Handbook of Batteries, 4th ed., McGraw_Hill, New York, New York, USA, 2011.

[81] K.R. Kambly, T.H. Bradley, Estimating the HVAC energy consumption of plug-in electric vehicles, J. Power Sources. 259 (2014) 117–124. doi:10.1016/j.jpowsour.2014.02.033.

[82] V.H. Johnson, Fuel Used for Vehicle Air Conditioning: A State-by-State Thermal Comfort-Based Approach, (2002). doi:10.4271/2002-01-1957.

[83] S.B. Peterson, J.F. Whitacre, J. Apt, Net air emissions from electric vehicles: the effect of carbon price and charging strategies., Environ. Sci. Technol. 45 (2011) 1792–7. doi:10.1021/es102464y.

[84] C. Samaras, K. Meisterling, Life cycle assessment of greenhouse gas emissions from plug-in hybrid vehicles: implications for policy., Environ. Sci. Technol. 42 (2008) 3170–6. http://www.ncbi.nlm.nih.gov/pubmed/18522090 (accessed November 10, 2014).

[85] J.S. Graff Zivin, M.J. Kotchen, E.T. Mansur, Spatial and temporal heterogeneity of marginal emissions: Implications for electric cars and other electricity-shifting policies, J. Econ. Behav. Organ. (2014) 1–21. doi:10.1016/j.jebo.2014.03.010.

[86] D. Anair, A. Mahmassani, State of charge: Electric vehicles' global warming emissions and fuel-cost savings across the United States, 2012. http://www.ucsusa.org/assets/documents/clean_vehicles/electric-car-global-warming-emissions-report.pdf (accessed April 15, 2014).

[87] D. Yawitz, A. Kenward, A Roadmap to Climate-Friendly Cars : 2013, 2013. http://assets.climatecentral.org/pdfs/ClimateFriendlyCarsReport_Final.pdf.

[88] M.-A.M. Tamayao, Urbanization and Vehicle Electrification in the U . S .: CO 2 Emissions Estimation and Implications for Climate Policy, Carnegie Mellon University, 2014.

[89] K. Siler-Evans, I.L. Azevedo, M.G. Morgan, Marginal emissions factors for the U.S. electricity system., Environ. Sci. Technol. 46 (2012) 4742–8. doi:10.1021/es300145v.

[90] K. Kambly, T.H. Bradley, Geographical and Temporal Differences in Electric Vehicle Range due to Cabin Conditioning Energy Consumption, J. Power Sources. (2014). doi:10.1016/j.jpowsour.2014.10.142.

[91] Advanced Technology Vehicle Lab Benchmarking - Level 1, (n.d.). http://www1.eere.energy.gov/vehiclesandfuels/pdfs/merit_review_2012/veh_sys_sim/vss030_lohsebusch_2012_o.pdf (accessed April 16, 2014).

[92] S. Wilcox, W. Marion, Users Manual for TMY3 Data Sets Users Manual for TMY3 Data Sets, 2008.

[93] NHTS Data Center, (n.d.). http://nhts.ornl.gov/download.shtml (accessed April 16, 2014).

[94] Nissan LEAF® Electric Car Charging, (n.d.). http://www.nissanusa.com/electric-cars/leaf/charging-range/charging/ (accessed July 30, 2014).

[95] Argonne TTRDC - D3 (Downloadable Dynamometer Database) - 2013 Nissan Leaf, (n.d.). http://www.transportation.anl.gov/D3/2012_nissan_leaf_electric.html (accessed January 28, 2015).

[96] 2013 Toyota Prius Energy and Environment Ratings, (n.d.). http://www.fueleconomy.gov/feg/Find.do?action=sbs&id=33324 (accessed January 30, 2015).

[97] O. US EPA, OAR, Clean Power Plan Proposed Rule, (n.d.). http://www2.epa.gov/carbon-pollution-standards/clean-power-plan-proposed-rule (accessed September 18, 2014).

[98] T. Yuksel, M.-A.M. Tamayao, C. Hendrickson, I.M.L. Azevedo, J.J. Michalek, Variation of Electric Vehicle Life Cycle Greenhouse Gas Reduction Potential across U.S. Counties due to Regional Electricity Sources, Driving Patterns, and Climate, (2015), (working paper).

[99] M.-A.M. Tamayao, J.J. Michalek, C. Hendrickson, I.M.L. Azevedo, Regional Variability and Uncertainty of Electric Vehicle Life Cycle CO_2 Emissions across the United States, Environ. Sci. Technol. (2015) 150630085437002. doi:10.1021/acs.est.5b00815.

[100] J. Neubauer, K. Smith, E. Wood, A. Pesaran, The Impact of Thermal Management, Geography, and Driving Habits on Plug-In Hybrid Electric Vehicle Battery Life and Economics, (2012).

[101] N. Meyer, I. Whittal, M. Christenson, A. Loiselle-Lapointe, The Impact of Driving Cycle and Climate on Electrical Consumption & Range of Fully Electric Passenger Vehicles, in: EVS26 - Int. Batter. Hybrid Fuel Cell Electr. Veh. Symp., Los Angeles, 2012.

[102] Argonne TTRDC - D3 (Downloadable Dynamometer Database), (n.d.). http://www.transportation.anl.gov/D3/ (accessed April 24, 2015).

[103] K.G. Gallagher, P. a. Nelson, D.W. Dees, Simplified calculation of the area specific impedance for battery design, J. Power Sources. 196 (2011) 2289–2297. doi:10.1016/j.jpowsour.2010.10.020.

[104] B. Barnett, J. Rempel, C. McCoy, S. Dalton-Castor, S. Sriramulu, PHEV and LEESS battery cost assessment, 2011. http://www1.eere.energy.gov/vehiclesandfuels/pdfs/merit_review_2011/electrochemical_storage/es001_barnett_2011_o.pdf.

[105] M.M. Doeff, Lawrence Berkeley National Laboratory Lawrence Berkeley National Laboratory, 2010.

[106] Interpolate scattered data - MATLAB griddata, (n.d.). http://www.mathworks.com/help/matlab/ref/griddata.html (accessed January 30, 2015).

[107] 2013 Nissan Leaf Fuel Economy Information, n.d. http://www.fueleconomy.gov/feg/Find.do?action=sbs&id=33558 (accessed April 16, 2014).

Appendix A. Supplemental Information for Plug-in Hybrid Electric Vehicle $LiFePO_4$ Battery Life Implications of Thermal Management, Driving Conditions, and Regional Climate

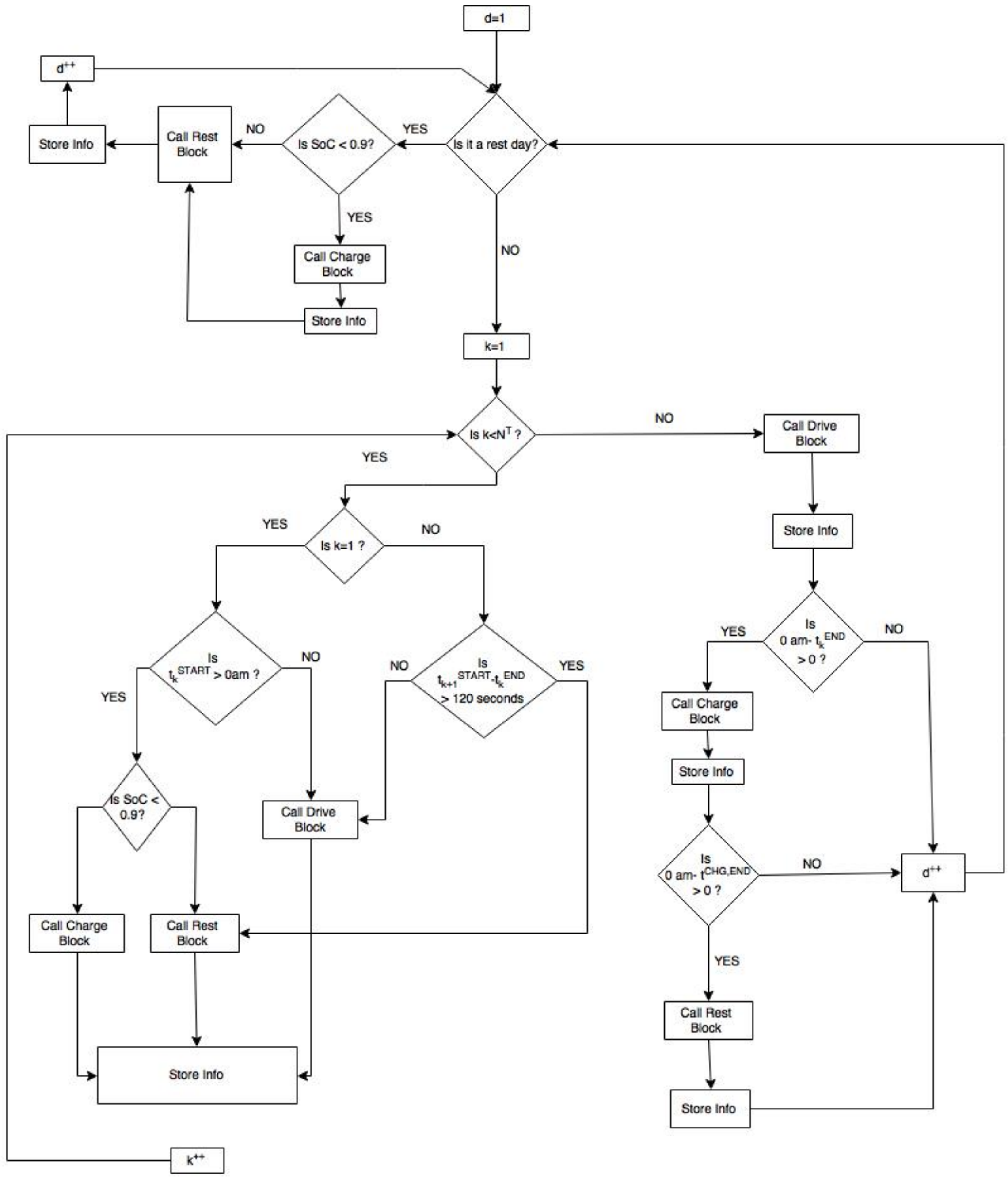

Figure A. 1 Decision Algorithm Schematic

Table A. 1 Parameters used in modeling and calculations

Parameter		Description	Model	Value
ψ^{VEH} (vehicle physical specs)	m^{VEH}	Vehicle mass	Performance	1355 kg
	C^{DRAG}	Vehicle drag coefficient	Performance	0.26
	A^{FRONT}	Vehicle frontal area	Performance	2.23 m^2
	C^{RR}	Vehicle tire rolling resistance coefficient	Performance	0.01
	η^{RB}	Efficiency of power transfer from regenerative braking to battery	Performance	0.4
	η^{BW}	Efficiency of power transfer from battery to wheels	Performance	0.8
ρ^{AIR}		Air density	Performance	1.23 kg/m^3
C^{RATED}		Cell rated capacity	Battery	2.3 Ah
$N^{\mathrm{CELL,PACK}}$		# of cells in the pack	Battery	616
$N^{\mathrm{CELL,PARALLEL}}$		# of cells connected in parallel	Battery	11
M^{CAB}		Vehicle cabin thermal mass	Thermal	101,771 J/K
M^{BAT}		Battery thermal mass	Thermal	45,500 J/K
K^{ac}		Inverse of the thermal resistance between cabin and ambient	Thermal	22.6
K^{ab}		Inverse of the thermal resistance between battery and ambient	Thermal	0.722
K^{cb}		Inverse of the thermal resistance between battery and cabin	Thermal	0.518

Appendix B. Supplemental Information for Effects Of Regional Temperature On Electric Vehicle Efficiency, Range and Emissions in the United States

1) Additional Details on Data and Analysis

In the main text, a brief description of each dataset is provided and the analysis approach is explained. We include additional details here.

Energy consumption versus temperature data: To find a relationship between energy consumption and ambient temperature, we use the Nissan Leaf average range versus ambient temperature data points provided by the Canadian company FleetCarma. The graph from which we obtained the data points is shown in Figure B. 1.

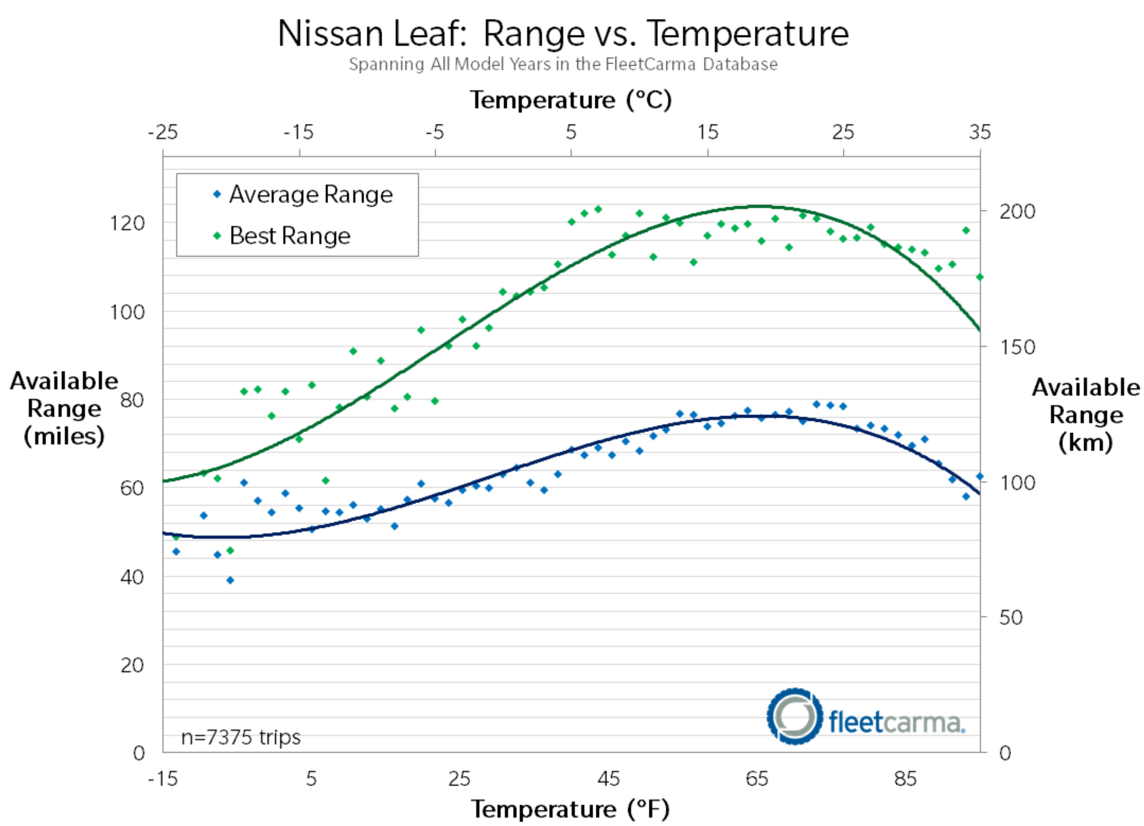

Figure B. 1 Nissan Leaf Range vs. Temperature graph as provided by FleetCarma [24]

In this study, we use the average range data points as shown with the blue dots in Figure B. 1. These data are collected via data loggers on vehicles across all North America for 7375 trips.

However, no specific details on the spatial resolution are provided. In our study, we convert each of the range data points s_i^{AER} to energy consumption per mile by using the relationship:

$$c_i = \frac{C^{\mathrm{BAT}}}{s_i^{\mathrm{AER}}} \tag{B.1}$$

where c_i refers to energy consumption per mile driven for data point i and C^{BAT} is the Nissan Leaf battery usable energy capacity. We then use the energy consumption versus ambient temperature information to obtain the functional relationship given in Equation (1) in the main text. Figure B. 2 shows the range data, as well as the energy consumption data points obtained using Equation (B.1).

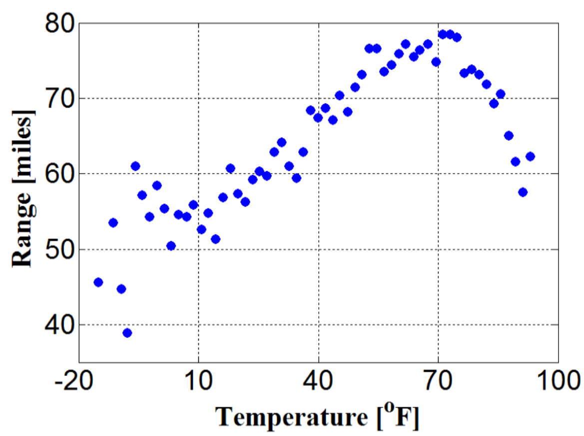

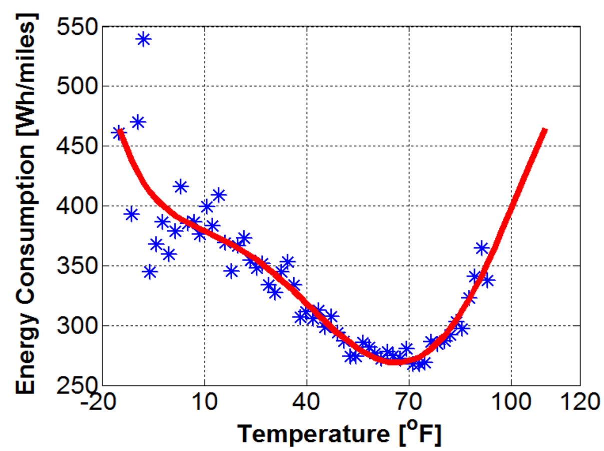

Figure B. 2 a) Nissan Leaf available range versus temperature data points from FleetCarma b) data points converted to energy consumption with function fit

Note that, the data points given in Figure B. 1 are obtained by measuring the energy consumption by data loggers and converting the data to range based on a battery capacity value. We lack information on FleetCarma's conversion method and assumption for battery capacity, however we do not expect the error in battery capacity assumption to change the relative effect of different temperatures.

Climate data. Figure B. 3 gives the locations of the stations where climate information in TMY3 was measured, as provided in the National Solar Radiation Data Base [76]. In our study, we make our estimations for each of these locations given in the map, and we show the results for the continental United States. To estimate the results at any location other than given in TMY3 results, we perform a triangulation-based cubic interpolation using the Matlab® function 'griddata'. [106]

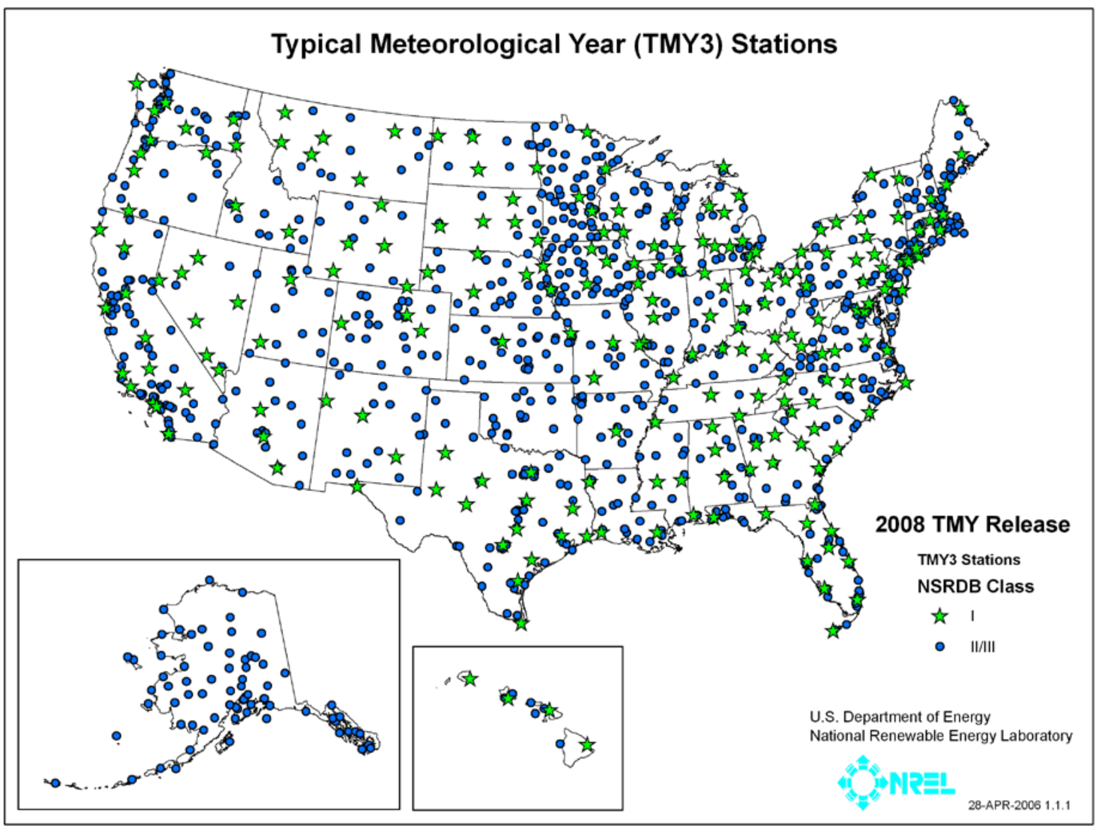

Figure B. 3 NREL TMY3 database measurement station locations

2) Sensitivity Analyses

In this section, we test several assumptions by simulating alternative cases.

Extrapolating range data. As mentioned in the main text, in this study we impose extrapolation limits to the ambient temperature vs. efficiency functional relationship. Here, we recompute the results without any lower or upper limits on extrapolation. The resulting daily range for selected cities is given in Figure B. 4. As can be seen from the figure, this approach does not cause any noticeable change in the results except in Rochester. In Rochester the average range on the worst day drops to 35 miles, about a 22% decrease from its previous value of 45 miles estimated in the main text.

The average range at the worst day of the year (day with the lowest predicted battery electric vehicle (BEV) range) calculated with the new approach in this section is plotted across the country in Figure B. 5. Looking at the figure, we see that the range of temperature values used in the calculations affect mainly cold regions, where it is possible to observe hourly temperatures less than -15ºF, the lower boundary used in the main text. There are only a few times per year when the temperature exceeds the upper data bound of 110ºF across the country, therefore hot climate regions are not affected from this change in the temperature range.

Note that in this study we only presented results for the continental US, although 86 of 1011 the location points mentioned in the main text are from Alaska and are from Hawaii. In addition, the most dramatic effect of temperature on range and energy consumption is observed in Alaska due to the cold climate. The worst-day range in Alaska is about 45 miles when using bounded extrapolation in the main text and drops to 8 miles when using full extrapolation. Given this wide uncertainty and the lack of data for extreme temperatures, we avoid making conclusions about range implications for Alaska.

We also recalculated the average energy consumption and average CO_2 emissions per mile using full extrapolation. However, the plots for these variables are not provided here since almost no change is observed in their values across the country. This might be explained by the fact that when these parameters are averaged over the year, the effect is negligible since temperatures fall outside the range of the data on only a small subset of days).

Figure B. 6 shows the expected vehicle range on an average day (rather than the worst day) across the fleet in each region. The plot uses bounded extrapolation, but results with full extrapolation are comparable.

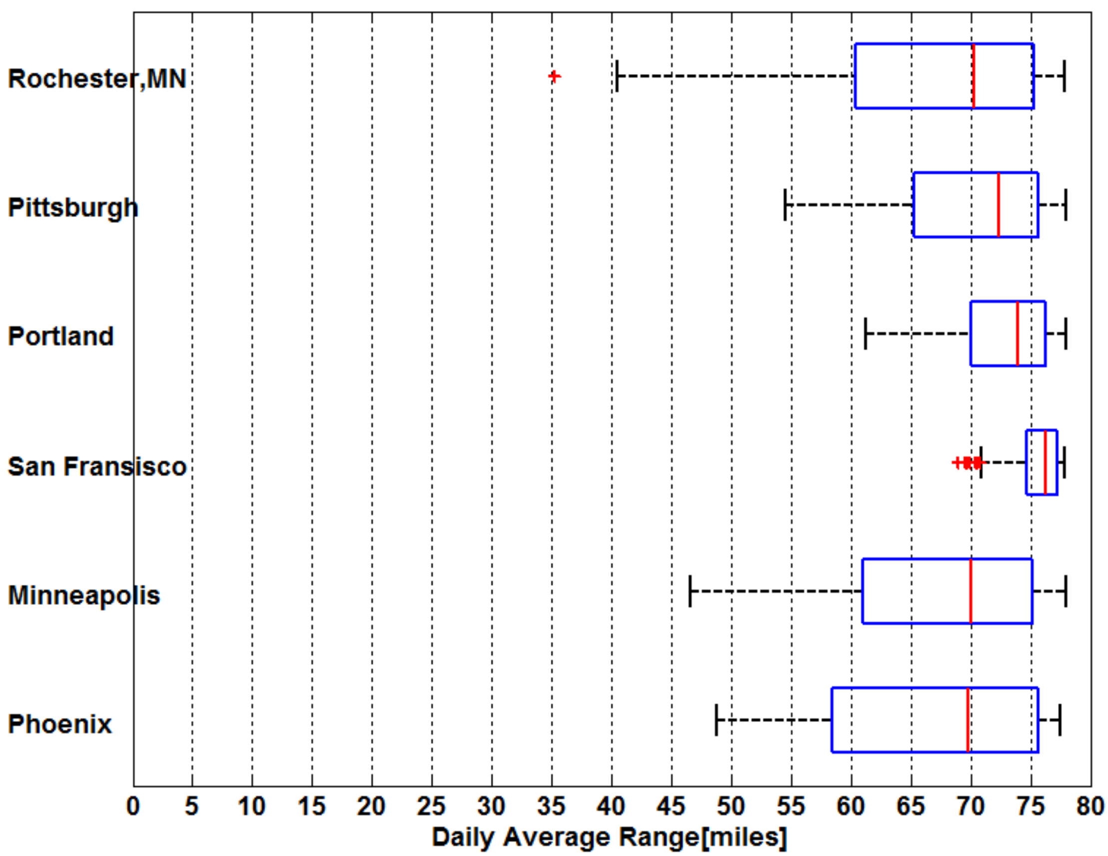

Figure B. 4 Updated daily driving range distribution for selected cities using full extrapolation

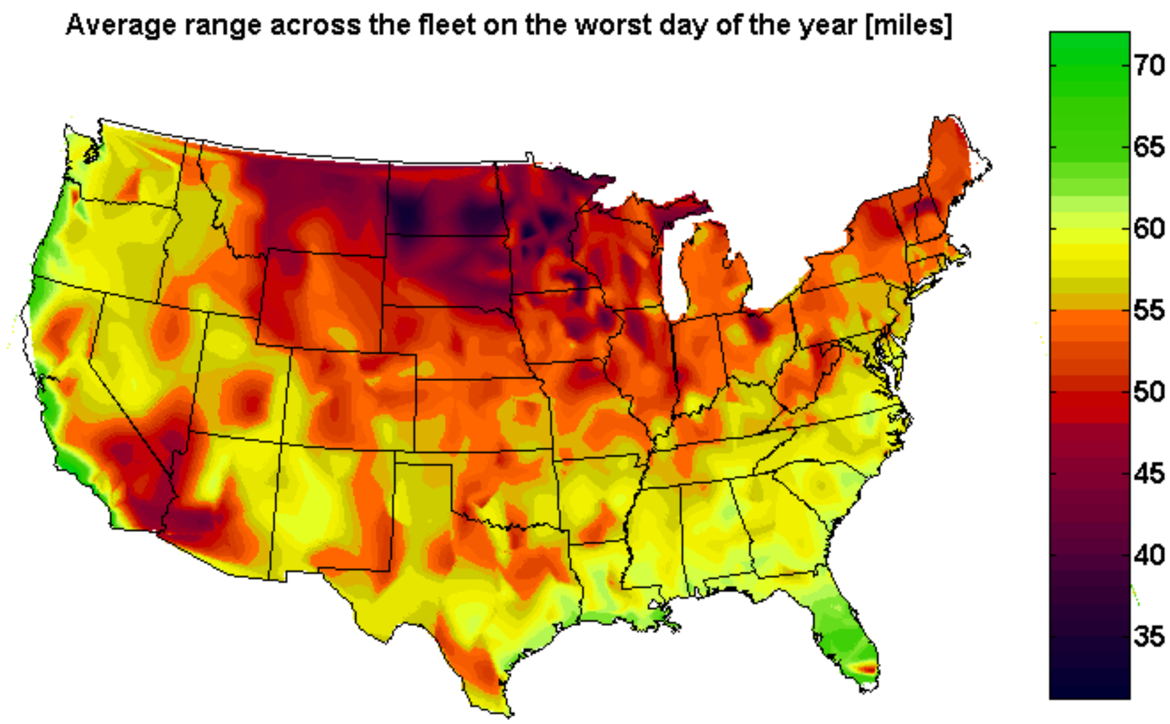

Figure B. 5 Average range across the fleet on the worst day of the year using full extrapolation

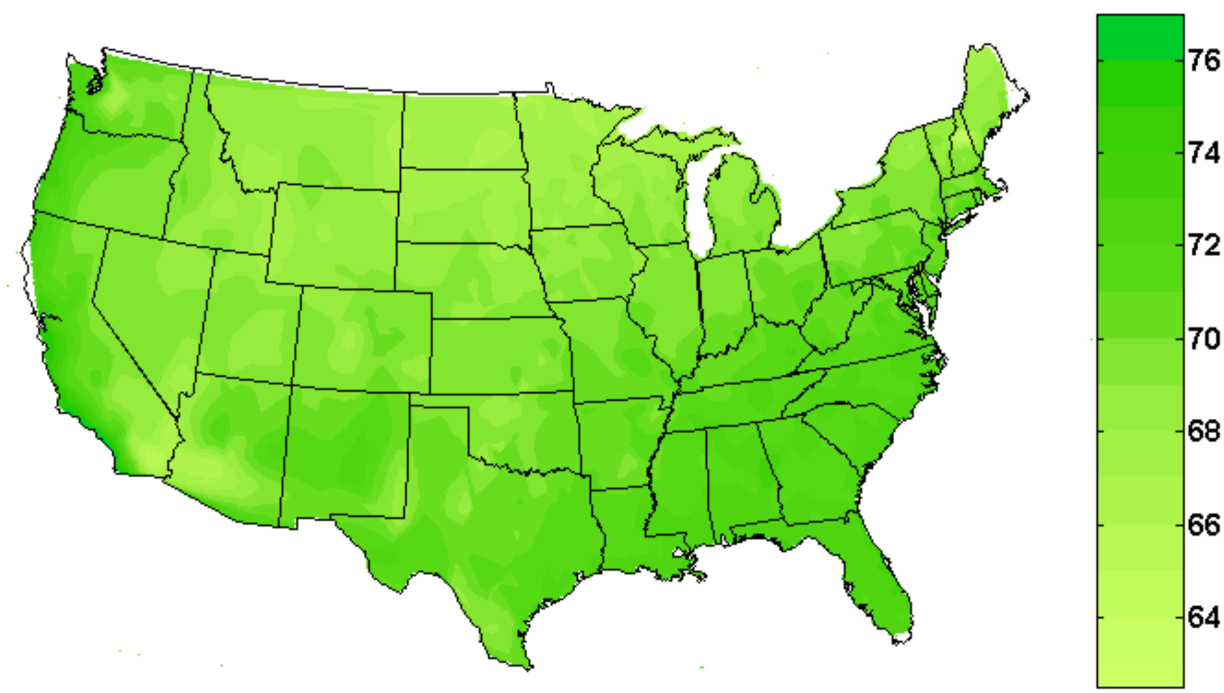

Figure B. 6 Expected range on an average day across the fleet (miles)

Expected range can drop to 64 miles in cold regions like the Upper Midwest and in hot regions like Southeast California and Southern Arizona. Therefore, the expected range in those regions is 11 miles less than the Environmental Protection Agency (EPA) rated 2013 Nissan Leaf range of 75 miles [107].

Battery Capacity. To understand the effect of battery size on the results, we repeated the simulations for an 85 kWh battery. In doing this, we assumed that the energy consumption per mile versus temperature relationship that we obtained in Equation (1) will still stay the same, i.e. increase in the capacity does not cause any change in vehicle and battery efficiency. Using the same ratio of usable capacity to actual capacity as the base case, we performed the simulations for a usable battery capacity of 74 kWh. The results for average range on the worst day are shown in Figure B. 7. As expected, we see an increase in the range; however the proportional reduction in range on the worst day remains similar for all locations. The average energy consumption shows a slight increase in most of the locations, with a maximum increase of 0.8%, since with increased battery capacity, more trips from NHTS are able to be completed, increasing the total energy consumption slightly. This affects emissions as well, and we see an increase in emissions in many locations as given in **Figure B. 8**. However, there are certain locations where we actually see about a 4% decrease in the emissions. This can be explained with the fact that, because the trip is longer now, the charging starts at a different time, when the emission factors may be lower.

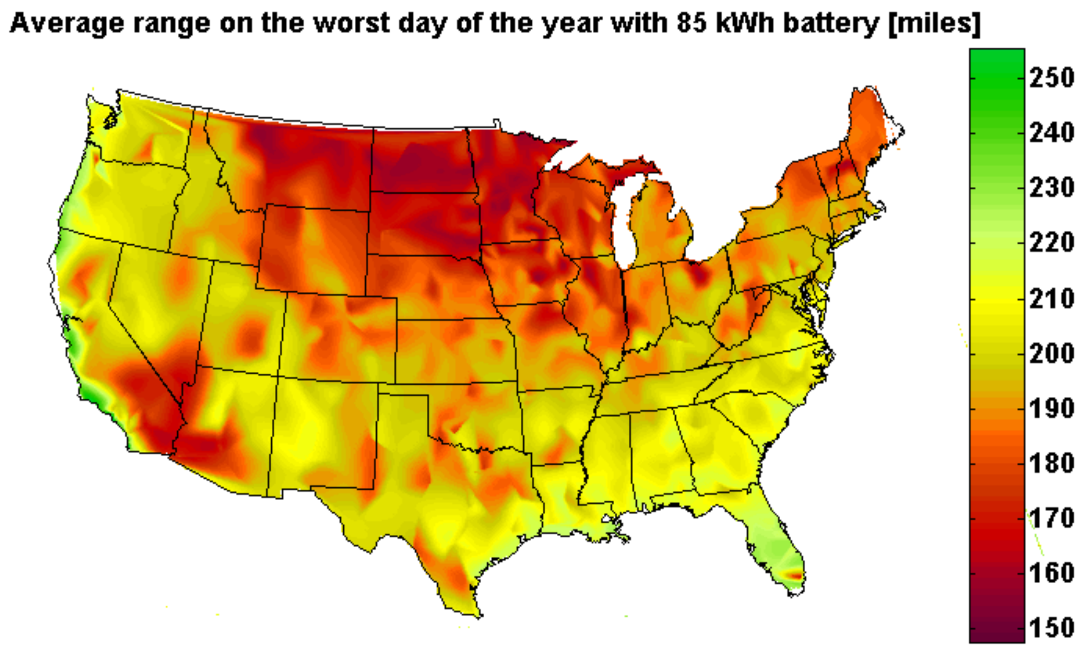

Figure B. 7 Average range on the worst day of the year with 85 kWh battery assumption

Charging Efficiency. In the main text, the average emissions are calculated using a charging efficiency of 87%. To see how much this assumption can change results, in **Figure B. 8** we provide the average emissions with 100% charging efficiency. As expected, we see a decrease of about 13% in the average emissions.

Charge Rate. In the main text, we assumed a 6.6 kW charging rate, which corresponds to Level 2 charging on a higher-current circuit. The Nissan Leaf also has the option to charge with Level 2 at 3.3 kW on a lower-current circuit (early models were limited to the lower rate). To see the effect of this assumption, we repeated our simulations using a charging rate of 3.3 kW. Emissions increase in most locations due to delayed charging and greater availability of coal-fired power plants on the margin at night; however, in certain locations emissions are up to 4.5% lower with lower charge rate. The emissions at selected cities for the base case and three sensitivity cases are provided in Figure B. 9.

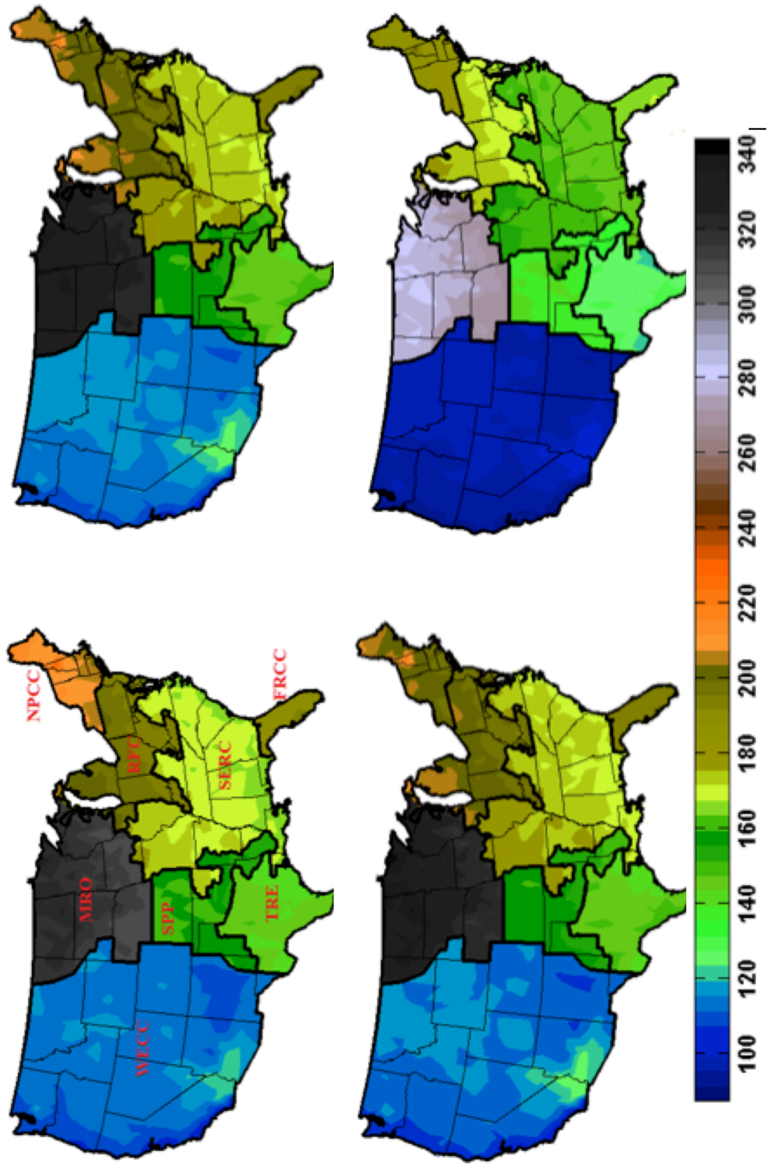

Figure B. 8 Average emissions for a) base case b) 85 kWh battery capacity c) 3.3 kW charge rate d) 100% charging efficiency.

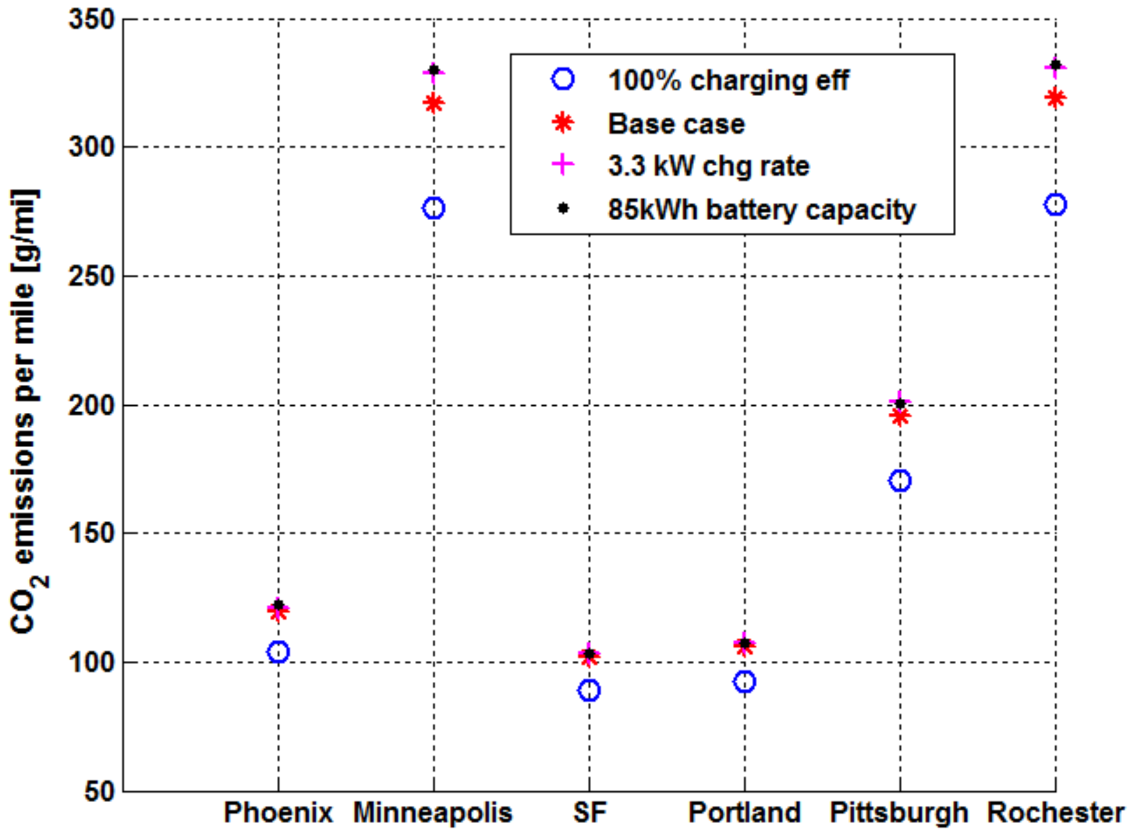

Figure B. 9 Emissions in selected cities, comparison of cases simulated. Base case represents simulations using 87% charging efficiency, 6.6 kW charge rate and 24 kWh battery capacity. For any other point, only the variable tested is given in the legend, other variables match the base case.

Marginal Emissions Factors. As mentioned in the main text, to estimate the grid emissions associated with increased load from BEV electricity consumption, we need to estimate marginal emissions from the power plants that are utilized to meet the extra demand. Although it is nearly impossible to identify exactly which power plants will change output in response to new demand, it is possible estimate the effect using past data. Two studies provide these estimates based on different approaches.

Graff Zivin et al. estimate the marginal emission factors (MEFs) by regressing emissions in each interconnect as a function of consumption in each North American Electric Reliability Corporation (NERC) regional reliability entity for each hour of the day[85] to identify marginal emission factors. They conduct the analysis both seasonally and annually. We use seasonal time of day estimates of the MEFs, an unpublished dataset that we obtained through personal communication with the authors, as our base case in the main text. To understand how much this time resolution affects our results, we perform the same analysis again using the overall time of day MEFs and present the results in Figure B. 10. Note that all of these MEFs we use here are point estimates (expectation of the marginal emission factor for each hour in each season).

Siler-Evans et al.[89] provide an alternative approach to estimating MEFs by regressing change in emissions as a function of change in Environmental Protection Agency's (EPA) Continuous Emissions Monitoring System (CEMS) fossil generation for each hour and in each NERC region. Their focus is on marginal electricity generation rather than consumption. Figure B. 10 shows analysis results using generation based seasonal and overall time of day point estimates for MEFs.

The results for consumption-based MEFs by Graff Zivin et al. show that using overall time of day estimates results in increased CO_2 emissions by about 4% on average (averaged over all the locations in the analysis) compared to seasonal time of day estimations. Figure B. 11 compares the results for selected cities (using a charging efficiency of 100%). In Phoenix, using the overall time of day MEFs can result in emissions 13% higher than using the seasonal MEFs. On the other hand, in Pittsburgh overall time of day MEFs result in about 2% lower emissions. The difference between overall and seasonal time of day MEFs is almost negligible for the generation based MEFs from Siler-Evans et al. When we compare the results using consumption based

MEFs versus generation based MEFs, we see that the difference is strongly regional. Two regions that show the most significant differences are WECC and MRO. In WECC, generation based MEFs result in emissions about 54% more than the consumption based MEFs. In MRO, on the other hand, the results with consumption based MEFs are on average about 10% higher. This shows that the estimation of CO_2 emissions due to extra load on grid from charging BEVs is strongly dependent on how MEFs are estimated. Figure B. 12 shows a comparison of the overall time of day MEFs predicted by two studies mentioned. For a more detailed comparison of the approaches, see Graff Zivin et al.[85] and Tamayao[88].

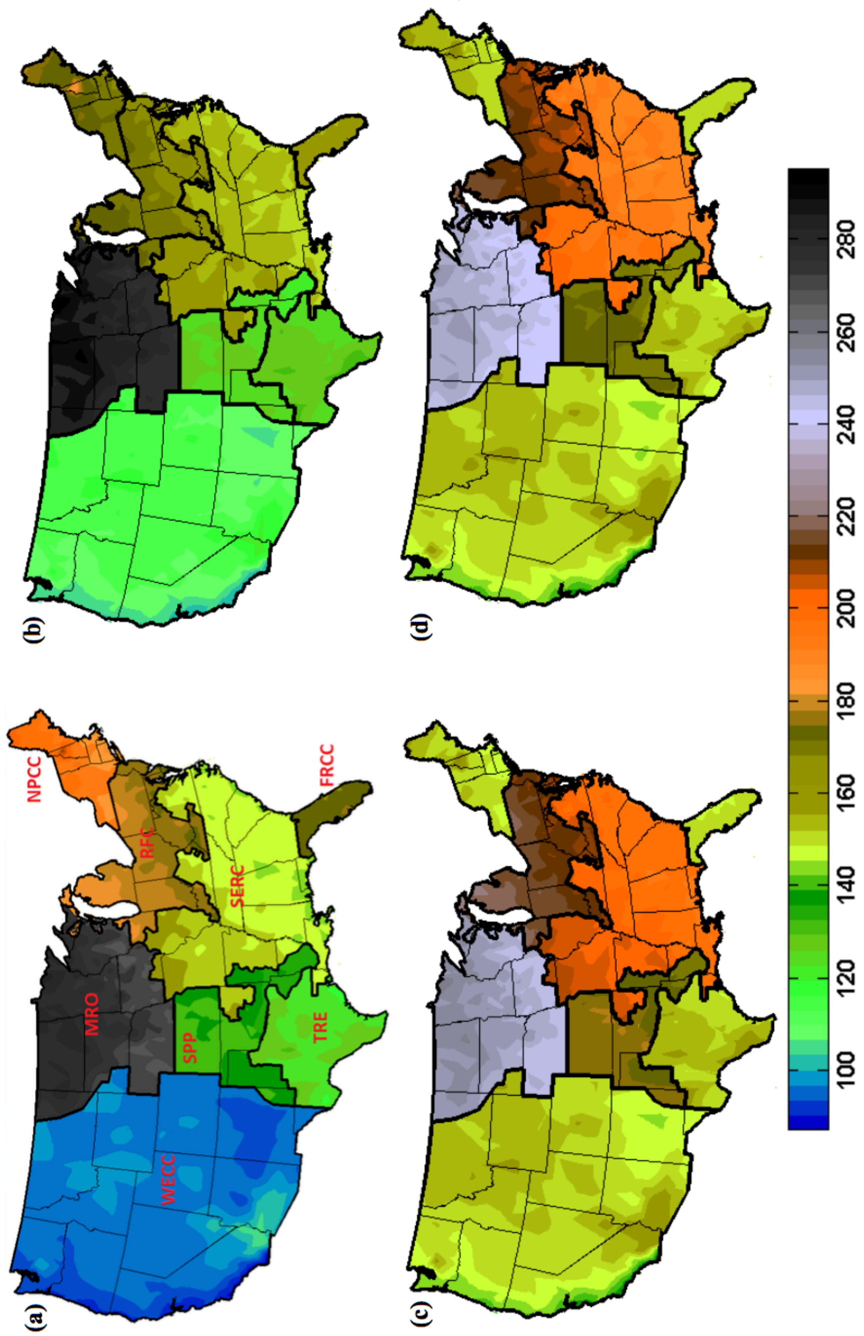

Figure B. 10 Average emissions using (a) Graff Zivin er al. seasonal time of day (b) Graff Zivin et al. overall time of day (c) Siler-Evans et al. seasonal time of day (d) Siler-Evans et al. overall time of day MEFs. 100% charging efficiency assumed**.**

.

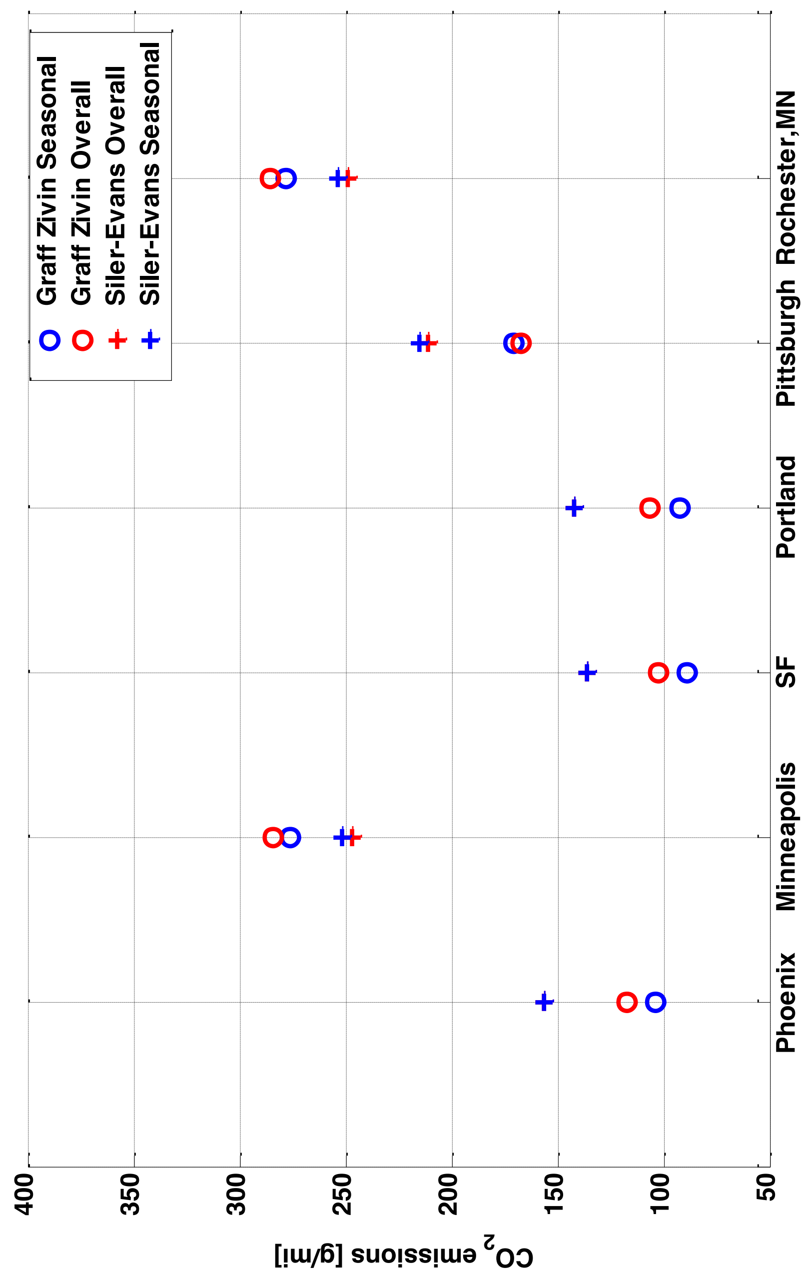

Figure B. 11 Average emissions for selected cities, comparison of using different values for MEFs from Graff Zivin et al. and Siler-Evans et al..

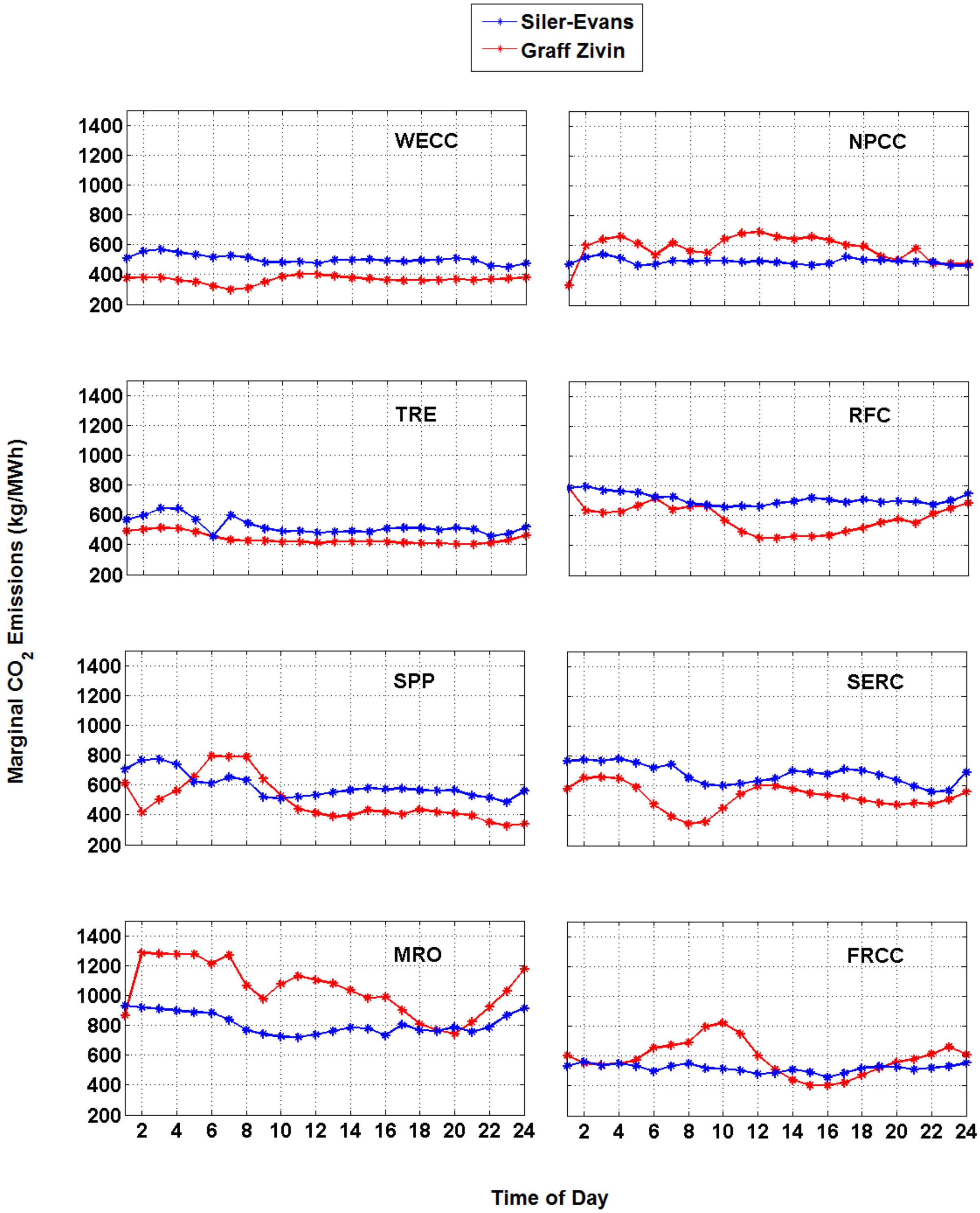

Figure B. 12 Comparison of overall time of day marginal CO_2 emissions at 8 NERC regions from two different sources: Graff Zivin et al. and Siler-Evans et al.

3) Extended Discussion on Limitations and Assumptions:

Battery Technology. All major US electric vehicles use lithium-ion (Li-ion) batteries. However, Li-ion batteries differ in material and design characteristics that affect temperature sensitivity The main reasons why cold temperature affects Li-ion batteries can be summarized briefly as follows:

- As temperature decreases, ionic mobility decreases. This causes the reaction rate to decrease and makes it harder for the Li-ion to be inserted in the "intercalation spaces". (Li-ion batteries depend on an "intercalation" mechanism where lithium ions are inserted into the crystalline lattice of the host electrode without changing its crystal structure)

- Decreased mobility causes the internal impedance to increase. Increase in internal impedance has negative effects both on life and performance: terminal voltage of the cell decreases, and the voltage needed during charging increases, thus reducing the battery effective capacity as well as decreasing its charge/discharge efficiency.

- With low temperatures electrolyte conductivity decreases.

Higher temperatures usually have positive effects in battery performance but negative effects on battery life.

Since all Li-ion batteries work on the same electrochemical principles, these effects will be observed in all currently available batteries. However, the extent of these effects may differ for different cell designs.

Driving Patterns. As mentioned in the main text, vehicle efficiency is strongly dependent on driving patterns and conditions. In particular, energy consumption is strongly dependent on the driving cycle[79], and driving cycle characteristics may be correlated with weather as well as location. We ignore regional variation in driving cycle to isolate effects of temperature from other effects such as degree of urbanization[88], but because our data are based on real-world driving, driving cycle effects that are correlated with temperature are implicitly captured in our efficiency vs. temperature model.

Further, BEV driving patterns may differ systematically from gasoline vehicle driving patterns obtained from the NHTS dataset. Figure B. 13 shows the cumulative distribution of daily vehicle miles traveled (DVMT) by NHTS vehicles. As can be seen from the figure, even when the range of a Nissan Leaf is the EPA rated value of 75 miles, 10% of the vehicles in NHTS cannot finish their daily trips using a Nissan Leaf on a single charge. When the range drops to lower values due to the temperature effect, this percentage increases. For example, in the case when the range drops to 45 miles, 25% of the vehicles are not able to perform their daily trips using a Nissan Leaf on a single charge. In this study, whenever the trip length is longer than the electric range, that trip is only completed to the point where the range allows. While BEV owner behavior may deviate from this assumption, our large battery sensitivity case suggests that the proportional effects we identify hold with longer-range BEVs as well.

Other climate elements. Temperature is not the only climate element that affects energy consumption. Other weather elements, such as snow, ice, rain and wind can all decrease vehicle efficiency due to resistance losses. Also, in addition to ambient temperature, humidity and radiation are other factors that determine cabin thermal comfort and therefore air conditioner use. With a temperature based comparison only, we may miss differences in efficiency between humid vs. dry regions that have similar temperature.

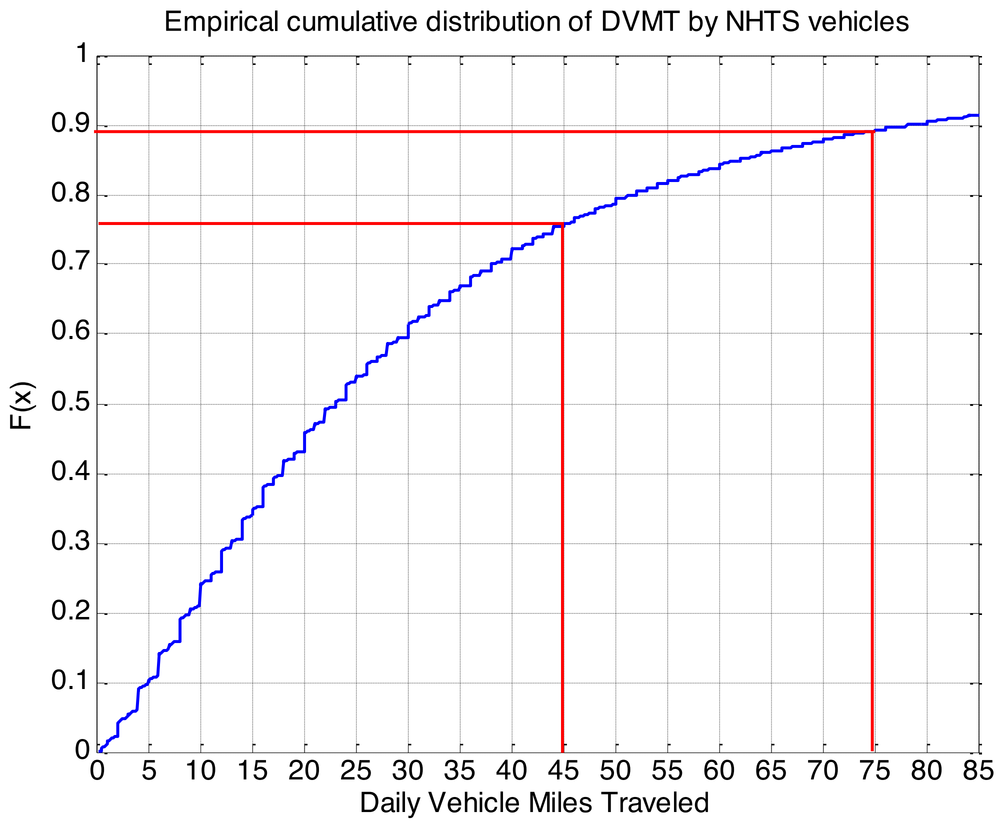

Figure B. 13 Cumulative distribution of daily vehicle miles traveled (DVMT) by NHTS vehicle

Appendix C. Supplemental Information for Variation of Electric Vehicle Life Cycle Greenhouse Gas Reduction Potential across U.S. Counties due to Regional Electricity Sources, Driving Patterns, and Climate

Testing the Importance of Temperature Effect

We test the effect of temperature on the results by ignoring the temperature dependency of the energy (electricity and/or gasoline) consumption and assuming a single constant value per drive cycle, which we obtain by using the dynamometer test results at 72^{o}F. In this case, hourly dependence of the energy consumption per mile is eliminated. The equations (3) to (5) can be removed from the analysis and Equation (6) becomes:

$$c_{ildvk}^{\mathrm{VEH}} = c_{ilk}^{\mathrm{DYNO}}(\phi_l) \tag{C.1}$$

The rest of the analysis remains the same.

Figure C. 1 shows results in comparison with the base case results. When temperature effect is ignored, the degree of comparison between Leaf and Prius emissions changes. Although relative comparison does not change, Leaf emissions decreases everywhere. Temperature affects the hourly and daily energy consumption of the vehicles. This also leads to changes in charge times and durations, shifting the MEFs. In addition, we also show results from simulations of a Nissan Leaf with model year 2012. We see that, with an older version of Nissan Leaf, the comparison between vehicles in terms of emissions is much more significant, and Nissan Leaf is has higher emissions in most of the US except Texas, Florida , the southwestern US, and urban counties of the western US and New England. This shows that, with improvements in battery and vehicle technologies, it is possible to diminish the effect of temperature on emissions.

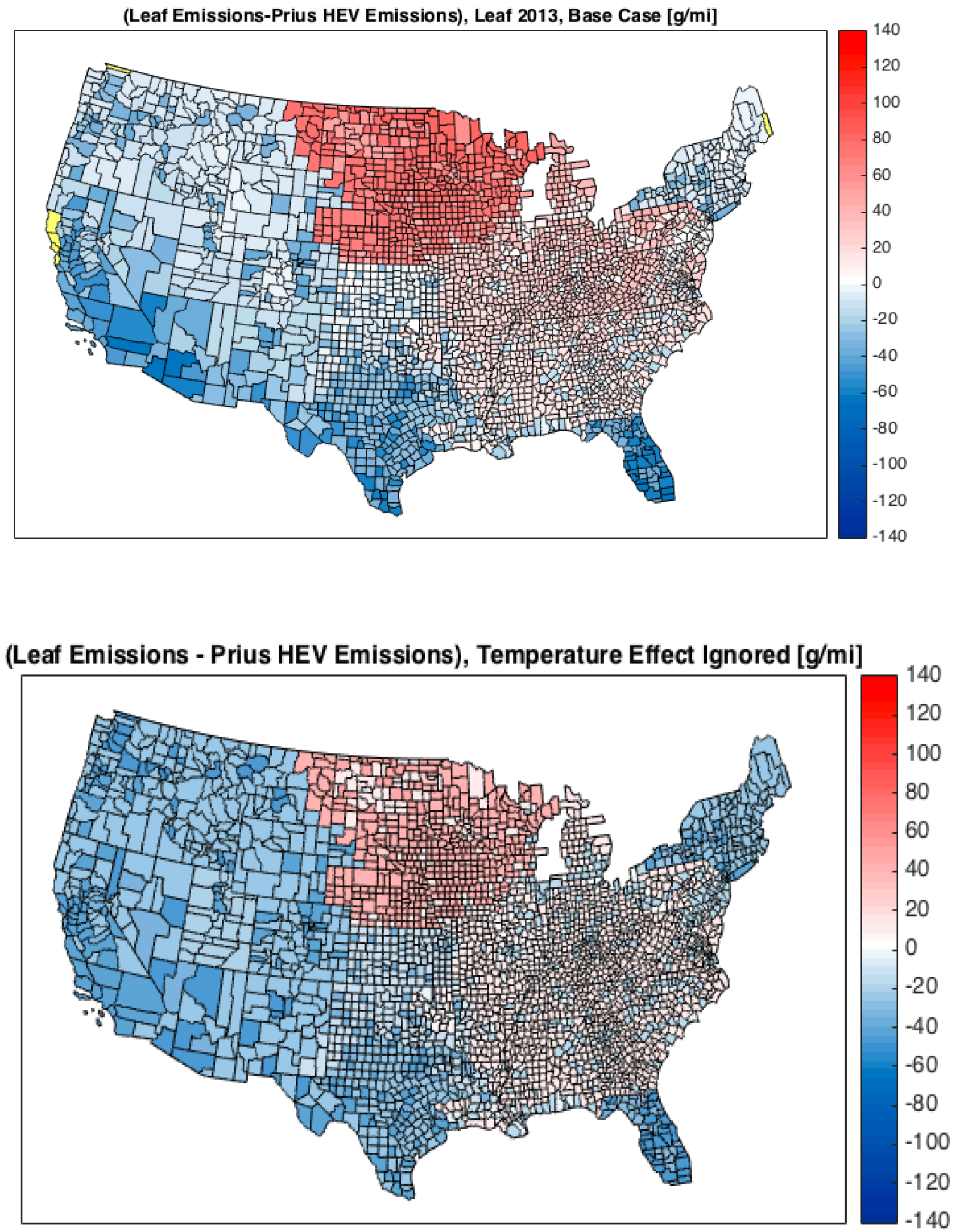

Figure C. 1 Leaf emissions-Prius HEV emissions, comparison of the temperature effect

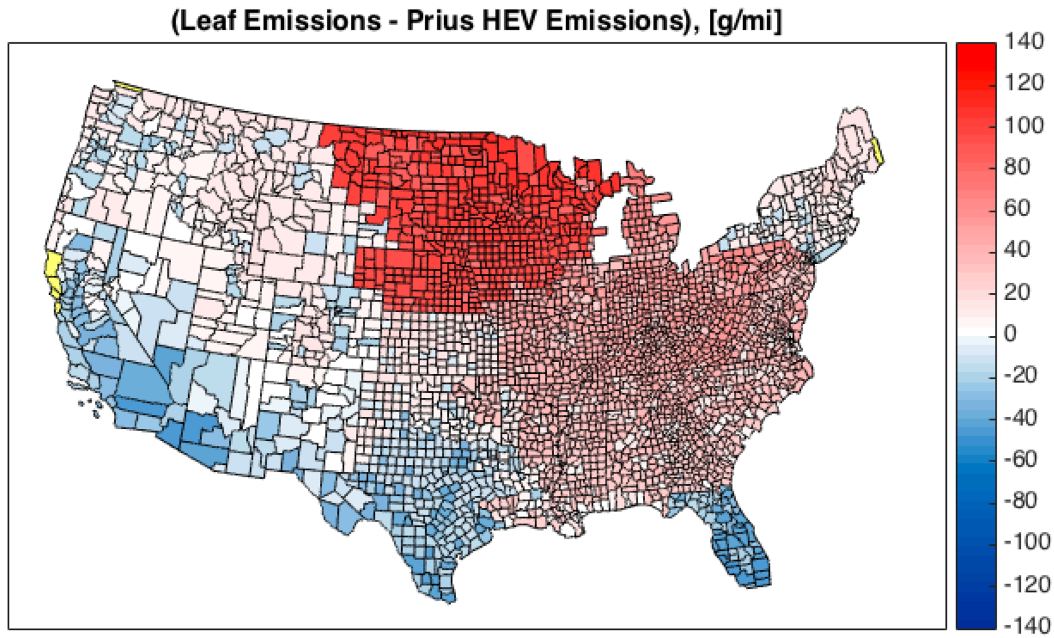

Figure C. 2 Leaf versus Prius, Leaf model year 2012

Testing the Importance of Regional Vehicle Drivng Patterns

We base our assumptions on vehicle driving patterns (time of driving, driving distance) on vehicle driving profiles available in NHTS 2009, data based on household surveys. NHTS does not provide the exact location of the households, therefore we do not know what kind of driving patterns are representative in each county exactly. However, NHTS provides the state where the surveyed household resides, as well as the urbanization level of the location (urban or rural). In our base case simulations, we match the driving patterns to counties based on their states only, i.e. all counties in the same state have the same vehicle driving patterns. To test the importance of this selection, we run another case, where we increase the level of accuracy by using both the states and urbanization levels in the matching. With this assumption, all urban (or rural) counties in the same state are assumed to be represented by the same driving patterns. We therefore include the differences in driving patterns both in regional (state) and urbanization level.

Figure C. 3 shows the results in comparison with the base case. No significant changes are depicted.

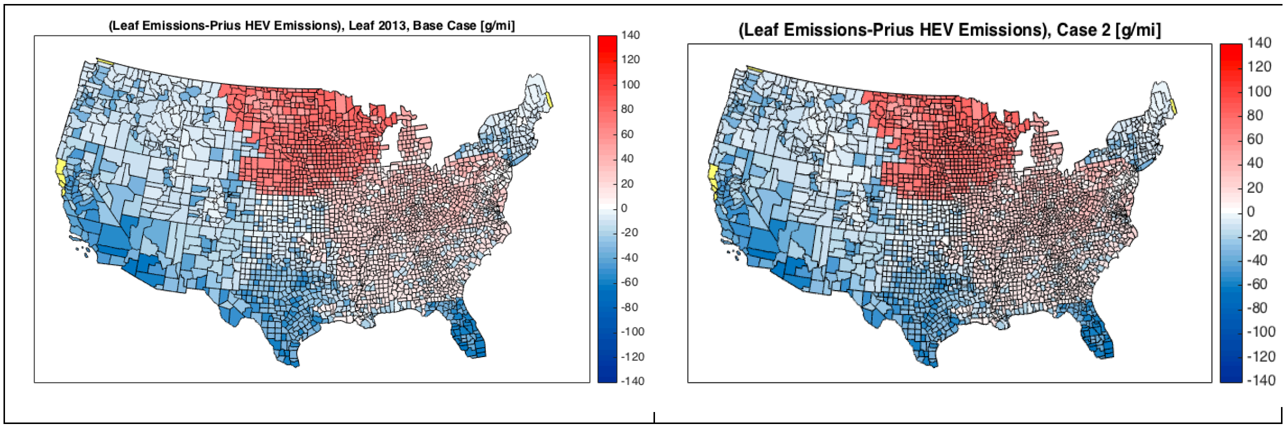

Figure C. 3 Leaf 2013 vs Prius Emissions, testing the importance of regional driving patterns, left: state level only; right: both state and urbanization level

Testing the Importance of Charging Scheme

In our base case simulations, we assume convenience charging, i.e. charging starts right after the last trip of the day. However, customers are usually advised to charge at night, due to lower electricity costs [Ref]. To test the effect of the decision on charging scheme, we simulate a case where charging starts at midnight for all vehicle profiles simulated.

Figure C. 4 shows the results in comparison with the base case. With delayed charging, Nissan Leaf emissions increase in general. This is due to the fact that, at nighttime, the marginal power plants are usually the low cost coal plants, which increases the MEFs at nighttime. This is the case for all NERC regions except NPCC, where we actually see an improvement in emissions with delayed charging. The results indicate that, although nighttime charging is a more economical option for the customer, it results in higher CO_2 emissions, with potential environmental and health costs. Note that this comparison was made using Nissan Leaf model year 2012.

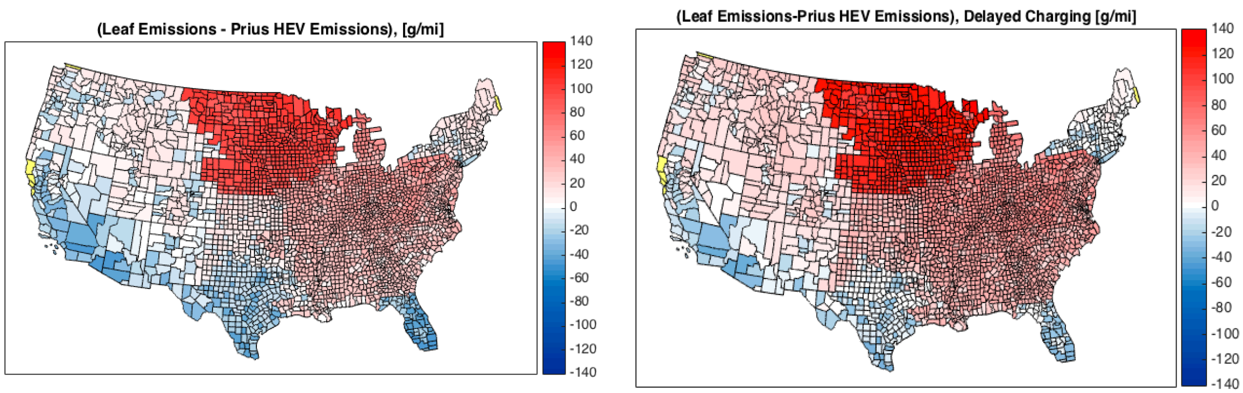

Figure C. 4 Leaf 2012 vs Prius emissions comparison, testing the importance of charging scheme. Left: convenience charging, right: delayed charging

Testing the Importance of Drive Cycle

As explained in the main text, in our base case simulations, we consider the regional differences in drive cycles (speed-time patterns) by assigning each county either a city, highway or combined driving based on county's MSA level. To test the importance of drive cycle, we also run a case where we neglect the differences MSA levels and consider combined driving only in all counties.

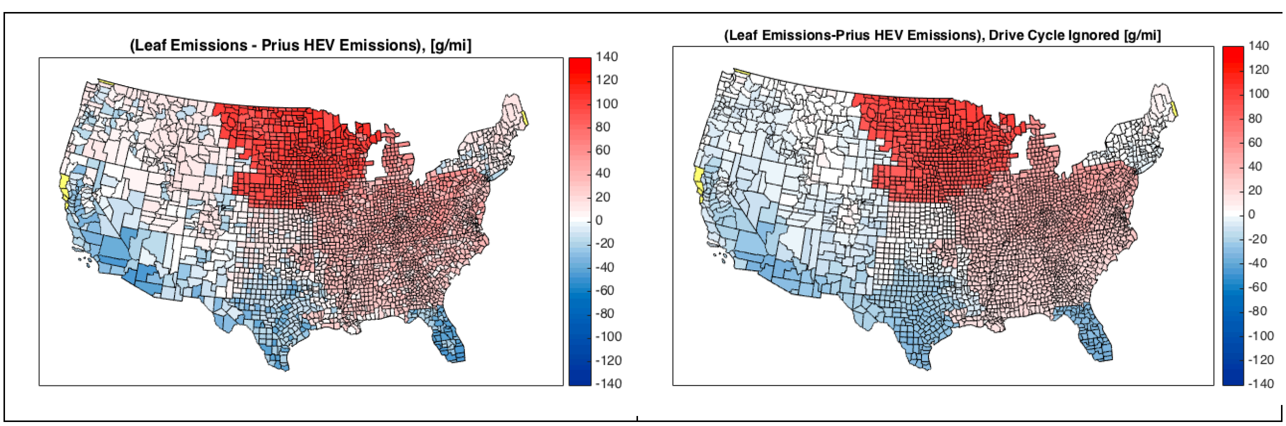

Figure C. 5 Leaf vs Prius emissions comparison, testing the importance of drive cycle. Left: base case, right: combined driving only